PETROGRAPHY AND MINERALOGY OF THE VERMICULITIZED PHLOGOPITIC METAGABBRO FROM THE KURANÇALI AREA (KIRŞEHİR-CENTRAL ANATOLIA)

A THESIS SUBMITTED TO
THE GRADUATE SCHOOL OF NATURAL AND APPLIED SCIENCES
OF
THE MIDDLE EAST TECHNICAL UNIVERSITY

75817

BY

FATMA TOKSOY

75817

IN PARTIAL FULFILLMENT OF THE REQUIREMENTS FOR THE DEGREE OF

MASTER OF SCIENCE

IN

THE DEPARTMENT OF GEOLOGICAL ENGINEERING

SEPTEMBER 1998

Approval of the Graduate School of Natural and Applied Science.

Prof. Dr. Tayfur ÖZTÜRK
Director

I certify that this thesis satisfies all the requirements as a thesis for the degree of Master of Science.

Prof. Dr. Vedat DOYURAN
Head of Department

This is to certify that we have read this thesis and that in our opinion it is fully adequate, in scope and quality, as a thesis for the degree of Master of Science.

Prof. Dr. M. Cemal GÖNCÜOĞLU
Supervisor

Examining Committee Members

Prof. Dr. Ayhan ERLER

Prof. Dr. M.Cemal GÖNCÜOĞLU

Assoc. Prof. Dr. Asuman G. TÜRKMENOĞLU

Assist. Prof. Dr. Sönmez SAYILI

Assist. Prof. Dr. Pırıl ÖNEN

ABSTRACT

PETROGRAPHY AND MINERALOGY
OF THE VERMICULITIZED PHLOGOPITIC METAGABBRO
FROM THE KURANÇALI AREA (KIRŞEHİR-CENTRAL ANATOLIA)

TOKSOY, Fatma

M.Sc., Department of Geological Engineering
Supervisor: Prof. Dr. M. Cemal Göncüoğlu

September 1998, 175 pages

The aim of this study is to understand the geological, petrographical and mineralogical characteristics of the Kurançalı Metagabbro in Kurançalı (Kırşehir) area and to determine the vermiculitization process of mafic minerals within the metagabbro.

The Kurançalı Metagabbro, an isolated member of the Central Anatolian Ophiolites, is thrusted onto the metamorphic ophiolitic complex of the Central Anatolian Metamorphics along a steep contact. Both the metagabbro and the underlying metamorphics are intruded by granitic rocks.

Compositional layering with variable grain size and presence of phlogopite-rich layers are the characteristic features of the Kurançalı Metagabbro. These features differentiate the unit from the other gabbroic rocks of the Central Anatolian Ophiolites.

Detailed petrographical and mineralogical studies are carried out on the gabbro samples by using x-ray diffractometry, combined differential thermal and thermogravimetric method, inductively coupled plasma spectrometry, scanning electron microscope and energy dispersive x-ray method, semi-quantitative electron microprobe and petrographic microscope.

Petrographically the major minerals of the metagabbro are diopsidic augite, hornblende, phlogopitic mica and plagioclase. Among them, the mafic minerals are mineralogically diopside, tschermakitic hornblende and Fe-rich phlogopite in composition. Based on the modes of the mafic minerals, the Kurançalı Metagabbro is mainly divided into pyroxene gabbro, hornblende gabbro and phlogopite gabbro.

In the metagabbro, secondary hornblende and actinolitic hornblende replacing clinopyroxene, secondary biotite replacing hornblende and clinopyroxene, and vermiculite occurrence from phlogopite are the most common alteration products those are formed at variable stages.

Transformation of primary phlogopite to vermiculite due to early stage weathering results in dioctahedral hydroxy-Al and anhydrous vermiculites.

Keywords: Kırşehir, Kurançalı Metagabbro, layering, petrography, mineralogy, phlogopite, vermiculite.

ÖZ

KURANÇALI BÖLGESİNDEKİ (KIRŞEHİR-ORTA ANADOLU) VERMİKÜLİTLEŞMİŞ FİLOGOPİT İÇEREN METAGABROLARIN PETROGRAFİSİ VE MİNERALOJİSİ

TOKSOY, Fatma

Yüksek Lisans, Jeoloji Mühendisliği Bölümü
Tez Yöneticisi: Prof. Dr. M. Cemal Göncüoğlu

Eylül 1998, 175 sayfa

Bu çalışmanın amacı Kurançalı (Kırşehir) bölgesindeki Kurançalı Metagabrosunun petrografik ve mineralojik özelliklerini ortaya koymak ve metagabro içinde yer alan koyu renkli minerallerdeki vermikülitleşme sürecini açıklığa kavuşturmaktır.

Orta Anadolu Ofiyolitlerinin izole bir birimi olan Kurançalı Metagabrosu, Orta Anadolu Metamorfiklerine ait metamorfik ofiyolitli kompleksinin üzerine dike yakın bir dokanak boyunca bindirmiştir. Metagabro ve alttaki metamorfiklerin her ikisi de granitik kayalarla kesilmişlerdir.

Değişik tane boyunda bileşimsel bantlaşma göstermesi ve filogopitli bantlar içermesi Kurançalı Metagabrosunun karakteristik özellikleridir. Bu özellikleri ile Orta Anadolu Ofiyolitlerine ait diğer gabrolardan ayırt edilir.

Gabrolardaki detaylı petrografik ve mineralojik çalışmalar, x-ışınları difraktometresi, birleşik diferansiyel termal ve termogravimetri metodu, endüklenmiş plazma spektrometresi, taramalı elektron mikroskop ve enerji yayılımlı x-ışınları metodu, yarı-kantitatif elektron mikroprob ve petrografik mikroskop ile yürütülmüştür.

Petrografiye göre metagabronun temel mineralleri diyopsidik ojit, hornblend, filogopitik mika ve plajiyoklasdır. Bunlardan mafik mineraller mineralojiye göre diyopsit, çermakitik hornblend ve demirce zengin filogopit bileşimindedirler. Mafik minerallerin türlerine göre Kurançalı Metagabrosu, piroksen gabro, hornblend gabro ve filogopit gabro olmak üzere üç temel gruba ayırtlanmıştır.

Metagabroda rastlanan klinopirokseni ornatan ikincil hornblend ve aktinolitik hornblend, hornblend ve klinopirokseni ornatan ikincil biyotit, filogopitten vermikülit oluşumu değişik aşamalarda oluşan en yaygın ayrışma ürünleridir.

Birincil filogopitteki vermikülitleşmenin erken aşamadaki ayrışma sebebi ile meydana geldiği, ve dioktahedral hidroksi-Al ve anhidrat vermikülit tiplerinin oluşumuna neden olduğu saptanmıştır.

Anahtar Kelimeler: Kırşehir, Kurançalı Metagabro, bantlaşma, petrografi, mineraloji, filogopit, vermikülit.

To Serhat KÖKSAL

ACKNOWLEDGMENTS

I am greatly thankful to my supervisor Prof. Dr. M. Cemal GÖNCÜOĞLU for his supervision throughout the research and for encouragements, valuable guidance and critisms.

I wish to express my thanks to Assoc. Prof. Dr. Asuman Türkmenoğlu for her critisms on analytical studies.

I am especially thankful to Miss. Serap İçöz and Mrs. Erçin Özgül from MTA, Assoc. Prof. Dr. Uğur Köktürk and Mrs. Hatice Yılmaz from University of Dokuz Eylül, Mr. Celal Şahin from Toprak Seniteri ve İzolatör Sanayii A.Ş. Eskişehir Karo Fabrikası, Mr. Abdullah Öner from Turkish Petroleum Corporation for providing laboratory facilities.

I would like to express my gratitude to my brother Kamil Toksoy, my sister Hatice Afacan and her husband Tanın Afacan, and my friends Atilla Ömerbeyoğlu, Murat Çetintaş, Hasan Sarıkaya for their help during the field studies.

Thanks are also extended to the BAYG Group of Scientific and Technical Research Council of Turkey (BAYG-TÜBİTAK) for their scholarship.

Finally, but never at least, I extend my gratitude to my parents and Serhat KÖKSAL for their patience and encouragements during my study.

TABLE OF CONTENTS

LIST OF TABLES

TABLE

LIST OF FIGURES

FIGURE

CHAPTER 1

INTRODUCTION

1.1. Purpose and Scope

Since the beginning of the century, there have been many geological studies in Central Anatolia. In the recent years, the important studies, done by METU Central Anatolian studies group, have shown that the Central Anatolian Crystalline Complex (CACC) consists of three main units: Central Anatolian Metamorphics, Central Anatolian Granitoids and Central Anatolian Ophiolites. The units of the Central Anatolian Ophiolites (CAO) are found as allochthonous bodies over the Central Anatolian Metamorphics (CAM) (Göncüoğlu et al., 1991, 1992, 1998).

Isotropic and layered gabbroic rocks occurring as isolated outcrops in the CACC have shown to be ophiolitic by Göncüoğlu et al. (1991, 1992, 1998), Yalınız et al. (1996), Yalınız and Göncüoğlu (1998). One of the isolated outcrops of layered gabbroic rocks is from Kurançalı town located at east of Kaman (Kırşehir). It is observed within a tectonic sliver having a sharp contact with the uppermost units of the CAM. This allochthonous unit and the underlying metamorphics are cut by K-rich granitic dykes. The Kurançalı Metagabbro shows variable compositions with intense alteration. The main mineral phases are clinopyroxene, amphibole of both primary and secondary origins, dark mica (phlogopite and secondary biotite) and plagioclase. The characteristic feature of the Kurançalı Metagabbro, differing from other mafic

and ultramafic rocks of the CAO, is the existence of vermiculitized phlogopite-bearing layers. Vermiculite occurrence due to alteration is especially along cleavages and at rims of primary phlogopitic mica crystals.

The purpose of this study is to interpret the contact relationships of the Kurançalı Metagabbro and the metamorphic ophiolitic complex of the CAM, petrographical features of the phlogopite-bearing metagabbro and the transformation of phlogopite to vermiculite. In these aims, detailed mapping, closely spaced sampling, petrographical and mineralogical studies have been done.

This Master's Thesis study, mainly based on mineralogy and petrography of the vermiculitized phlogopite bearing gabbros, is carried out to learn the analytical methods and to interpret the mineral alterations associated with the Kurançalı Metagabbro. The mineral separates (mica, hornblende and pyroxene) which were purified by Frantz isodynamic magnetic separator and hand picking were analysed by x-ray diffractometry, associated differential thermal and thermogravimetric method, and inductively coupled plasma spectrometry. In addition, chips of rock samples were analysed by scanning electron microscope and energy dispersive x-ray method. Thin sections of rock samples were examined semi-quantitatively using electron microprobe as well as petrographic microscope.

1.2. Geographic Setting

The study area covers 9 km^2 just at south of the Kurançalı town of Kırşehir which is included in J31-b3 quadrangle of the 1:25 000 scaled topographic map of Turkey within latitudes 39°17'41"-39°19'17" N and longitudes 33°53'33"-33°55'39" E in the Central Anatolia (Figure 1).

The main topographic high is Karaöne Hill (1703 m) with Sivri Sırtı stretching in NE-SW direction. Karagedik stream is just at east of the Karaöne

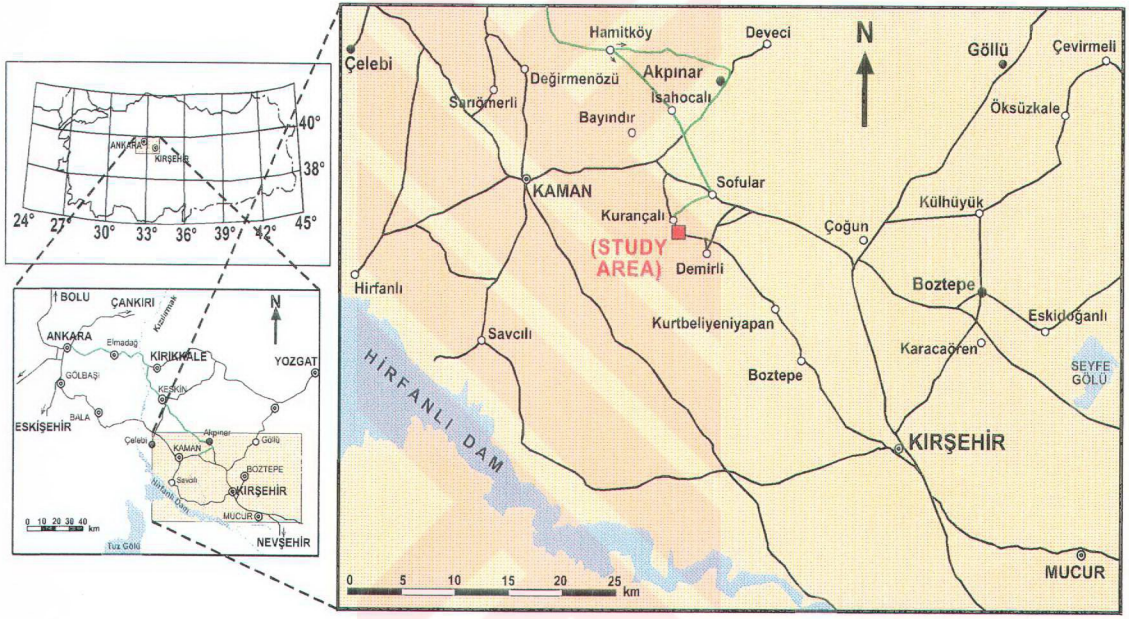

Figure 1. Location map of the study area.

Hill. The typical continental climate of Central Anatolia is effective in the study area.

It is easy to arrive from Ankara to Kurançalı town along Ankara - Kırıkkale - Keskin - Akpınar - Sofular - Kurançalı or Ankara - Kırıkkale - Keskin - Hamitköy - İsahocalı - Sofular - Kurançalı with a distance of about 180 km. The distance of the town to Kırşehir is about 43 km.

1.3. Methods of Study

This study was mainly performed in two major steps; field and laboratory studies.

1.3.1. Field Work

Although the field work was mainly performed for sampling, geological map was also prepared on the 1:25 000 scale topographic map of Kırşehir sheet during the summer months of 1996-1997. In geological map, although there are no good outcrops arbitrary boundaries between metamorphics and gabbros were indicated. In addition, gabbros were differentiated into three main groups on the basis of their modal compositions in hand specimens.

106 samples from the study area and 10 more from outside of the study area were collected. Among them, 40 samples are from metamorphic rocks, 59 samples are from gabbros and 17 samples are from felsic dykes.

1.3.2. Laboratory Work

Laboratory work, mainly based on petrographical and mineralogical analyses of the collected samples, were carried out by many analytical methods such as; mineral purification using Frantz isodynamic magnetic

separator and by hand picking, x-ray diffractometry, associated differential thermometry and thermogravimetry, scanning electron microscope with energy dispersive x-ray diffractometry, inductively coupled plasma spectrometry, spectrophotometry, semi-quantitative electron microprobe and petrographic microscope.

Petrographic examinations were carried out by petrographic microscope, scanning electron microscope and semi-quantitative electron micropobe. For microscopic study, 73 thin sections were prepared from fresh surfaces of selected samples at Department of Geological Engineering of Middle East Technical University. Microscope studies were carried out by using James Swift (Prior) model polarizing microscope revealing mineralogical and textural properties. James Swift (Prior) Model F point counter attached to polarizing microscope was used to make modal analyses of representative dyke samples with point counts of between 1000 and 2000 points per sample by which the compositions of rocks are expressed by percentages.

Scanning electron microscope (SEM) was utilized to examine the actual three-dimensional crystal relationships on 4 gabbro samples that were petrographically interpreted, because SEM has advantages over optical microscope (e.g., greater depth of field and resolution, and a significantly higher magnification range). Together with SEM, energy dispersive x-ray analyser (EDS) was used to check the phase changes semi-quantitatively. Specimens mounted as chips on aluminum stubs and coated with gold were analysed by a JEOL LTD. JSM-840A scanning electron microscope equipped with a TRACOR-NORTHERN 5502 energy dispersive analysis (EDS) system which is available at Turkish Petroleum Corporation. The samples were examined at 20 kV accelerating voltage with a range of magnification from 80X to 5000X.

Electron microprobe analyses were semi-quantitatively applied on polished thin sections of selected 4 gabbro samples. The samples were analysed by JEOL superprobe 733 (microprobe) equipped with energy

dispersive system (EDS) with an accelerating voltage of 15 kV which is available at Department of Mining Engineering of Dokuz Eylül University. These samples were carbon coated by JEOL JEE-4X vacuum evaporator and mounted on Al stubs using double stick tape. The elements, Si, Al, Mg, Na, were routinely analysed using counter TAP (001) crystal of 2d (25.757Å) with proportional counter while Ca, Ti, K were analysed using PET(002) crystal of 2d (8.742Å) with scintillation counter. In addition, Fe was analysed using LIF (002) crystal of 2d (4.0267Å) with scintillation counter.

Samples usually contain an admixture of mica flakes, amphibole, pyroxene, plagioclase and magnetite. Therefore, prior to mineralogical analyses, 12 representative gabbro samples were ground and passed through magnetic separator to purify the minerals at Department of Geological Engineering of Middle East Technical University. Firstly primary minerals of the samples ground to less than 1 cm size in a Spex 4200 model jaw crusher were tried to be selected by hand picking. Since this purification was not enough, separated samples were wet ground with alcohol either in an agate mortar and pestle or Bico LC-115 shatter box with a ceramic holder to avoid excessive damage to the structure, and fully dispersed in distilled water by shaking and ultrasonic treatment. After they were dried, samples were sieved to the range of 90-150 μm for subsequent mineral separation in a Frantz isodynamic magnetic separator because the size of the grains should be as uniform as possible. These two fractions and those that lie between were the best suited for separation. Variable electromagnetic force, controlled by altering the current flow and variable degrees of longitudinal and cross slope of the chute, were applied according to the behavior of the minerals. Although there are some charts giving the current amount applied at which longitudinal and cross slopes for every mineral (e.g., Appendix A), experience in using a separator led to more accurate and rapid results during the mineral separation. After magnetite was separated using a small magnet, the other minerals were purified at various conditions by Frantz isodynamic magnetic separator. Purified minerals, mica, pyroxene, hornblende, were progressively controlled under a binocular microscope during separation by

Frantz isodynamic magnetic separator. At the end of separation, approximately 100% pure mica samples from 8 samples were obtained. Moreover, the purity of the 2 clinopyroxene samples and of 2 amphibole samples are estimated to be more than 95%. The elimination of amphiboles from the micas was difficult because of their similar Fe content. In this case, electricity of micas on paper due to friction was used to separate them from amphiboles.

8 purified mica samples were examined using X-ray diffractometry (XRD) at General Directorate of Mineral Research and Exploration. The X-ray analyses were carried out using a Rigaku Geiferflex X-ray diffractometry with Ni-filtered CuKα radiation at voltage of 40 kV and current of 20 mV. Count data on both oriented and random samples were recorded at steps of 2°2θ/min with a starting angle of 2°2θ. Random samples, placed into the glass sample holder (2.5x3 cm), were run up to 70°2θ while oriented samples on glass slides were run up to either 30°2θ or 40°2θ at setting of $2x10^3$ cps (count per second). The d(060) values were measured only for untreated random specimens. Oriented samples were prepared by slurring them with acetone and allowing to dry slowly at room temperature to form thin layers on glass slides in order to enhance the basal reflections on the patterns. Parallel oriented specimens of each sample were heated to 170°, 350° and 600°C for 1 hr and treated with glycerol (G) and ethylene glycol (EG) as well as air-dried specimen (i.e., 6 mounts were prepared for each sample). Saturation with EG and G was performed by placing the samples (on glass slides) above the organic liquid at 65°C for 24 hr (vapor method) in a desiccator. The heated and organic matter saturated specimens were kept in a desiccator having 0% relative humidity until they were x-rayed. The records of the specimens, EG saturated and heated to 350° and 600°C as well as air-dried one, were obtained in the range of 2°2θ and 40°2θ while the specimens, G saturated and heated to 170° were recorded to 30°2θ.

For purified mica samples, connected differential thermal-thermogravimetric analyses (DTA-TGA) were also carried out by a Rigaku

thermal apparatus at General Directorate of Mineral Research and Exploration. 20 mg of samples placed into platinum was analysed using calcined Al_2O_3 as reference at static air atmosphere in the range from room temperature to 1100°C with a heating rate of 10°C/min.

Chemical analyses for 7 mineral separates of the vermiculite-bearing phlogopite gabbro, pyroxene gabbro and hornblende gabbro were carried out using standard inductively coupled plasma spectrometry (ICP) method in an automated PERKIN ELMER Optima 2000 at Toprak Seniteri ve İzolatör Sanayii A.Ş. Eskişehir Karo Fabrikası, Eskişehir. Since the total iron is reported as Fe_2O_3 by ICP, the same samples were decomposed in an orthophenanthroline complex to allocate ICP total-iron values to Fe^{2+} and Fe^{3+}. Fe^{2+} was measured colormetrically in the prepared complex using Unicam SP 600 Series 2 spectrophotometry available at Department of Geological Engineering of Middle East Technical University. The used standard was DTS-1 (dunite sample). The details of solution preparation for the chemical analyses by ICP and spectrophotometry are given in Appendix B.

1.4. Previous Work

Previous work is reviewed on three subjects; geology of the Central Anatolia, phlogopite and vermiculite.

1.4.1. Previous Work on the Geology of the Central Anatolia

Previous work on the geology of the Central Anatolia includes studies on all the rock units (metamorphics, ophiolitic rocks and granitoids).

Buchardt (1954) prepared a 1/100000 scaled geological map of an area between Kırşehir-Çiçekdağ-Keskin and north of Tuz Gölü. He identified rock types in terms of mineralogy and petrography. He concluded that gabbro

exposures are generally surrounded and injected by syenites containing gabbro xenoliths. He identified that the pyroxenes of gabbros were completely uralitized, and other alteration products (chlorite, epidote, sericite, calcite) were formed at the contacts between gabbros and syenites.

Ketin (1955, 1963) defined the crystalline rocks as metamorphic rocks, plutonic rocks of acidic, intermediate and basic compositions intersecting the metamorphics.

Ayan (1963) studied various rock types, both felsic and mafic, around Kaman region in the Central Anatolian Massif and suggested that they are products of the successive intrusions from the same magma chamber. His suggestion is that first basic rocks (gabbros), than granitic rocks and finally alkaline rocks (nepheline syenite, nordmarkite, foyaite) were intruded. He reported that gabbros contain as major minerals, diallage, green and brown hornblende and plagioclase (labradorite). He also mentioned that the alteration products are uralite, serpentine, epidote and tremolite. Ayan (1963) radiometrically determined the intrusion age of Baranadağ monzonitic granite by the Pb-Pb method on a zircon sample and gave an age of 54 my.

Erkan (1975) studying the prograding metamorphism in Central Anatolian Massif, around Kırşehir suggested that high temperature (approximately 700°C) - medium pressure (3 kb) were effective factors during metamorphism.

Göncüoğlu (1977, 1981) studied the geology of Niğde Massif and differentiated from bottom to top; Gümüşler Formation (composed mainly of metaclastics), Kaleboynu Formation (comprising the alternation of metacarbonates and metaclastics), Aşıgediği Formation (consisting of metacarbonates). He suggested that they are the products of metamorphism from medium to high grade (up to partial melting). Göncüoğlu (1977) also interpreted that the Niğde group is overlain by an ophiolitic melange which has undergone deformation and metamorphism together with the underlying

formations. He also stated that the metamorphics and metaophiolites are intruded by post-tectonic Üçkapılı Granodiorite.

Erkan and Ataman (1981) obtained geochronological data by using K-Ar method on biotite and hornblende from gneisses, mica-schists and amphibolites exposed at NW of Kırşehir (among the analysed hornblende samples, one is from amphibolites at SE of Kurançalı town). They compared the ages obtained from hornblende and biotite of the same sample and showed that while biotites of the samples gave 69.7±1.7 my average age, hornblendes of the samples have 74.1±3.2 my average age. They suggested that the isotopic system of the metamorphics were wound up by the thermic effect of the intrusion of the granodioritic masses and concluded the average age (71 my) obtained by averaging the two minerals as the intrusion/cooling age of the intrusives. The authors also concluded that evolution of the main phase of regional metamorphism was completed in pre-Cretaceous time.

Oktay (1981) described the gabbroic rocks in the southwestern part of the study area as Karakaya ultramafics.

Seymen (1981a,b, 1982) stated that the oldest units of the Kırşehir Massif are metamorphic rocks at S-SW of Kaman and named them as the Kaman Metamorphics. Seymen (1981a) defined the gabbroic rocks as gabbro, diorite-gabbro, quartz-gabbro in composition. All of the magmatic rocks were suggested to cut the metamorphics and at some places ophiolitic units. Seymen (1982) proposed that the metamorphics, divided into three subunits, were formed under prograde and retrograde conditions of regional metamorphism and completed its evolution before Mesozoic. Metamorphics are tectonically overlain by ophiolites and ophiolitic melange (Ankara melange and Karakaya ultramafics) during the Campanian-late Maastrichtian. They all together were cut by granitoids and alkaline plutons of Baranadağ and Buzlukdağ, respectively.

Göncüoğlu (1985, 1986) obtained geochronological data using Rb/Sr wholerock, and Rb/Sr and K/Ar mineral methods for the Üçkapılı Granitoids and gneisses of Gümüşler Formation. He calculated the crystallization age of Üçkapılı Granitoids as 95±11 my based on the Rb/Sr wholerock data. He interpreted the source of the granitic magma considering the initial Sr value (Sr=0.7104) obtained from the wholerock isochron. His statement is that the melting of continental crust itself or by the extensive contamination by the continental crust caused Üçkapılı granitic magma. He interpreted cooling ages of granodiorite and gneisses to cool together down to 300±50°C using the ages, 77.8±1.2 my of Rb/Sr wholerock-mineral method and 76.5±1.1 my of K/Ar method. Göncüoğlu (1986) also suggested that the main metamorphism and ophiolite emplacement occurred during pre-Cenomanian in the Niğde Massif by correlating his data with other radiometric ages from other parts of the Central Anatolian Massif and considering both the metamorphics and ophiolites were cut by granodiorite.

Önen (1985) investigated the mineralogy-petrography and geochemistry of the gabbros of Central Anatolian Massif from northeast of Kaman region. She observed that the major minerals are plagioclase, hornblende, augite and rarely olivine. Besides, the alteration products observed are chlorite, calcite, tremolite, quartz, albite, epidote and biotite. Önen (1985) defined the gabbros as; hornblende-gabbro and fine grained gabbro. Önen (1985) and Önen and Unan (1988) also concluded that gabbros were geochemically derived from subalkaline tholeiitic magma and they are ophiolitic in origin not intrusive.

Bayhan (1986) studied the Çelebi granitoid which is located at the western proximity of the Kırşehir Massif and cutting the ultramafic rocks and metamorphics tectonically underlying them. He interpreted that the ultramafics are composed of pyroxenite, hornblendite and lastly gabbros having cumulate structure. He observed intense uralitization in pyroxenite and gabbros.

Tarhan (1987) stated that the metaophiolites in Aksaray area are of Paleozoic age. According to him, metaophiolites were overlain by metamorphic rocks of Permian-Campanian island arc origin and by granitic rocks. Tarhan (1987) put forward that there are no granitic intrusions but magmatic rocks were formed by in situ partial melting of the metamorphics. He accepted that all the units, metamorphics, ophiolites and granitoids, belonging to the Central Anatolian Massif form a nappe that was emplaced from north or northwest during the Middle-Upper Miocene time interval.

Kara and Dönmez (1990) mapped the Kırşehir region in a 1:100 000 scale and investigated the geology of the area. According to the authors, the oldest unit of the area is Kırşehir Massif. The Kırşehir Massif was lithostratigraphically divided into four formations; Kalkanlıdağ, Bozçaldağ, Kervansaraydağ and Hacıselimli. The Hacıselimli Formation was represented by metabasic rocks (metagabbro, metadiabases, amphibolites). The metabasic rocks were interpreted to intrude the sedimentary units during syn- and/or post-sedimentational period, and then they were altogether metamorphosed.

Erler et al. (1991) studied granitoids and alkaline rocks from N and NW parts of the Central Anatolian Massif in terms of petrographical and geochemical features. They stated that granitoids cut ophiolite and ophiolitic melange which are observed as roof-pendants within them. Erler et al. (1991) identified seven subgroups of granitoids based on their field occurrences, petrographical and geochemical compositions.

Göncüoğlu et al. (1991) used new terms; Central Anatolian Crystalline Complex (CACC) for whole Massif including Kırşehir Massif, Akdağ Massif and Niğde Massif, Central Anatolian Metamorphics (CAM) for metamorphic units, Central Anatolian Ophiolites (CAO) for ophiolitic masses and Central Anatolian Granitoids (CAG) for granitoid bodies. They divided the metamorphic units comprising mainly gneiss, mica-schist, metacarbonate, amphibolite and metaquartzite as; Gümüşler Formation, Kaleboynu

According to his investigation, there are mainly three rock types, Çokumkaya gabbro, Ağaçören granitoid and Kurtkaya basalt in the area. Geochemical data of Kadıoğlu from these rocks provide a crustal source for the Ağaçören granitoid and a mantle source for the Çokumkaya gabbro. The gabbro was suggested to be intrusive.

Türeli (1991) interpreted the metagabbros which are thrusted onto metamorphics and cut by the Ekecikdağ Granitoids from Ekecikdağ region. According to Türeli (1991), the metagabbros exposing in this region, are of the CAO and not related to granitoids in the region. They are tholeiitic in character and derived from oceanic crust (mantle).

Göncüoğlu et al. (1992) studied the geology and petrography of the rock units at western part of Central Anatolian Crystalline Complex, around Ortaköy-Aksaray. The authors stated that the CAM forming the basement are overlain by ophiolitic rocks. They observed that the metagabbros are widely distributed in Kötüdağ, Küçükdağ, Harundağ, Dededağ, Ekecikdağ, Keleşdağ and Küçükekecekdağ which are tectonically emplaced from NW to S. The authors also recognized them at lower parts of other ophiolitic units (sheeted dykes and pillow lavas) at Çatallıdağı, Devedamı, Bozdağ-Ceceli, Karadağ, Alayhanı-Ağaçlı. Granitic rocks cut both the metagabbroic rocks and metamorphics, metagabbros are observed as roof-pendants within them. Göncüoğlu et al. (1992) stated based on petrographic and geochemical

features that there are two subtypes of granitoids, leucogranite derived from syn-collisional partial melting of continental crust and biotite-hornblende granite having late-collisional - post-collisional character. The first one has geochemical characteristics of S-type while the latter has both I- and S-type characteristics.

Göncüoğlu and Türeli (1993) petrologically and geodynamically investigated ophiolitic rocks in Ekecikdağ area, east of the Aksaray. They stated that the metamorphics were overthrusted by an ophiolitic unit comprising different types of gabbros, dolerites and diabases with minor plagiogranites. They recognized that both the metamorphic and ophiolitic rocks were cut by granitoids, moreover, ophiolitic masses are found as roof-pendants within them. The contact zone of granitoids with gabbroic rocks is characterized by the presence of enclaves and hornblende-biotite rich reaction zones. The authors provided trace element data for the plagiogranites petrographically characterized by the absence of K-feldspar. The data suggest that the plagiogranites were generated by the fractionation of basic magma and were formed in a fore-arc setting. The authors concluded that the intra-oceanic subduction within the İzmir-Ankara ocean, in close relation with an ensimatic arc, resulted in the formation of the ophiolites.

Göncüoğlu et al. (1993a,b) indicated that the CAG must have resulted from a collisional type magmatism. According to their investigation, the İzmir-Ankara Ocean was consumed by both subduction beneath the Pontides and through the intra-oceanic subduction zones. Firstly S-type syncollisional and then S- and I-type post-collisional granitoids of late Campanian age are intruded into the area due to the emplacement and crustal thickening resulted from collision of island arc (formed from subduction of İzmir-Ankara Ocean beneath Pontides) with the Tauride-Anatolide belt and obducted onto this belt during the closure of İzmir-Ankara Ocean.

Göncüoğlu and Türeli (1994) described the geological, petrological and geochemical features of Ekecikdağ Granitoids and discussed their tectonic

setting. They suggested based on major, trace and REE element data that Ekecikdağ granitoid, post-collisional in character, was essentially generated by partial melting of the continental crust with minor contamination from lower crust/mantle because of a two-stage collision related to the closure of İzmir-Ankara branch of Neotethys during Late Upper Cretaceous.

Göncüoğlu et al. (1994) studied the petrological and geodynamic characteristics of the Central Anatolian Ophiolites thrusted on metamorphic basement of Paleozoic-Mesozoic and cut by granitoids of Late Cretaceous-Paleocene. They investigated the composition of alkaline plutonics cutting the ophiolitic rocks in Central Anatolia. According to them, the studied ophiolites were derived in supra-subduction zone, and not in the mid-ocean ridge from İzmir-Ankara-Erzincan ocean during Turonian-Santonian period.

Güleç (1994) obtained Rb/Sr isotopical data from the granitoids of Ağaçören located along the western margin of the CACC. She showed that the Rb-Sr isochron yields initial isotopic ratio of 0.708616±42 with an age of 110±14 my. She suggested that this age must have pre-dated at least the initiation of the Neotethyan closure.

Yalınız et al. (1994, 1996, 1997), Yalınız and Göncüoğlu (1998) studied the Sarıkaraman Ophiolite, one of the ophiolitic bodies of Late Cretaceous age. The Sarıkaraman Ophiolite comprises a somewhat dismembered ophiolite body retaining a recognizable and well-preserved magmatic pseudostratigraphy. According to the authors, the ophiolitic body includes isotropic gabbros, plagiogranites (trondhjemite), dolerite dyke complex, basaltic volcanics of a co-magmatic tholeiitic source and sedimentary cover. They concluded that the Sarıkaraman Ophiolite formed in a supra-subduction zone through northward subduction of Vardar-İzmir-Ankara-Erzincan oceanic lithosphere during Middle Turonian-Early Santonian. Yalınız et al. (1997) suggested that the studied ophiolite was very short lived and rapidly obducted during the Campanian to pre-Upper Maastrichtian times onto the CACC in the south.

Köksal (1996) studied the geology and petrology of the rocks of CACC around İdiş Dağı-Avanos area and prepared a 1/25 000 scaled geological map. He stated that Aşıgediği Metamorphics representing the uppermost unit of the CAM were cut by Early Maastrichtian aged İdiş Dağı syenitoids which are quartz syenite, alkali-feldspar syenite and quartz monzonite in composition. He suggested on the basis of geochemical data that these syenitoids are A-type and products of post-collisional intrusions resulted from the partial melting of mainly the upper mantle. Köksal also stated that there are volcanic equivalents of the syenitoids cut by them. He proposed that in the late Middle Eocene period, Aşıgediği metamorphics and İdişdağı syenitoids were thrusted over the Tertiary cover units due to a compressional regime.

Yılmaz-Şahin and Boztuğ (1997) interpreted the Akçakent gabbro in Çiçekdağ region as a product of an underplating mafic magma rather than of an ophiolitic suite. However, later Yılmaz-Şahin and Boztuğ (1998) interpreted the same gabbroic rocks as a part of the CAO. The authors stated that the Akçakent gabbro thrusting onto the Çökelik volcanics, shows a preserved ophitic texture and mineralogical composition. The gabbros were called as uralite-gabbro. Based on major and trace element geochemical data, Yılmaz and Boztuğ suggested a depleted mantle source and low-K tholeiitic characteristics in composition. They also investigated the Halaçlı monzogranite, characterizing the post-collisional, high-K calcalkaline, hybrid I/HLO type magmatism intruding the ophiolitic units.

Floyd et al. (1998) studied the geochemical and petrological features of plagiogranites belonging to the Sarıkaraman Ophiolite in CACC and discussed their origin relative to basic members of the complex. The provided data resulted in supra-subduction origin for the plagiogranites which are largely concentrated near the top of the gabbro section.

Göncüoğlu et al. (1998) concluded that the most of the ophiolitic rocks from CACC were generated above an intra-oceanic subduction within İAE

ocean during Middle Turonian-Early Santonian and thrusted onto the CAM representing the Tauride-Anatolide Platform during Early Santonian - pre-Late Maastrichtian time interval. Moreover, they recognized the transition of supra-subduction zone type ophiolite to initial volcanic arc complex since the rhyolitic volcanics are co-genetic with plagiogranites of ophiolites. They, however, interpreted metabasaltic rocks of the metamorphosed ophiolites (partly within the CAM) having the alkaline character must have been related to transitional crust or a material developed during the syn-opening or just post-opening of İzmir-Ankara-Erzincan ocean. These rocks were emplaced onto metamorphosed platform rocks before emplacement of the ophiolitic rocks. Also some MORB-type basaltic rocks which are not completely consumed during intra-oceanic subduction resulted in Central Anatolian Ophiolites.

Kadıoğlu et al. (1998) made geological and geophysical studies on the gabbros which are observed as roof-pendants in the Ağaçören Granitoid from east of Tuz Gölü. According the authors, the gabbroic rocks are coeval with the main granitic body, but not allochthonous ophiolitic bodies representing the remnants of Neotethyan ocean floor.

1.4.2. Previous Work on Phlogopite

Nemecz (1981) proposed the structural formula of phlogopite with Fe substitution of 27% as $[Si_3FeO_{10}(OH)_2Mg_3]K_{0.9}Mn_{0.1}$ with cell dimensions of a=5.36, b=9.29, c=10.41 Å and â=100°. However, there are differences in cell parameters of phlogopite given by Hazen and Burnham (1973) where a=5.3078, b=9.1901, c=10.1547 Å, ß=100.08°. The ideal structural formulae based on the crystal structures given by Nemecz (1981), trioctahedral mica (phlogopite) $[Si_3AlO_{10}(OH)_2Mg_3]^{-1}K^+$ indicates an absence of excess charges in the octahedral sheets of micas. Octahedral cations seem far more restricted in their ability to substitute into phlogopite structure (Hazen and Wones, 1972). From the crystal chemical viewpoint, the most important task is to clarify the range of possible substitutions in the tetrahedral and

octahedral layers. If any specific mica is considered as an isomorphous mixed crystal, this essentially means the setting up of a system of pure extreme terms. There are two approaches to this problem: a statistical processing of numbers of analyses (Foster, 1960), and experimental, hydrothermal synthesis (Yoder, 1959; Crowley and Roy, 1964). A combination of the results leads to the assumption of the following extreme terms:

Trioctahedral types

$[Si_3AlO_{10}(OH)_2Mg_3]K$	ideal phlogopite
$[Si_3AlO_{10}(OH)_2Fe^{2+}_3]K$	annite
$[Si_4O_{10}Fe_2AlLi_2]K$	polylithionite
$[Si_5Al_3O_{20}(OH)_4Mg_5Al]K_2$	eastonite
$[Si_5Al_3O_{20}(OH)_4Fe_5Al]K_2$	Fe-eastonite

Transitional di-trioctahedral types

$[Si_3AlO_{10}(OH)_2AlMg_{1.5}]K$	hypothetical
$[Si_{2.67}Al_{1.33}O_{10}(OH)_2AlFe^{2+}_{1.66}]K$	siderophyllite
$[Si_{2.67}Al_{1.33}O_{10}(OH)_2Fe^{3+}Fe^{2+}_{1.66}]K$	lepidomelane (iron-rich biotite)

Foster (1960) showed the relationship of the trioctahedral micas on the triangular diagram of the Mg-R^{2+}-R^{3+} system (see Figure 64) where the octahedral cation content for over 200 natural phlogopites, biotites, and siderophyllites were plotted. It is conspicuous that the composition of ledikites (apart from the oxidation of the R^{2+} cations Fe^{2+} and Mn^{2+}) corresponding essentially to those of phlogopite and biotite (lying to the left of those in the diagram). As the Fe^{2+} content of these micas increases, so does the octahedral aluminum content. Trivalent aluminum in R^{2+} sites requires a corresponding substitution of aluminum for silicon in the tetrahedral layer. Thus, aluminum has the dual effect of increasing the size of the tetrahedral layer, while decreasing the effective octahedral cation radius. The maximum

observed effective octahedral ionic radius, for the most iron-rich, aluminum poor specimens, is 0.74 Å.

Phlogopites were suggested to have trioctahedral triple-layer complex (Pabst, 1955) in which the vector joining the centers of the O and the H atom are perpendicular to the (001) plane (with the H atom exactly beneath the interlayer K ion) (Bassett, 1960). The studies on variation between composition and the various polymorps in the biotite-phlogopite series (Levinson and Heinrich, 1954) showed that (a) in phlogopites there is no discernible relationship between structure and either composition or paragenesis, (b) in biotites there is no relationship between structure and composition, but geologic environment may be a factor in determining the polymorphic type, (c) the optic plane of all 2-layer polymorps is normal to (010), (d) 1-layer polymorps nearly always have the optic plane parallel with (010). Hendricks and Jefferson (1938a) investigated that the relative position of the triple-layer complexes resulting in polytypes in mica structure is not fixed and there are many possibilities. The differences observed between polytypes was suggested due to differences in site-filling distribution over the Si, Al and Fe populations (Nemecz, 1981). After the discovery of a number of polytypes, Smith and Yoder (1956) attempted to provide a theoretical foundation of polymorphism in micas and proposed a notation involving the number of layers in the unit cell, combined with the symbol of lattice symmetry. If a certain symmetry admits more than one arrangement, these are distinguished by numerical suffixes. In terms of this notation, the six basic types are 1M, $2M_1$, $2M_2$, 2Or, 3T, 6H. Of these, $2M_1$ is first variant of the two-layered monoclinic polytype with alternating rotation by 120 and 240°. The alternation of 60 or 300° gives $2M_2$. 1M is the result of zero-degree rotation, and 2Or of 180° rotation. Repeated rotation by either 120 or 240° gives rise to 3T. Nemecz (1981) and Bailey (1984) stated that the most mica minerals belong to the types 1M, $2M_1$, $2M_2$, 3T and the disordered types are subordinate. Phlogopites show two types of ordered staking; one example (1M) is very common, the other ($2M_1$) much rarer (Bailey, 1985; de la Calle

and Suquet, 1988). In both cases pseudohexagonal cavities on the surface of adjacent layers face each other and enclose the interlayer K cations.

Ferromagnesian micas with low Fe^{2+}, the join between phlogopite and annite, behaves essentially as an ideal solution (Hewitt and Wones, 1984). These biotite compositions, common constituents of igneous rocks, are important in the determination of temperature, water pressure, oxygen pressure and compositional variations for magmatic processes. Biotite compositions represent some general trends summarized by stating that the biotites from the more siliceous igneous rocks tend to be more iron-rich than biotites from the less siliceous rocks (Heincrich, 1946; Nockolds, 1947). The authors assumed two reasonable interpretations for these trends; (a) the bulk compositions of these rock types are related and the biotites merely reflect that effect, (b) the less siliceous rocks represent higher temperature of crystallization and only Mg-rich biotites are stable at those magmatic conditions. In this aim, Wones and Eugster (1965) experimentally investigated schematic f_{O_2}-T curve in the range from 400° to 900° for biotite-sanidine-pyroxene-magnetite-quartz assemblage and concluded that biotite crystallizing from a magma may follow either a more Fe-rich or a more Mg-rich trend, depending upon the f_{O_2} conditions during cooling. The Mg-rich (phlogopitic) trend in the biotite compositions is represented by constant or slightly increasing f_{O_2} (through loss of hydrogen) and leads to an increase in the amount of magnetite present and a decrease in the Fe/Fe+Mg ratio of the biotites crystallizing from the melt (i.e., increase in Mg/Fe ratios of the associated ferromagnesian phases). This phlogopitic trend in biotite compositions represents saturation of melt in H_2O during crystallization and cooling. On the other hand, Fe-rich biotites are crystallized from the melt with low content of H_2O. The H_2O undersaturated melt is buffered by the anhydrous mineral assemblages and results in crsytallization of ferromagnesian silicates and very little magnetite as well as Fe-rich biotite. Each mica bearing assemblage requires a minimum H_2O pressure for a particular mica to coexist with a hydrated siliceous melt and a particular phase assemblage. In the deep crust and mantle, where vapor is usually not present

as a phase, the fusion of a particular mineral yield a hydrated, but H_2O saturated melt. Maaloe and Wyllie (1978) showed that the crystallization sequence for biotite changed as a function of H_2O content, with biotite crystallizing out earlier at higher H_2O contents. The increasing water content lowers the melting points of the anhydrous minerals and enhances the stability of biotite. The combined effect gives different sequences of crystallization, and this becomes a valuable indicator of the nature of the fugitive components within a crystallizing magma. Partin (1984 in Hewitt and Wones, 1984) suggested that biotites having 24% phlogopite component do not require the presence of Fe^{3+} to satisfy the structural fit between the octahedral and tetrahedral sheets and will have an Fe^{3+} content dependent only on f_{O_2} and composition. Phlogopite stability is bounded by a series of subsolidus dehydration reactions that terminate in a series of invariant points that lie at total pressures less than 1.2 kb (Hewitt and Wones, 1984). At higher total pressure, the phlogopite stability curves are a series of melting reactions. In this series of invariant points the (SiO_2) decreases with increasing temperature, and f_{H_2O} increases with increasing temperature. The dependence of phlogopite stability on silica activity explains the wide variations in the occurrence of the mineral in gabbroic rocks. An important result of the several studies in the model system is the change in the composition of the liquid generated by the vapor absent melting of the different phlogopite-bearing assemblages. Not only is the liquid a function of the phase assemblage, but it varies significantly with pressure.

The relationships between biotites and amphiboles are quite complex and the relative stabilities of them in a crystallizing magma depend on the activity of K_2O, CaO, H_2O and SiO_2 (Wones and Gilbert, 1982). According to Wones and Gilbert, biotites by themselves are equal in thermal stability to amphiboles considering that Bowen's reaction series is as successful as it is. K_2O activities are usually lowered by Na_2O contents of melts and feldspars. CaO is relatively insoluble in silisic melts, so that clinopyroxene or hornblende crystallizes earlier than biotites in most magmas. However, in ultrapotassic rocks, the sequence can be reversed, and rocks exit in which amphibole is

only present as a late stage alteration product (Eriksson and Wones, 1983). Wones and Dodge (1977) examined the relations between phlogopite, quartz and diopside in an idealized system. These results are very similar to those of Naney (1983) so that the occurrence of biotite euhedra as inclusions in hornblende, and the presence of biotite and diopsidic pyroxene in ash-flow tuff indicate that the early part of the magmatic crystallization in these instances took place under conditions of relatively low H_2O content of the melt. It was also reviewed that the estimates of H_2O contents of magma and concluded that most begin to crystallize at low water contents, gradually building up to saturation with crystallization of anhydrous minerals.

There are many studies on the melting of ultrapotassic rocks and the crystallization of phlogopite from ultrapotassic magmas (see references in Hewitt and Wones, 1984). The suggestions about the origin of the phlogopite rich regions of the mantle have ranged from metasomatism of the upper mantle (Bailey, 1982) or the interaction of siliceous liquids with peridotitic mantle (Sekine and Whllie, 1982a,b,c, 1983; Whllie and Sekine, 1982). In the latter studies, it is argued that siliceous liquids rising into a peridotitic mantle would precipitate zones of phlogopite. Hewitt and Wones (1984) concluded that the ultrapotassic magmas are generated from portions of the mantle that contain phlogopite, but at different depths. There are no logical fractionation sequences that relate the several kinds of ultrapotassic magmas, but phlogopite-bearing peridotites will react at different pressures to produce melts of higher silica contents at low pressures, and lower silica contents at higher pressures. Any melt that containing several percent H_2O, a high K_2O activity, and greater than 0.2% MgO should crystallize biotite early in the crystallization sequence. Phlogopites can crystallize directly from the melt, or to be in a reaction relationship with forsterite and/or diopside at crustal pressures. Drops in temperature while maintaining H_2O pressure and total pressure would lead olivine to react with a potassic liquid to form phlogopite. Orthopyroxene will also react to form phlogopite under similar conditions. Drops in pressure of magmas that contain phlogopite phenocrysts might also

lead to resorption of phlogopite, or its decomposition to glass or feldspar and pyroxene or olivine.

Cerny and Burt (1984) reviewed the phlogopite occurrence around the rare-element pegmatites as metasomatic auroles. Phlogopite is common in contacts with peridotites, pyroxenites and serpentinites. It also forms among pegmatites emplaced into marbles. In both ultrabasic and carbonate environments, the phlogopite is occasionally associated with endocontact margarite, replacing plagioclase.

1.4.3. Previous Work on Vermiculite

Vermiculite is a mineral resembling mica that, when exfoliated by rapid heating, has an appearance of little worms. The term vermiculite, used for mineral occurring as large crystals as well as in the clay size range, is a somewhat basket term. Basically, the name, derived from the Latin *vermiculare* (Deer et al., 1980), is given to the 2:1 phyllosilicate expandable minerals which have layer charge, $0.6<x<0.9$ per $O_{10}(OH)_2$, and containing Mg, Fe (Fe^{3+}) or hydroxy-Al complexes in between the 2:1 layers (Velde, 1985; de la Calle and Suquet, 1988; Deer et al., 1980, Nemecz, 1981; Moore and Reynolds, 1989). This is not just an argument over terms but it in fact represents a compositional and physicochemical reality in many instances.

Many studies have been done on mineral samples of large size, well characterized as trioctahedral vermiculites according to the definition of Gruner (1934). In addition to macroscopic vermiculites MacEvan (1948), Jackson et al. (1952), Walker (1950a), Brown (1953), Hattaway (1955) first found the mineral in soils. X-ray diffractometry analysis shows that the vermiculite is dioctahedral as well as trioctahedral (Brown, 1953; Hattaway, 1955; Walker, 1957; Barshad and Kishk, 1969; Gruner, 1934, 1939; Hendricks and Jefferson, 1938a,b; Deer et al., 1980). In addition to the soil and macroscopic vermiculites, authigenic vermiculites forming hydrothermally

(Singer and Stoffer, 1981) and vermiculites (metamorphic type) found in metamorphosed pelitic rocks (Black, 1975; Velde, 1978, 1985; McDowell and Elders, 1980) were also identified.

Vermiculite has been considered for a long time as a variety of trioctahedral mica. Gruner (1934, 1939) studied on the samples of large crystals and determined its structure. He showed it to be composed of talc sheets separated by a double water layer, similar in thickness to the brucite layer of chlorites. Hendricks and Jefferson (1938a,b) pointed out that the structure is neutral, and that it is balanced by the interlayer ions, most commonly Mg and sometimes Ca. Hendricks and Jefferson (1938b) postulated a hypothetical arrangement of the interlayer water molecules in planar hexagonal rings with the oxygen of each water being tetrahedrally bonded to four neighboring oxygens through hydrogen atoms. Alternating water molecules in each of the two interlayer planes bond to the adjacent talc surfaces. High cation exchange capacity ($0.6<x<0.9$ per $O_{10}(OH)_2$) (Walker, 1949, 1957; Barshad, 1948, 1950, 1952; Grim, 1968; Moore and Reynolds, 1989), the ability to form complexes with organic substances (Walker, 1950b; Barshad, 1950; Moore and Reynolds, 1989) and a variable interlamellar distance depending on the exchangeable cation present and the humidity of the sample (Barshad, 1949; Walker, 1951) are the characteristic properties of the vermiculite.

Most vermiculites form by the degradation of pre-existing sheet silicates and much of their characters are determined by those of the starting minerals. That is to say, the chemistry of vermiculites is quite closely related to that of the parent micas, although there is little disruption of the mica structure (Jelitto et al., 1993). The two main distinguishing features from micas are lower net negative layer charge and oxidized form relative to the parent mica. The lower net charge correlated closely with the oxidation of Fe^{2+} to Fe^{3+} (Norrish, 1973). However, as pointed out by Foster (1963), there is not 1:1 relation between the layer charge reduction below 1 per $O_{10}(OH)_2$ and the

content of Fe^{3+} in the vermiculite, so that additional changes in composition must also occur. These include the coupled oxidation-reduction reaction:

$$Fe^{2+} + OH^{-}\ (\text{structural}) \longrightarrow Fe^{3+} + O^{2-}\ (\text{structural})$$

which causes no overall change in net charge balance, and ejection of Fe^{3+} from the structure when the octahedral sites become overpopulated with trivalent cations (Farmer et al., 1971). The Fe^{2+} present in the parent mica is oxidized to Fe^{3+} during transformation of trioctahedral mica to vermiculite, and part of the Fe^{3+} may have moved into the interlayer space to produce heterogeneous, unorganized layers. On the other hand, Proust et al. (1986) recognized vermiculitization process which does not appear to have taken place by the oxidation of Fe^{2+}, but rather, by the simultaneous leaching of Fe^{2+} and Mg with increase in Si and Al. The initial Fe^{3+} content of the parent mineral is almost the same as that of the last weathering product, vermiculite.

Vermiculites resulting from alteration of micas express the replacement of the interlayer K by a hydrated cation, generally Mg (e.g., Moore and Reynolds, 1989; Nemecz, 1981). K-Mg exchange process is reversible. It was implied the fact that the crystal structure of the vermiculite contracts in the presence of K (Gruner, 1939; Barshad, 1948, 1950, 1954a,b; Walker, 1949; de la Calle et al., 1976). The pseudo-hexagonal cavities on the surface of the vermiculite layers may be partially filled by K cations because the size of the K cations is so small as to allow to enter in cavities. Thus neighboring layers are linked by strong electrostatic bonds and resulting structure is equivalent of that of a trioctahedral mica. The biotite having high iron content is not likely to alter to vermiculite. When ferrous iron content is sufficiently high, oxidation will result in positive charge and extension of octahedral sheet to such extent that basic layer would be unstable and break up quite rapidly (de la Calle and Suquet, 1988).

The element losses in the order of $K^{+} > Fe^{2+} > F^{-} > Mn^{2+} > Si^{4+} > Mg^{2+} > Al^{3+} > Ti^{4+}$ as well as some gains in the order of $H^{+} > Ca^{2+} > Fe^{3+} > Na^{+}$ were

recognized during transformation of biotite to vermiculite (Pozzuoli et al., 1992). The transformation of different micas obviously follows quite different paths with general trends of K leaching and a continuous decrease in Al-for Si tetrahedral substitutions and a progressive increase in Al-for-(Fe^{2+}-Mg) octahedral substitutions depending on composition of parent mineral and conditions of weathering (Moon et al., 1994). The alteration of biotite to vermiculite was given in a two-step process by Hindman (1994). Using a hypothetical biotite and ferric iron solution, the ferrous iron is first oxidized within the octahedral layers as follows: $K_2(Mg_4,Fe^{2+}_2)[(Si_6Al_2O_{20}](OH)_4+Fe^{2+} \rightarrow K_2(Mg_4,Fe^{2+}Fe^{3+})[(Si_6Al_2O_{20}](OH)_4+Fe^{3+}$. This process, unless accompanied by the loss of interlayer K, results in an imbalance of charge and an increased separation between 2:1 silicate layers. The second step begins when the silicate layers of the mica are separated sufficiently to allow exchange. This excess K content of the interlayer is taken into the groundwater according to $K_2(Mg_4,Fe^{2+}Fe^{3+})[(Si_6Al_2O_{20}](OH)_4 \rightarrow K(Mg_4,Fe^{2+}Fe^{3+})[(Si_6Al_2O_{20}](OH)_4+K^+$ and the content of the remaining interlayer exchangeable ion is altered to reflect the ionic content of groundwater within the vermiculite formation area by: $(Mg_4,Fe^{2+}Fe^{3+})[(Si_6Al_2O_{20}](OH)_4+0.25Ca^{2+}+0.25Mg^{2+}+3H_2O \rightarrow (Ca^{2+}_{0.25},Mg^{2+}_{0.25}.3H_2O)K(Mg_4,Fe^{2+}Fe^{3+})[(Si_6Al_2O_{20}](OH)_4$.

The chemical composition of macroscopic vermiculites, generally, ranges in 37-42% SiO_2, 10-13% Al_2O_3, 5-17% Fe_2O_3, 1-3% FeO, 14-23% MgO, 8-18% H_2O, in addition, up to 5% K_2O may be present. But there may be different compositions other than given compositional ranges. Justo et al. (1986) related chemical composition and geological locations. He suggested that ultramafic zones have higher Ti, Ni, Cr, Zn and lower Mn than that of other locations. Chemical analyses on natural vermiculites show that there is no any relationship between major element content and geological location while there is a relationship between minor element content and geological location (de la Calle and Suquet, 1988).

Although vermiculite material as a common constituent of soils is unquestionably the product of low temperature weathering, there are too

many unanswered questions about the formation of macroscopic vermiculite. The occurrence of vermiculite is attributed to either hydrothermal (e.g., Varley, 1948; Hadley, 1949; Hagner, 1944; Morel, 1955) or supergene (e.g., Gevers, 1948; Kulp and Brobst, 1954; Clabaugh and Barnes, 1959; Justo et al., 1986; de la Calle and Suquet, 1988; Lvova, 1974) origins, or combination of two (Palabora Mining Co. Staff, 1976; Bassett, 1959; Zhelyaskova-Panayotova, 1989; Zhelyaskova-Panayotova et al., 1992, 1993). Therefore some experimental studies at atmospheric and room temperature (Barshad, 1948; Bassett, 1959) and hydrothermal conditions ranging from low temperature metasomatism to the highest ranking metamorphism (Bassett, 1959; Roy and Romo, 1957; Komarneni and Roy, 1981) were applied. According to the experimental studies, vermiculite is alteration product of micas due to the effects of dilute solutions having very low alkali content. Hydrothermal experiments also support the supergene solution effects. Because it was clearly stated that primary vermiculite could not have crystallized nor continue to be stable under even mild hydrothermal conditions (over 200°C at 700 atm). On the other hand, some field evidences suggest the hydrothermal fluids effects such as; association of vermiculite with high temperature minerals and rocks, its presence at depths over 200 ft, the presence of vermiculite in proximity to pegmatites while some other field evidences indicate supergene formation such as; the increase in the proportion of biotite and phlogopite with depth, the presence of unaltered biotite in the interior of pyroxenite.

Occurrence of macroscopic vermiculites were investigated by many authors. The first classification was done on the basis of parent rock type by Bassett (1963). According to him, (a) vermiculite associated with ultramafic and mafic rocks and dispersed among them, low temperature hydrothermal alteration, (b) vermiculite associated with metamorphic rocks, especially gneiss and schist, effects of hydrothermal fluids, (c) vermiculite associated with carbonate rocks, supergene solutions, (d) vermiculite associated with granitic rocks, supergene effects. Vorovikov (1973) did a more detailed classification on the basis of Bassett's (1963) classification. Group I:

vermiculites in ultramafic and alkaline rocks including subgroup 1 (phlogopite and vermiculite in Fe-free ultramafic and alkaline rock complexes), subgroup 2 (biotite and hydrobiotite (vermiculite) in the ferruginous ultramafic rocks), subgroup 3 (biotite and hydrobiotite (vermiculite) in serpentinites); Group II: vermiculite in altered carbonate rock complexes including subgroup 1 (phlogopite and vermiculite in diopsidic rocks, at the contacts between carbonates and aluminosilicate), subgroup 2 (phlogopite and vermiculite occurrences in diopsidic rocks, at the contacts between carbonates and the basic rocks), subgroup 3 (vermiculite occurrences in calciphyres, that is recrystallized dolomites altered to macrocrystalline calciphyres by the action of post-magmatic acid solution); Group III: vermiculite in reaction zones of pegmatites, talc, corundum, asbestos, and also in metasomatic veins in serpentinites; Group IV: vermiculite in micaceous gneisses and other metamorphic rocks.

Lvova (1974) classified the vermiculite deposits on the basis of the associated rocks and the geodynamic conditions of their formation on the basis of previous classifications. In this classification, he used characteristic features of the parent mica (structure, Fe common (f_{com}=($2Fe_2O_3$+FeO)x ($2Fe_2O_3$+FeO+MgO)$^{-1}$x100), F quantity, etc.) which depend on the host rock considering them as main controlling factor of the vermiculite occurrences. Lvova (1974) proposed four groups and nine types of vermiculite deposits. Among them, the most important types are Group A (Type 1 and 2) and Group B (Type 3 and 4). Group A, Type 1 and 2: In this group, the vermiculite - phlogopite associated with alkaline-ultrabasic and carbonatite complexes occurrences. Group B, Type 3 and 4: Type 3 is associated with tectonites which are highly or completely serpentinized and includes vermiculite-hydrophlogopite transformed from parent mica high-Mg phlogopite. Type 4 is associated with the magmatic (cumulate) sequence of ophiolite complexes (peridotites, pyroxenites and gabbros). Group C, Type 5 include very small vermiculite occurrences associated with magnesian skarns. Group D, Type 9 include hydrobiotite mineralizations in biotite gneisses and schists. Among them, Groups A and B are divided mainly based on f_{com} value of phlogopite.

Bush (1976) prepared another classification; Type 1 (hydrothermal) is formed within large ultramafic intrusive masses (pyroxenite plutons, cut by syenite or alkalic granite or carbonatitic rocks and pegmatites); Type 2 (hydrothermal) is associated with ultramafic intrusive bodies (dunite and unzoned pyroxenite and peridotite, cut by pegmatite and syenitic or granitic intrusives), Type 3 (weathering) is derived from ultramafic metamorphic rocks such as amphibole schist in contact with pyroxenite or peridotite and cut by pegmatite.

CHAPTER 2

GEOLOGY OF THE STUDY AREA

2.1. General

The assemblage of magmatic and metamorphic rocks, cropping out in Central Anatolia, is called Central Anatolian Crystalline Complex (CACC) (Göncüoğlu et al., 1991, 1992, 1993a) (Figure 2). The rock groups of ophiolites are called as Central Anatolian Ophiolites (CAO), of granitoids as Central Anatolian Granitoids (CAG) and of metamorphics as Central Anatolian Metamorphics (CAM) (Göncüoğlu et al., 1991, 1992, 1993a, 1998; Göncüoğlu and Türeli, 1993, Yalınız et al., 1996). According to the authors, the metamorphics present in the CACC are overthrusted by ophiolitic units, and later both units are cut by granitoids (Figure 3).

The layered metagabbro with phlogopite and vermiculite studied in this thesis from Kurançalı-Kırşehir area, belong to the ophiolites of Central Anatolian Crystalline Complex (CACC) (Göncüoğlu et al., 1992; Yalınız, 1996; Yalınız and Göncüoğlu, 1998) (Figure 4). In the study area only the uppermost part of the CAM (Metamorphic Ophiolitic Complex) and the tectonically overlying the CAO (Kurançalı Metagabbro) are cropping out. Both units are cut by the Kurançalı Granitoid that belongs to CAG.

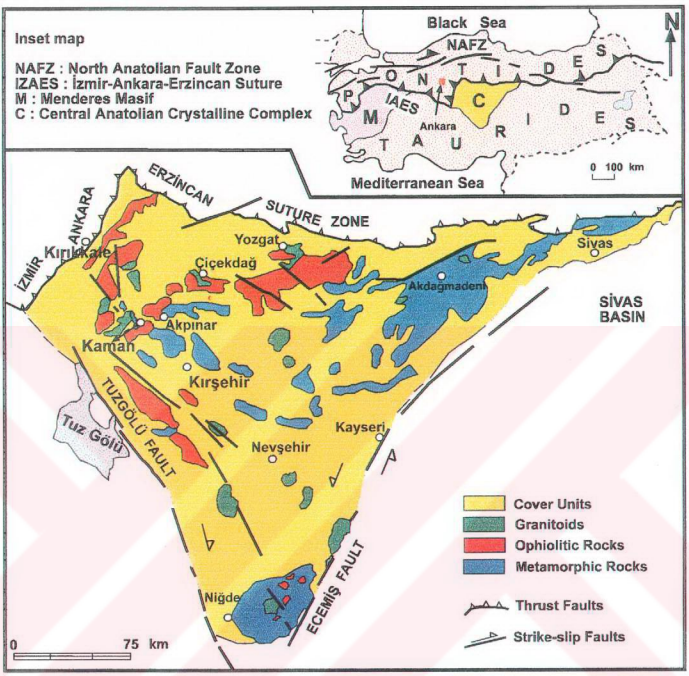

Figure 2. Simplified map of the Central Anatolian Crystalline Complex showing geological setting and main lithological units (After Yalınız and Göncüoğlu, 1998).

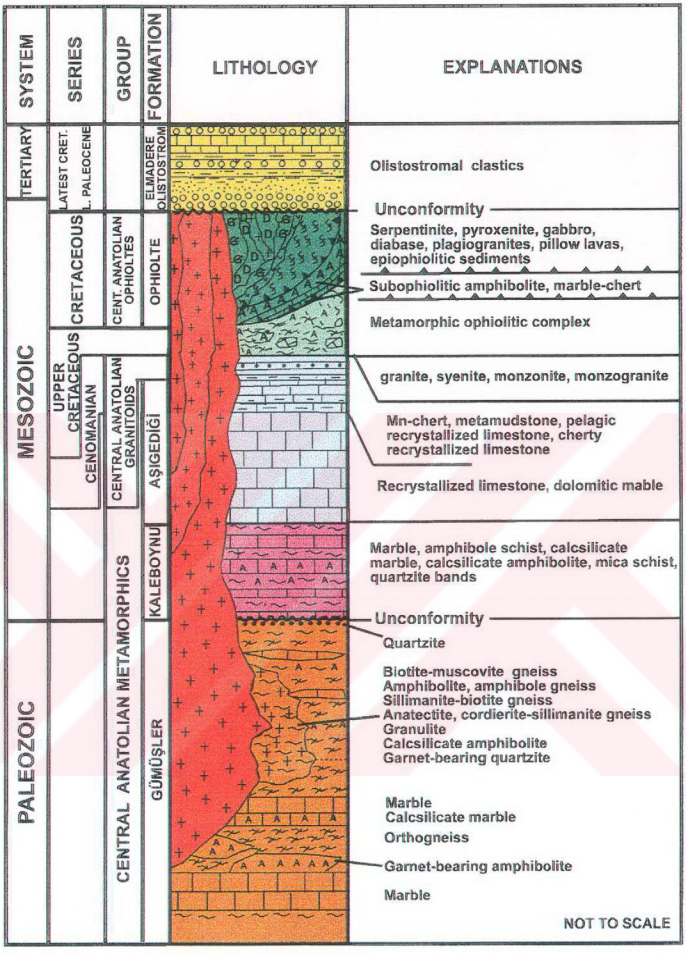

Figure 3. Generalized columnar section of the Central Anatolian Crystalline Complex (Modified from Göncüoğlu et al., 1991).

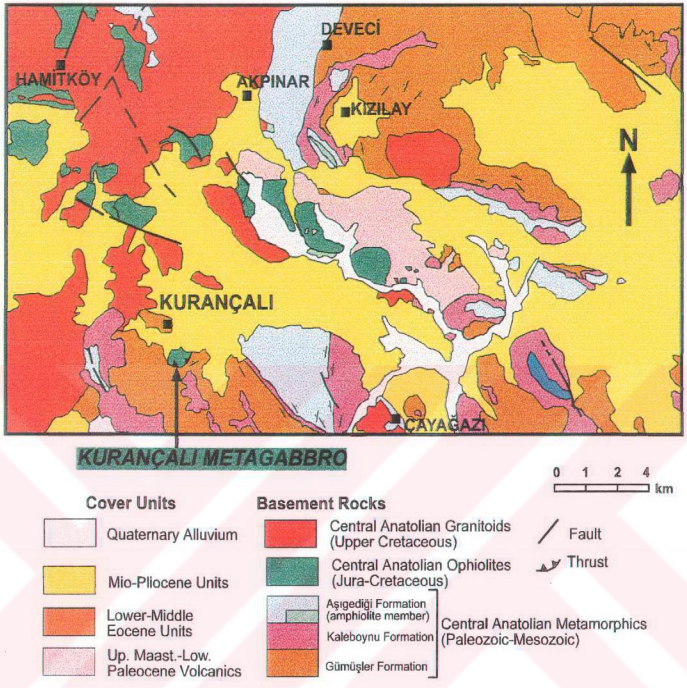

Figure 4. Geological map of the Kurançalı and surrounding region to illustrate the main lithological units (After Göncüoğlu et al.,1992).

2.2. Central Anatolian Metamorphics

Central Anatolian Metamorphics (CAM) mainly exposed in central and along western and eastern-northeastern parts of the of Central Anatolian Crystalline Complex (CACC) (Göncüoğlu et al., 1991, 1992, 1993a, 1998) (Figure 2). The metamorphics which were assumed to be resulted from multiphase deformation and metamorphism were grouped into three from bottom to top (Göncüoğlu, 1977, 1981, 1986; Göncüoğlu et al., 1991, 1992, 1993a, 1998) (Figure 3): (1) Gümüşler Formation is composed mainly of well-foliated gneisses with marble interlayers and amphibolite bands. The assumed protoliths are clastics for paragneisses, felsic intrusives or extrusives for orthogneisses, basic magmatic rocks for amphibolites, carbonate rocks for marble. (2) Kaleboynu Formation contains mainly pure marble interbedding with calcsilicate marble, calcsilicate, mica-schist, gneiss, bands of amphibolite and calcsilicate amphibolites. The protoliths of the formation are alternating carbonates and clastics, basic magmatic rocks. (3) Aşıgediği Formation consists mainly of massive marble with cherty-marble and amphibolite alternations. The protolith is mainly carbonates.

At the uppermost part of the Aşıgediği Formation, the complex of metaophiolitic rocks and the units developed during the emplacement onto the CAM appear (Göncüoğlu et al., 1991, 1992, 1998). The complex consisting of schist, gneiss and amphibolite were named as Metamorphic Ophiolitic Complex by Göncüoğlu et al. (1998). The complex which is typical of sedimentary complex with blocks of ophiolite and marble were affected by the same deformation and metamorphism with the CAM. The rocks of the complex found as tectonic slices over CAM may show foliation similar to that at lower parts of the Gümüşler Formation. The complex is mainly composed of blocks of alternating pink colored marble and garnet-bearing amphibolite. In addition, metaserpentinite, metagabbro, amphibolite and marble blocks within hornblende-biotite gneissic matrix are also present in the complex. The age of the Metamorphic Ophiolitic Complex is given as post-Cenomanian - Turonian to pre Upper Campanian by Göncüoğlu et al. (1998).

2.2.1. Metamorphic Ophiolitic Complex in Kurançalı Area

The ophiolite bearing metamorphic rocks covering 3.5-4 km^2 of the study area, are part of the Metamorphic Ophiolitic Complex (Figures 5, 6).

The Metamorphic Ophiolitic Complex in the study area is dominated by alternations of regular calcsilicate, calcsilicate amphibolite, calcsilicate cherty-marble and calcsilicate biotite-gneisses, biotite-gneiss bands including amphibolite and metaserpentinite lenses. The amount of calcsilicate becomes lesser while the biotite gneiss increases away from the contact with the overlying sheared sliver to contact with the underlying Aşıgediği Metamorphics (outside of the study area).

The amphibolites show banding of white colored plagioclases and dark green colored amphiboles with foliation. The calcsilicate rocks differ in character in accordance to their constituents. They vary from light to dark in color and are highly foliated.

Metaserpentinities, which are mostly green in color and have massive texture with some foliation, are highly fragmented and distributed in the tectonic slice of the Metamorphic Ophiolitic Complex as well as in the Sheared Zone.

The protoliths of the metamorphic ophiolitic rocks are considered to be clastics, carbonate, felsic and basic igneous as described by Göncüoğlu et al. (1991, 1992, 1998).

The metamorphic ophiolitic rocks in the Kurançalı area are thrusted onto massive marbles of the Aşıgediği Metamorphics of the CAM at the outside of the study area at a steep angle (80-85°) from N to S. That is to say, there is a tectonic slice of metamorphic ophiolitic complex together with a sheared zone between the Kurançalı Metagabbro and the Aşıgediği Metamorphics. However, the studied units were assumed to be emplaced on Gümüşler

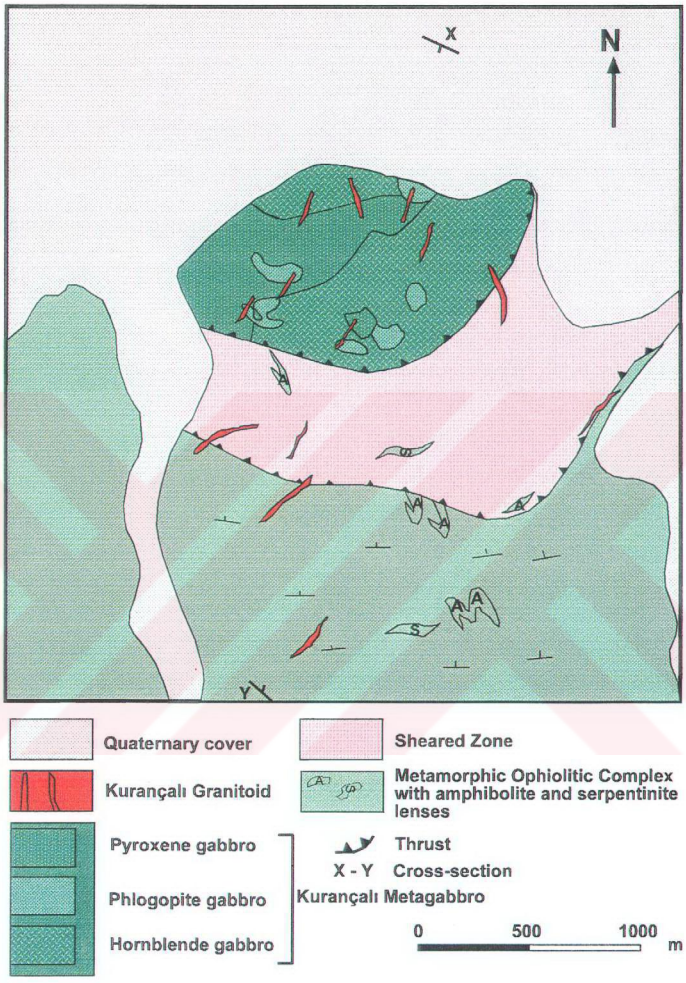

Figure 5. Geological map of the Kurançalı area.

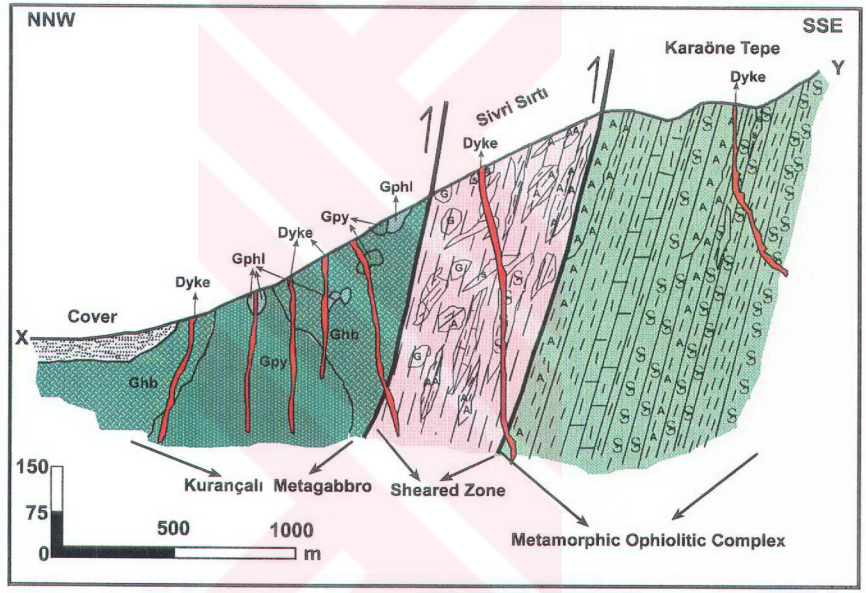

Figure 6. Cross-section of the study area showing the main rock types and their relationships (Gpy: pyroxene gabbro; Gphl: phlogopite gabbro; Ghb: hornblende gabbro).

Metamorphics by Göncüoğlu et al. (1992) considering that the amphibolites of metamorphic ophiolitic complex are of the Gümüşler Formation (Figure 4). The interpretation given by Göncüoğlu et al. (1998) explains that at the uppermost part of the Aşıgediği Metamorphics, the units of the metamorphic ophiolitic complex showing vertical transition from cherty marbles are present in Central Anatolia. According to them, clastic originated hornblende-biotite gneiss, calcsilicate gneiss, and calciturbiditic originated calcsilicate marble, amphibolite-bearing marble, and bands of amphibolite, chert are observed together with metaserpentinite and gabbro. Their investigation is conformable with the suggestion given in this study.

2.3. Central Anatolian Ophiolites

All of the ophiolitic rocks emplaced on CAM were named as Central Anatolian Ophiolitic Complex by Göncüoğlu et al. (1991, 1992). Later, Central Anatolian Ophiolites (CAO) was used to define the supra-subduction zone type oceanic crust material which is affected low grade metamorphism, and the rocks related to ophiolitic units developed in an ensimatic arc environment at Late Cretaceous (Göncüoğlu and Türeli, 1993; Göncüoğlu et al., 1998; Yalınız et al., 1996; Yalınız and Göncüoğlu, 1998). The ophiolites in CACC comprise ultramafics, both isotropic and layered gabbro, trondhjemite/plagiogranite, diabase dyke complex, basaltic pillow lavas, pelagic sediments and epiophiolitic cover units. The relationships of the units of the ophiolites are not obvious. Among them, the Sarıkaraman Ophiolite of the CAO was described to have dismembered pseudostratigraphy by Yalınız (1996), Yalınız et al. (1996) and Yalınız and Göncüoğlu (1998).

The ultramafic (peridotite) of the ophiolites which are found generally at contacts of the CAO and the CAM are completely serpentinized. These serpentinized rocks, in general, alternate with bands of cumulate gabbros although they tectonically overly the gabbros at some locations. The gabbros, having variable sizes ranging from fine grained to pegmatitic as well as their variable compositions (leuco to melano), are extensively exposed units of the

CAO. At two locations, Kurançalı and Koçkar, the gabbros showing layering are characterized by dark mica. The irregular diabase dykes of the ophiolites cut the gabbros. In addition, plagiogranites those are characterized by the absence of K-feldspar and cutting only the gabbros, are usually found between amphibolitized gabbros and diabase dyke complex.

2.3.1. Central Anatolian Ophiolites in Kurançalı Area

The ophiolite bearing units of the Kurançalı area (Kırşehir) at SW of Akpınar, exposed at an area of about 8-9 km^2, were thrusted along a steep contact onto massif marbles of the Aşıgediği Formation of the CAM which is outside of the study area. The ophiolite bearing units are divided into three different lithological tectonic slices in the study area; a 800-1000 m thick basal sliver dominated by calcsilicates and biotite-gneisses with amphibolite and metaserpentinite lenses; an intermediate 500-600 m thick, sheared slice composed of blocks and lenses of metagabbro, calcsilicate cherty-marble, calcsilicate amphibolite, amphibolite, metaserpentinites, biotite-gneiss; an upper slice composed of 250-300 m of either isotropic or layered metagabbro (Figures 5, 6). In this study, the first slice is attributed to the metamorphic ophiolitic complex while the third slice is called as the Kurançalı Metagabbro. They are separated by a sheared zone containing boudens of both the metamorphic ophiolitic complex and the Kurançalı Metagabbro.

2.3.1.1. Kurançalı Metagabbro

The metagabbro, having phlogopite and vermiculite studied in this thesis, from Kurançalı-Kırşehir area was investigated to be a part of the CAO (Göncüoğlu et al., 1992; Yalınız, 1996; Yalınız and Göncüoğlu, 1998) (Figure 4). The gabbroic rocks are called as Kurançalı Metagabbro due to its exposure close to the Kurançalı Town of Kırşehir. The gabbros, which are tectonically emplaced on the metamorphic ophiolitic complex, outcrop at an area of 1 km^2 (Figures 5, 7). The Kurançalı Metagabbro is characterized by

the presence of phlogopitic biotite as well as major pyroxene and hornblende mineral phases. The metagabbro is heterogeneous either in composition or in size (from microscopic to pegmatitic) and show modally-graded rhythmic layering (Figure 8).

Figure 7. Gabbro exposures along lower part of the Sivri Sırtı viewed from NE of the Karaöne Hill.

The Kurançalı Metagabbro, in general, consisting mainly of green-prismatic pyroxenes, is dark green to black in color except for plagioclase-rich leucocratic parts. Hornblende, phlogopitic biotite and plagioclase are major minerals of the rock after pyroxene. On the basis of modal compositions of the mafic minerals, three major metagabbro types are identified in the field for mapping; pyroxene gabbro, hornblende gabbro, phlogopite gabbro (Figures 5, 6). Moreover, the metagabbro could be differentiated in more detail on the basis of modes, into phlogopite gabbro, pyroxene-phlogopite gabbro, pyroxene gabbro (at some locations it is pyroxenite), pyroxene-hornblende gabbro, pyroxene-plagioclase gabbro, hornblende gabbro, hornblende-plagioclase gabbro, plagioclase-hornblende pegmatitic gabbro, hornblende pegmatitic gabbro which are not mappable (Toksoy and Göncüoğlu, 1998).

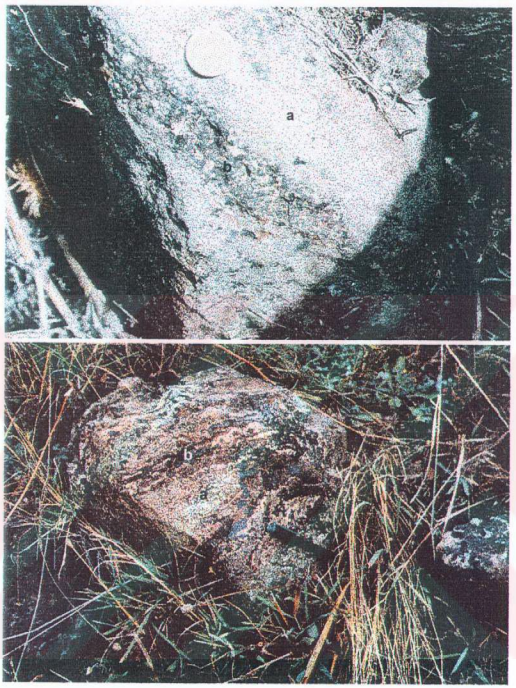

Figure 8. Thin pyroxene-plagioclase rhythmic layering together with pegmatitic hornblende-plagioclase layers (a: layers of fine-grained pyroxene-plagioclase, b: pegmatitic hornblende-plagioclase layers).

Even with closely spaced samples, mineralogically defined boundaries are difficult to draw precisely. The metagabbro with its characteristic layering is not well exposed except for at few locations (Figure 9). Exposures of the gabbro are highly dissected and deformed. The contact relationships of the types of the gabbro, therefore, could not be traced accurately. The small outcrops of the layered metagabbro showing compositional and size variation are distributed into the study area among the outcrops seem to be isotropic. But isotropic outcrops may also be parts of the thick layering. Since the contact of the outcrops are so poorly exposed this matter could not be understood. That is to say, compositional and petrographical variations are too irregular.

Figure 9. Gabbro outcrops from the best-exposed part in the study area.

Pyroxene gabbro is found as either massif or layered (Figure 10). The pyroxene gabbro is variable in size from coarse to fine. The coarse grained types are most readily distinguished in the field by the absence of cumulate layering and by almost absence of plagioclase from fine to medium grained type having cumulate layering and plagioclase. Layered type of the pyroxene

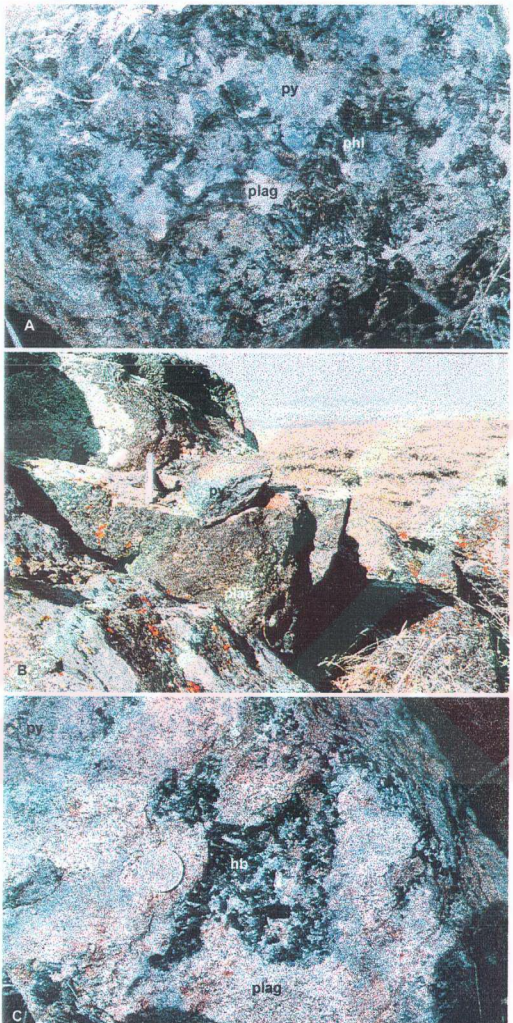

Figure 10. Pyroxene gabbros: (A) pegmatitic containing phlogopite, (B) medium grained with some thin layers of plagioclase, (C) fine-grained, layered, including irregular shaped pegmatitic hornblende enclave (py: pyroxene, phl: phlogopite, hb: hornblende, plag: plagioclase).

gabbro mainly shows rhythmic alternations of pyroxene and plagioclase. In addition to the compositional layering, layering of different size of the major minerals is dominant. The isotropic parts of the pyroxene gabbro also have phlogopite flakes ranging in size from few mm to 1-2 cm and hornblende. Phlogopite bearing pyroxene gabbro is generally found close to the phlogopite gabbro with increasing phlogopite amount. The presence of primary hornblende in pyroxene gabbro is not abundant although it is dominant within fine grained pyroxene gabbro either as pegmatitic enclaves or irregular layers at some locations (Figures 8, 10, 11). Most commonly pyroxenes are uralitized and micatized which are distinguishable in coarse-grained hand specimens.

Hornblende gabbro is observed either in massif or layered form in variable sizes like pyroxene gabbro (Figures 12). Hornblende gabbro is mainly composed of blackish amphibole with lesser amounts of plagioclase although at some places, hornblende-gabbro, which is commonly associated with coarse, acicular pegmatitic amphiboles (up to 20 cm in size), has plagioclase dominated leucocratic parts usually characterized by well defined irregular to angular margins (Figures 11, 13). The fine-grained types are generally massive. The amphiboles typically occur as black, long prismatic, euhedral prisms (from few mm to 15-20 cm long). Hornblende gabbro may have anhedral pyroxene crystals at areas close to the pyroxene gabbro while it does not have any pyroxene in leucocratic type which generally increases in amount as far as away from phlogopite and pyroxene gabbros. That is to say, where the pyroxene and phlogopite is rich, plagioclase amount of the hornblende gabbro is less.

The irregular isotropic masses of phlogopite gabbro consisting mainly of phlogopite with lesser amount of pyroxene (Figures 10, 14). Phlogopite crystals are brittle, dark brown and black in color and have sizes varying up to 2-2.5 cm. Almost no plagioclase is present in phlogopite gabbro. In addition, the presence of hornblende is also less and it is only found close to the hornblende gabbro. Most of the phlogopite gabbro outcrops are found as

fresh but occasionally some of them are started to altered to gold-yellow colored vermiculite.

Figure 11. Pegmatitic hornblende-plagioclase gabbro with fine-grained pyroxene. The constituent minerals form monomineralic aggregates (py: pyroxene, hb: hornblende, plag: plagioclase).

Although it is not certain, it can be suggested that pegmatitic hornblende gabbro intrude the pyroxene gabbro. Because the pegmatitic hornblende gabbro either layered or irregularly is distributed within the layered finer grained pyroxene gabbro (Figures 8, 10c, 11).

One of the characteristic feature of the Kurançalı Metagabbro is the "absence" of the plagiogranites of the CAO which cut the other gabbro exposures from Sarıkaraman Ophiolite (Yalınız, 1996; Yalınız et al., 1996; Yalınız and Göncüoğlu, 1998), from Ekecikdağ region (Göncüoğlu and Türeli, 1993), from Kerkenezdağ region (Göncüoğlu et al., 1998). However, Yalınız (1996) indicated that plagiogranites cut the metagabbro around Kurançalı.

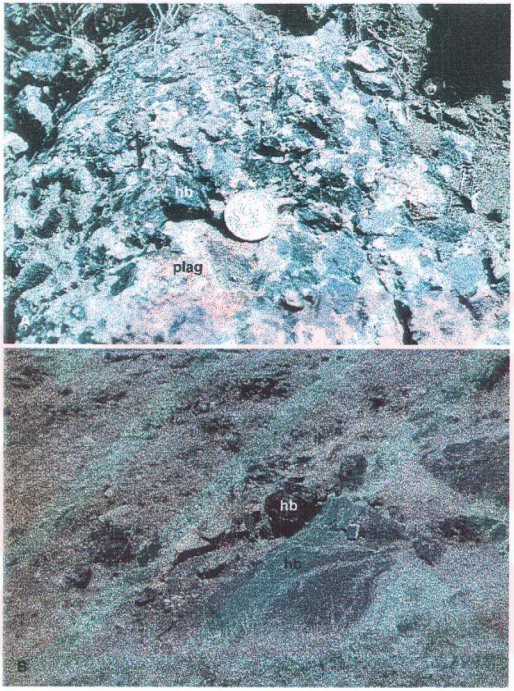

Figure 12. (A) Pegmatitic hornblende gabbro rich in plagioclase, (B) Fine-grained hornblende gabbro poor in plagioclase (hb: hornblende, plag: plagioclase).

Figure 13. (A) Pegmatitic hornblende gabbro rich in leucocratic plagioclase parts, (B) Close up view of the (A) where long prismatic hornblende crystals are disseminated in leucocratic parts.

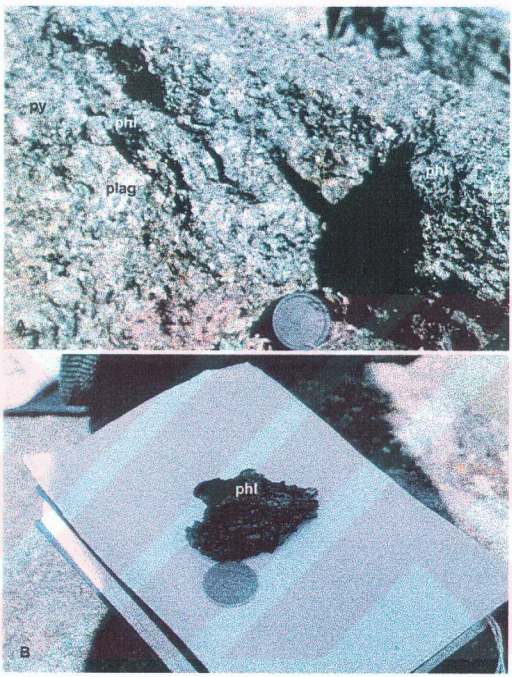

Figure 14. Phlogopite gabbro containing small amount of pyroxene and plagioclase (A) outcrop of phlogopite gabbro, (B) hand specimen of phlogopite gabbro (phl: phlogopite, py: pyroxene, plag: plagioclase).

The Kurançalı Metagabbro tectonically overlies the metamorphic ophiolitic complex in the direction of about N to S, which emplaced onto the Aşıgediği Metamorphics of the CAM at out of the study area. The ophiolite-bearing metamorphics are highly sheared close to the contact with the Kurançalı Metagabbro and have boudens of metaserpentinite and metagabbro. In the study of Göncüoğlu et al. (1992), however, only the metagabbro of the CAO was investigated to thrust on the Gümüşler Formation of CAM without any metamorphic ophiolitic complex.

2.4. Sheared Zone

The sheared tectonic slice with a thickness of 500-600 m including the blocks of both the metagabbro and the metamorphic ophiolitic complex is found between the underlying 800-1000 m thick ophiolite bearing metamorphic slice and the overlying metagabbro slice (Figures 5, 6). The sheared section outcrops along the upper parts of the Sivri Sırtı.

The sheared slice is composed of blocks and lenses of metagabbro, calcsilicate cherty-marble, cherty-marble, calcsilicate amphibolite, amphibolite, metaserpentinites, calcsilicate interbedding biotite-gneiss, biotite-gneiss. The small blocks of amphibolites and metaserpentinites are abundant within the more regular calcsilicate, cherty-marble calcsilicate, biotite-gneiss bodies of this slice. Besides these, at the lower part of the sheared zone fine grained and massive metagabbro appear and become abundant with similar characteristics of the rocks of upper metagabbro slice. The effects of cataclastic deformation is abundant in this zone. The outcrops are not regular (Figure 15). They are highly fractured and fragmented. They are highly foliated in either micro or macro scale (Figure 16).

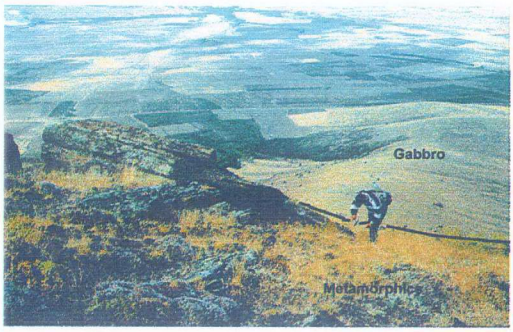

Figure 15. A large calcsilicate, calcsilicate amphibolite block in the sheared zone just at contact with the Kurançalı Metagabbro.

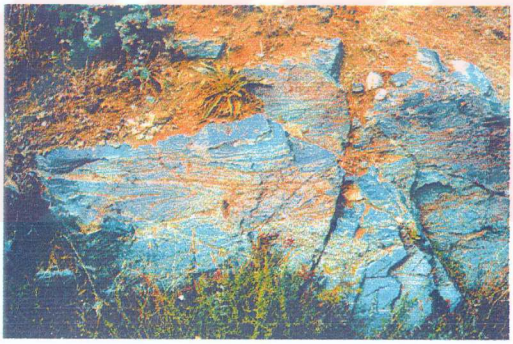

Figure 16. Well-foliated calcsilicate outcrop from the sheared zone.

2.5. Central Anatolian Granitoids

The granitoids of Upper Cretaceous age, intruding both metamorphics and ophiolites, are described as Central Anatolian Granitoids (CAG) by Göncüoğlu et al. (1991, 1992), Göncüoğlu and Türeli (1993). The granitoids exposing mainly along the northern part of the CACC, are variable in composition which are leucogranite, biotite-hornblende granite, alkali-feldspar megacrystic granite, granodiorite and aplitic alkali-feldspar granite in general (e.g.; Bayhan, 1990; Göncüoğlu et al., 1991, 1992; Erler et al., 1991; Türeli, 1991; Akıman et al., 1993). Among them, leucogranite and biotite-hornblende granite intrudes the mafic rocks. Aplitic type of the granitoids is generally found as dykes.

2.5.1. Kurançalı Granitoid

The Kurançalı Granitoid term used to describe the leucocratic felsic dykes cross-cutting all the Kurançalı Metagabbro, the Sheared Zone and the Metamorphic Ophiolitic Complex in the study area. The intruding dykes are generalized in NW-SE direction with few exceptions. They are strongly deformed and fragmented into irregular discontinuous masses like the metagabbroic rocks in the study area (Figure 17). Dykes exhibit lengths generally less than 20-30 m and thickness ranging between a 10 and 25 cm. Both highly fragmented and non-fragmented dykes exhibit a sharp contact with the host metagabbros and metamorphic ophiolitic complex rocks. They have effects of cataclastic deformation while some have foliation. Foliation and cataclastic deformation is more effective on dykes cutting the Metamorphic Ophiolitic Complex. They vary in size from very fine to fairly medium. The rocks are not homogeneous in composition ranging from granitic to quartz syenitic with changing amounts of biotite, hornblende, K-feldspar, K-Na feldspar, and quartz. Angular to subrounded mafic mineral rich darker colored enclaves are also recognized in few dykes.

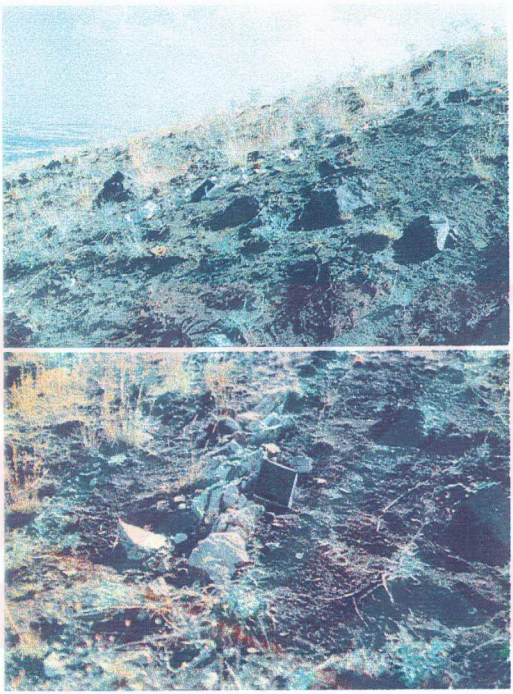

Figure 17. Granitic dykes cutting the Kurançalı Metagabbro.

CHAPTER 3

PETROGRAPHY

3.1. Introduction

In petrographical study, 36 samples from the Kurançalı Metagabbro, 20 samples from the Sheared Zone and the Metamorphic Ophiolitic Complex, and 17 dyke samples from the Kurançalı Granitoid were examined under microscope. The textural characteristics (degree of crystallinity, granularity and fabric) were determined. Modal analyses either by point counting or by visual estimation methods were also done to investigate the modal compositions of the gabbro and dyke samples.

3.2. Kurançalı Metagabbro

The Kurançalı Metagabbro macroscopically ranges in size from very fine grained to pegmatitic. It is essentially composed of pyroxene, phlogopitic biotite, hornblende, plagioclase in varying amounts. These phases are extremely distributed through the metagabbro. The holocrystalline rock samples also have secondary hornblende (uralite), actinolitic hornblende, secondary biotite, vermiculite, albite, calcite, sericite and rarely epidote. The accessory minerals of the metagabbro are mainly sphene, magnetite and hematite of opaque minerals.

The Kurançalı Metagabbro is characterized by a distinct compositional layering reflected by grain size and mineralogy. It is differentiated into several types based on different modes. Although the Kurançalı Metagabbro was divided into three main types for the field mapping (pyroxene gabbro, hornblende gabbro, phlogopite gabbro) (Figure 5), detailed petrographic investigation revealed the following types: phlogopite gabbro, pyroxene-phlogopite gabbro, pyroxene gabbro (pyroxenite), pyroxene-hornblende gabbro, pyroxene-plagioclase gabbro, hornblende gabbro, hornblende-plagioclase gabbro, plagioclase-hornblende pegmatitic gabbro, hornblende-plagioclase pegmatitic gabbro. The sample location map given in Figure 18 shows that most of the samples are closely spaced (therefore the samples numerated without prefix FT although they are numerated starting from FT-1). It is difficult and meaningless to interpret the modes of gabbro samples under microscope by point counting method due to varying degree of alteration, composional layering of the almost monomineralic phases with varying thickness (centimetric to decimetric), layering of the different grain sizes, presence of very coarse crystals up to pegmatitic size. Therefore, modes of gabbro samples were examined by visual estimation method and controlling the properties of the hand specimens. That is to say, thin sections may not be useful and representative for point counting method.

In general, although altered in varying degree, the metagabbros exhibit well-preserved igneous textures, straining and cataclasis. They are characterized by cumulus texture that is well observed in pyroxene gabbro with fresh pyroxene crystals. Cataclastic and mylonitic textures, recognized by crystal bending (especially in micas), granulation and brecciation commonly at grain boundaries, are identified in zones close to thrust surface onto the metamorphic ophiolitic complex (Figure 19). They have predominately coarse grained, equigranular and secondary recrystallization texture.

The essential and the most abundant mineral of the metagabbro is a clinopyroxene with a composition of diopsidic augite. Short prismatic crystals of diopsidic augite are colorless to pale green - pale grayish green in color. It

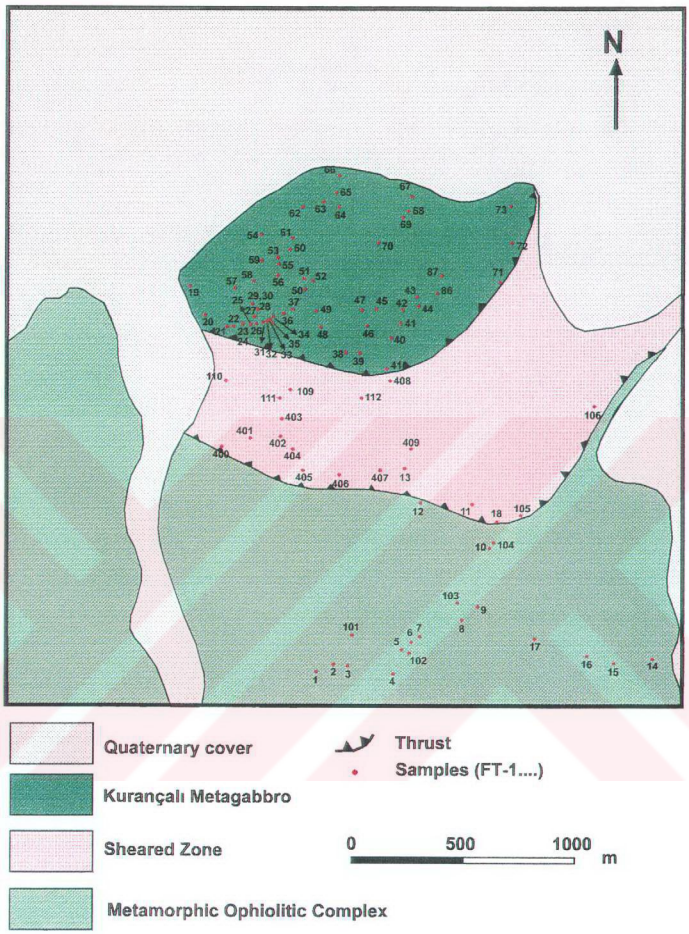

Figure 18. Sample location map.

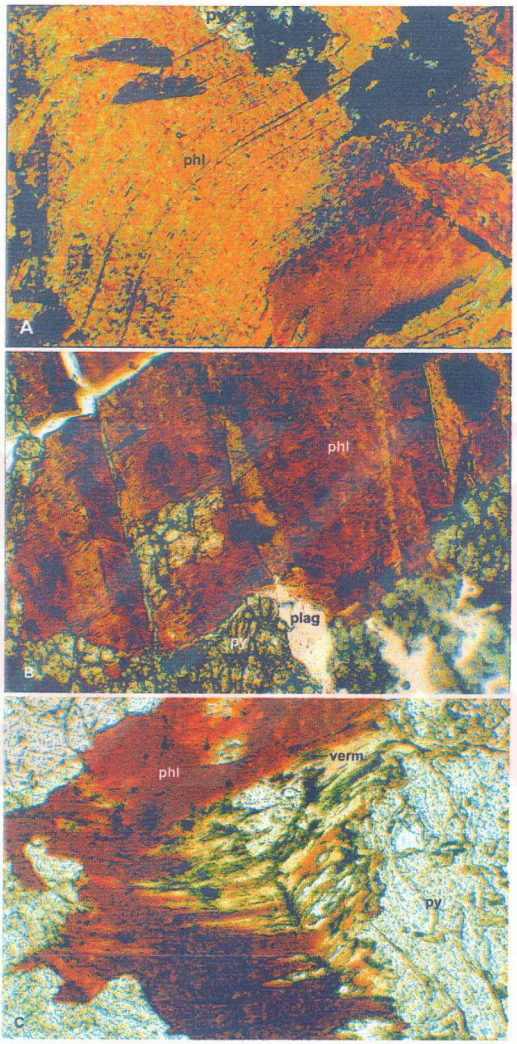

Figure 19. Photomicrographs of bent micas. A: (XPL, x10), B: (PPL, x10), C: (PPL, x10) (phl: phlogopite, py: pyroxene, plag: plagioclase, verm: vermiculite).

has an extinction angle of 40°-45° and interference colors of middle to upper second order. Diopsidic augites are present nearly in all samples except for hornblende-plagioclase and hornblende gabbro samples. Coarse-grained clinopyroxene encloses plagioclase with poikilitical texture or forms patches interstitial to this mineral (Figure 20).

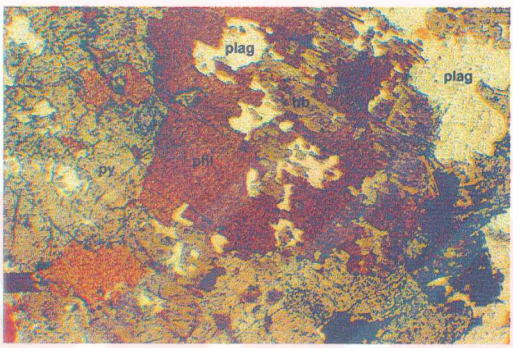

Figure 20. Photomicrograph showing poikilitic texture (PPL, x2.5) (phl: phlogopite, py: pyroxene, hb: hornblende, plag: plagioclase).

The clinopyroxenes are found as very fresh, euhedral form to intensely altered, fractured and fragmented anhedral forms due to variable amounts of deformation and alteration (Figure 21). While some are completely fragmented, the others are fragmented only at outer parts with solid central parts. Fresh and clear pyroxenes are generally found in pyroxene gabbro and pyroxene-plagioclase gabbro. In most of the samples, however, clinopyroxenes with cloudy appearance have been replaced by secondary hornblende and biotite (Figures 21b, 22). They are, in most cases, observed as anhedral relicts within secondary minerals. Uralitization is the most common alteration type in these clinopyroxenes probably formed due to

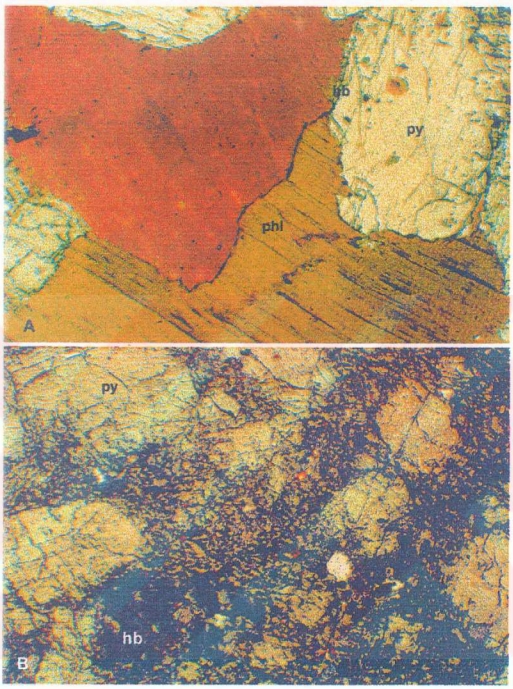

Figure 21. Photomicrographs showing forms of clinopyroxene crystals. A: (PPL, x2.5), B: (PPL, x2.5) (phl: phlogopite, py: pyroxene, hb: hornblende).

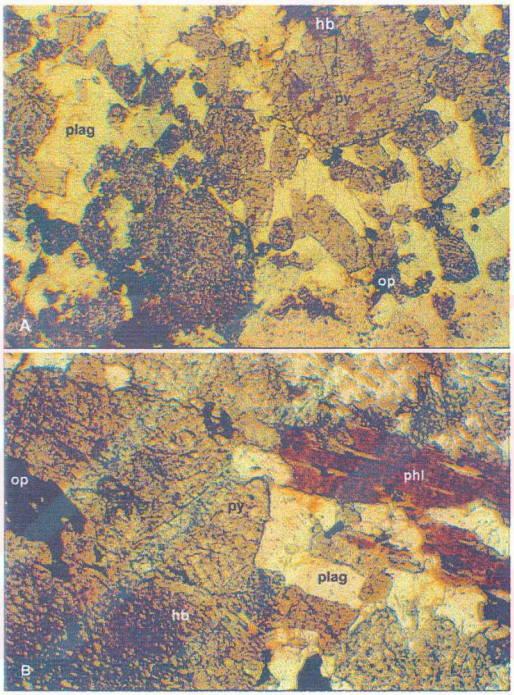

Figure 22. Photomicrographs showing alteration on pyroxene crystals. A: (PPL, x2.5), B: (PPL, x10) (py: pyroxene, plag: plagioclase, phl: phlogopite, hb: hornblende, op: opaque).

effects of hydrothermal solutions during the late stage magmatic crystallization. In some samples, they are almost completely replaced by secondary hornblende while in others they are partially replaced by patchy and needle like hornblendes along cleavage and fracture surfaces and at rims (Figure 23). Green actinolitic hornblende replacement is also recognized along cleavages of clinopyroxene and as patches in few studied samples (Figure 24). Beside transformation of pyroxene to hornblende, secondary biotite from pyroxene and/or hornblende is also observed on fracture and cleavage surfaces probably due to K-rich solutions rising with the intrusion of granitic dykes (Figure 25). This observation was also made by Bayhan (1986) from gabbros which are thrusted onto the metamorphics and intruded by Çelebi Granitoid. He suggested that secondary biotite is due to increasing alteration. Önen (1985), Önen and Unan (1988) observed secondary biotite in gabbros from NE of Kaman. In addition to these alteration products, calcitization and epidotization are also present in very less amount (Figure 26).

Hornblende, one of the major mineral phases, is essentially found as the primary magmatic phase in hornblende gabbro, hornblende-plagioclase gabbro, plagioclase-hornblende gabbro of the Kurançalı Metagabbro either in fine grained or pegmatitic size while the secondary type replacing diopsidic augite is present almost in all of the gabbro types in varying amounts. Primary hornblendes are light yellowish green, green, brownish in color while secondary type has generally brownish green to greenish brown color. Primary hornblendes have usually euhedral long, twinned prisms with faint optical zoning. Epitaxitic growth of the hornblende with pyroxene is also recognized in the samples (Figure 27). The primary hornblendes are generally too coarse to examine under microscope while patches and rims of secondary type are found in variable sizes on clinopyroxene crystals as anhedral grains. Actinolitic hornblende is poorly developed along grain margins of the secondary type of hornblendes where they may have been derived from the latter one (Figure 24). This alteration sequence of pyroxene through uralitization to actinolitic hornblende for metagabbros was also

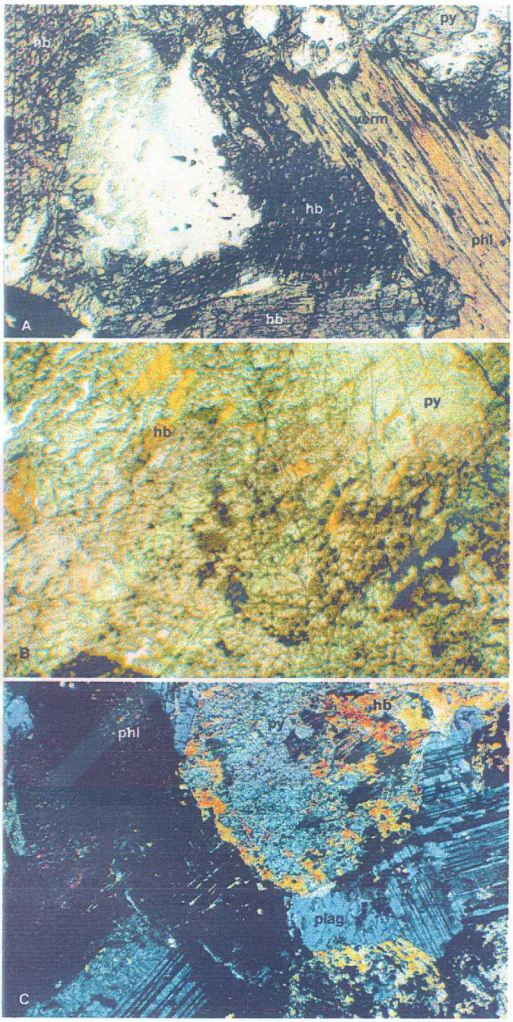

Figure 23. Photomicrographs showing hornblende replacement from pyroxene. A: (PPL, x10), B: (PPL, x2.5), C: (XPL, x2.5) (py: pyroxene, hb: hornblende, phl: phlogopite, plag: plagioclase, verm: vermiculite).

interpreted by Göncüoğlu et al. (1991) from different locations of the Central Anatolia. Uralitization is the most common alteration type observed in gabbros of the CAO (e.g., Bayhan, 1986; Önen, 1985; Önen and Unan, 1988; Kara and Dönmez, 1990; Yalınız, 1996). The common inclusions within hornblende comprise pale green diopsidic augite, reddish brownish secondary biotite as well as opaque minerals.

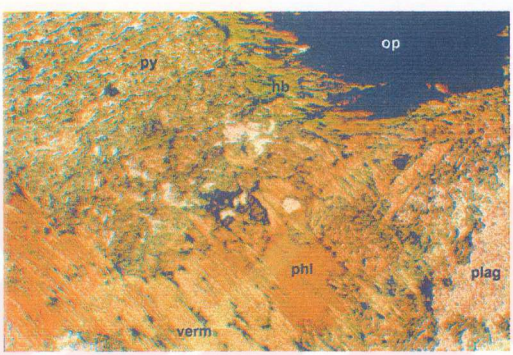

Figure 24. Photomicrograph showing actinolitic hornblende development (PPL, x2.5) (py: pyroxene, hb: hornblende, phl: phlogopite, plag: plagioclase, verm: vermiculite).

In brief, based on textural data, three types of hornblende are present in the studied samples, primary magmatic hornblende, uralite formed during the late stage magmatic crystallization under the effects of hydrothermal solutions, and late stage actinolitic hornblende formed from pyroxene and earlier stage hornblende.

The phlogopitic mica (Mg-rich biotite) is the essential mineral of the phlogopite gabbro although it is also present in variable amounts and size in

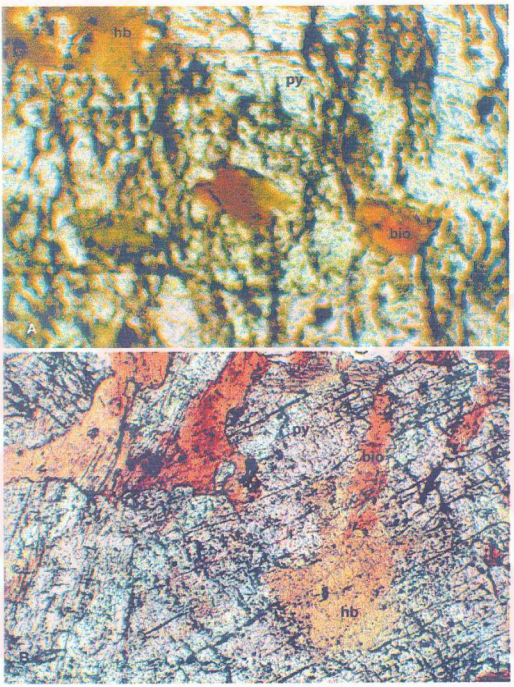

Figure 25. Photomicrographs showing development of secondary hornblende and biotite. A: (PPL, x2.5), B: (PPL, x10) (py: pyroxene, hb: hornblende, bio: secondary biotite).

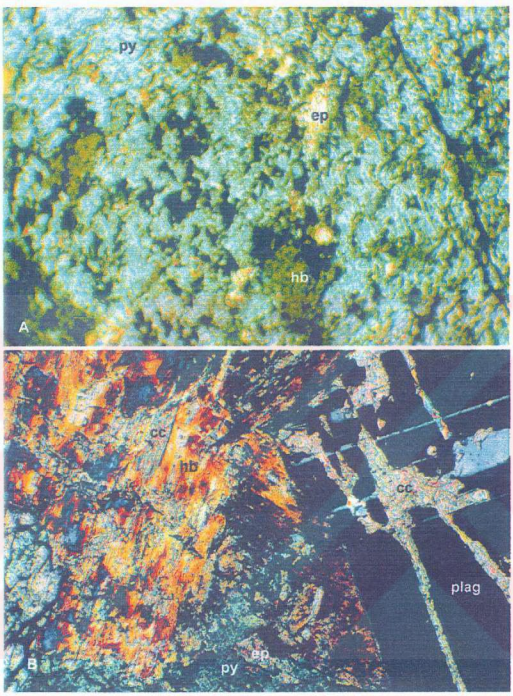

Figure 26. Photomicrographs showing alteration products (calcite, epidote) on constituent mafic minerals. A: (XPL, x10), B: (XPL, x2.5) (py: pyroxene, hb: hornblende, plag: plagioclase, cc: calcite, ep: epidote).

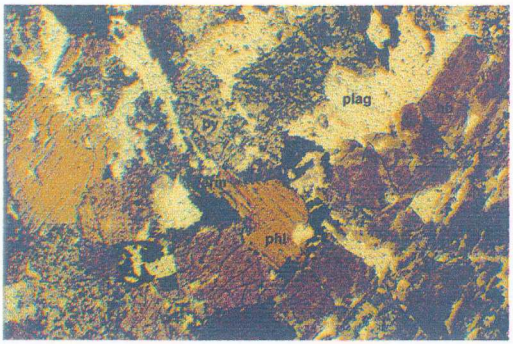

Figure 27. Photomicrograph showing epitaxitic growth of hornblende on pyroxene (PPL, x2.5) (phl: phlogopite, py: pyroxene, hb: hornblende, plag: plagioclase, verm: vermiculite).

other gabbro types. The phlogopitic mica crystals are mainly pegmatitic (2-2.5 cm) in hand specimens. The primary phlogopitic mica, having strong pleochroism with light yellowish brown to reddish brown, purplish to greenish brown, is developed in form of large plates with some degree of ragged terminations (Figure 28). The mineral display lighter coloration near the margins of the some plates. The yellowish reddish brown colored dark mica show bright interference colors of 2nd and 3rd order. Optic axial angle (2V) of the mica is 2°-8°. It is Fe-rich variety of phlogopite with parallel extinction. It occurs usually together with diopsidic augite, magnetite, and sphene (Figures 20, 21a, 28, 29). Small flakes of phlogopite also occur, most of which associated with bigger, phlogopite plates (Figures 19a, 30). Alteration of phlogopite to vermiculite along cleavages and at rims is poorly developed (Figures 19c, 23c, 24, 30b, 31). Unaltered relicts of phlogopite parallel to the cleavage planes are common in altered crystals. These two distinct modes of occurrence, together with the textural features described above indicate that this brown phlogopite is primary. Due to oxidation during the transformation of phlogopite to vermiculite, phlogopite has high relief, numerous tiny iron oxide

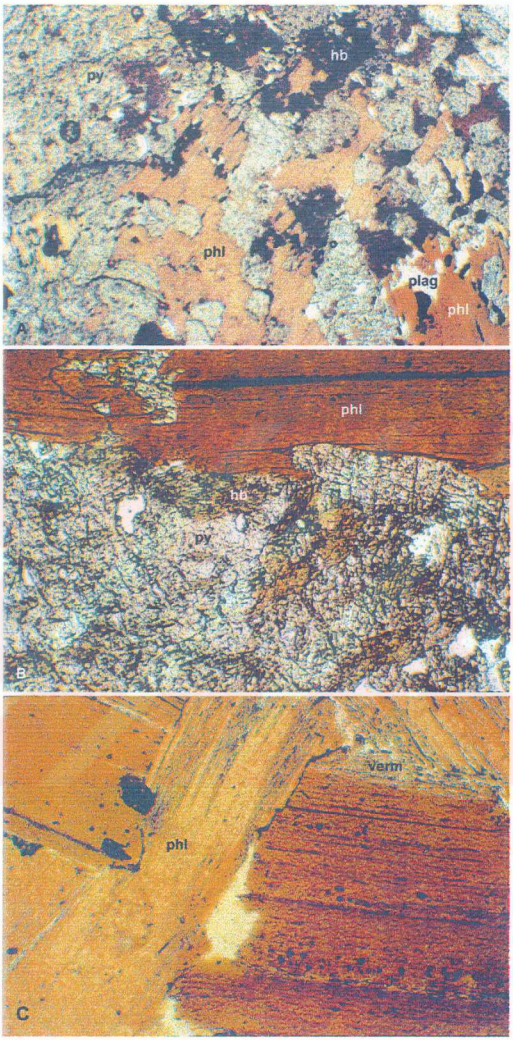

Figure 28. Photomicrographs showing primary phlogopite crystals. A: (PPL, x2.5), B: (PPL, x10), C: (PPL, x2.5) (phl: phlogopite, py: pyroxene, hb: hornblende, plag: plagioclase, verm: vermiculite).

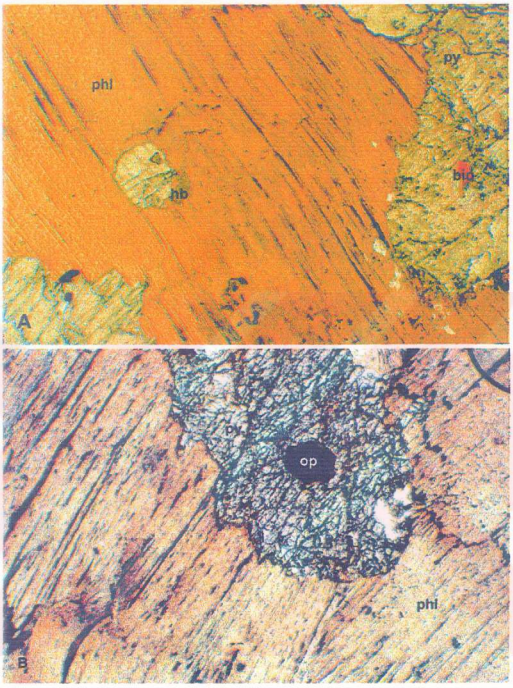

Figure 29. Photomicrographs showing phlogopite crystals together with pyroxene and opaque minerals. A: (PPL, x10), B: (PPL, x10) (phl: phlogopite, py: pyroxene, hb: hornblende, bio: secondary biotite, op: opaque).

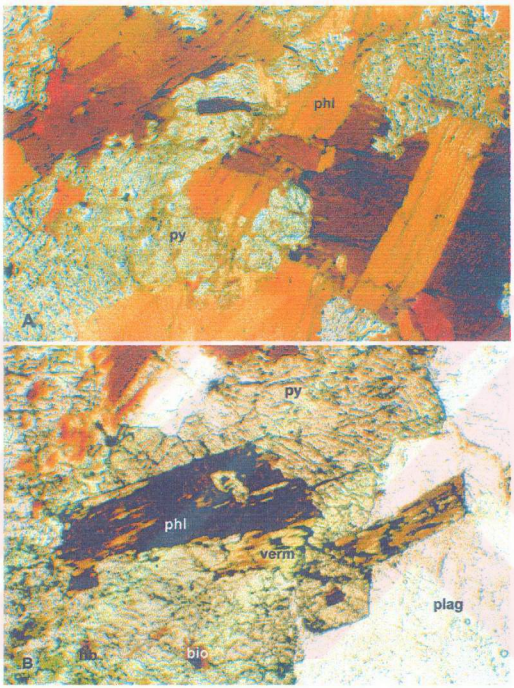

Figure 30. Photomicrographs showing phlogopite crystals in various sizes. A: (PPL, x2.5), B: (PPL, x2.5) (phl: phlogopite, py: pyroxene, plag: plagioclase, hb: hornblende, bio: secondary biotite, verm: vermiculite).

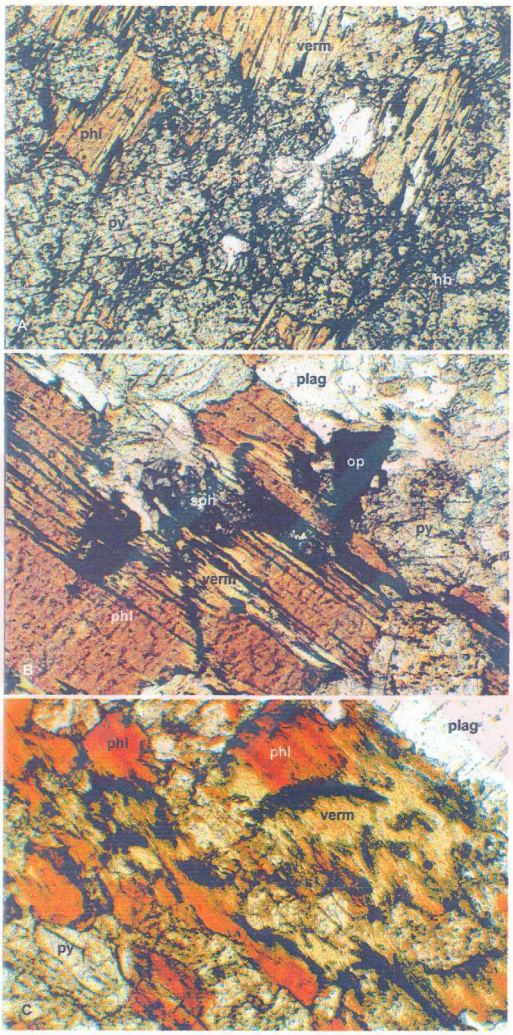

Figure 31. Photomicrographs showing vermiculite replacing phlogopite. A: (PPL, x10), B: (PPL, x10), C: (PPL, x10) (phl: phlogopite, py: pyroxene, plag: plagioclase, hb: hornblende, verm: vermiculite, sph: sphene).

inclusions along fractures and cleavages (Figures 31, 32). Meunier and Velde (1979) and Rowins et al. (1991) indicated that in the earlier stages of weathering, the phlogopites appear little altered to vermiculite but show a strong tendency for iron to migrate to grain edges where it accumulates as amorphous oxides. According to them, the morphological evolution appears to include sheet splitting, destruction structure and crystallization of the secondary phase; all of which seem to manifest at the same time.

Phlogopites are present, commonly in close association with Fe-oxides and sphene (with pleochroism indicating high Ti-content). However, it can not be excluded that some small flakes of the mica are resulted from the replacement from the primary pyroxene and both of the primary and secondary hornblende along cleavages and fractures (Figures 23, 25, 33) due to the rise of the K-rich solutions during the intrusion of granitic dykes. The biotitization of amphibole and pyroxene is also identifiable in coarse-grained pyroxene and hornblende gabbros in hand specimen.

Vermiculite replacing the phlogopite plates shows optical continuity with the parent mineral. It is colorless to pale yellow with very weak pleochroism. It has parallel extinction and very weak interference color.

Plagioclase exists almost in all types of gabbros but it is very less in phlogopite gabbro, pyroxene-phlogopite gabbro with a mode of up to 10%. However, it has 90% mode in plagioclase-rich leucocratic parts of the plagioclase-hornblende and/or hornblende-plagioclase gabbro. The plagioclase in these samples, ranges in composition from labradorite to bytownite (An_{50-70}) which is measured by Michel Levy method. They have euhedral to anhedral forms in subophitic relation to pyroxene and hornblende. They display albite, Carlsbad, pericline twinning as well as zoning (Figure 34). Due to alteration, secondary plagioclase developments with higher albite content at rims are recognized (Figure 35). Sericite and calcite which are alteration products from plagioclases result in cloudy, dirty appearance (Figures 26b, 34, 36). Epidotization is very rarely observed.

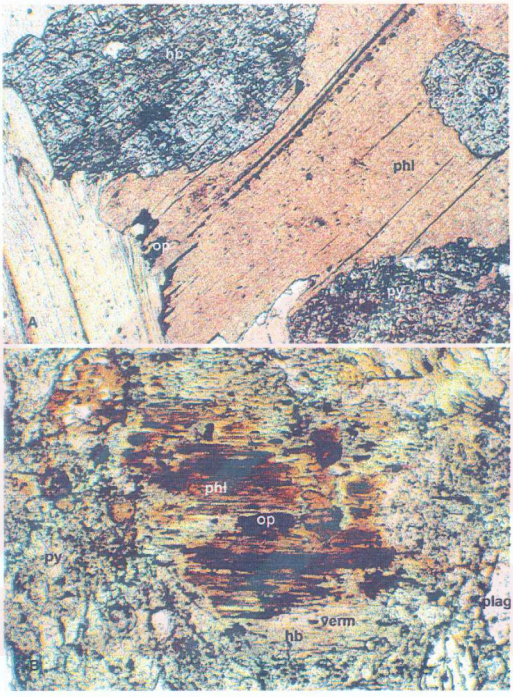

Figure 32. Photomicrographs showing oxide inclusion within phlogopite. A: (PPL, x10), B: (PPL, x10) (phl: phlogopite, py: pyroxene, hb: hornblende, plagioclase:plagioclase, verm: vermiculite, op: opaque).

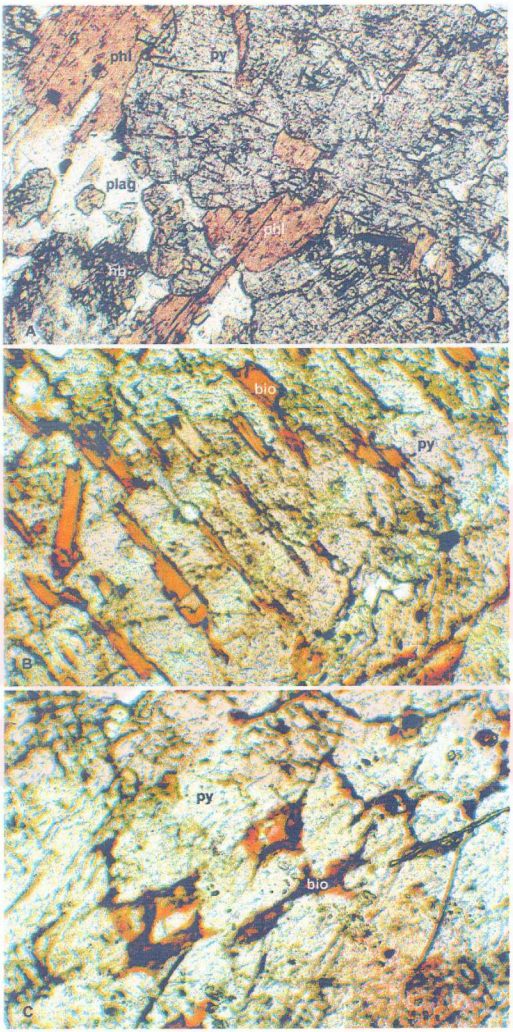

Figure 33. Photomicrographs showing secondary biotite development on mafic minerals. A: (PPL, x10), B: (PPL, x10), C: (PPL, x10) (phl: phlogopite, py: pyroxene, hb: hornblende, plag: plagioclase, bio: secondary biotite).

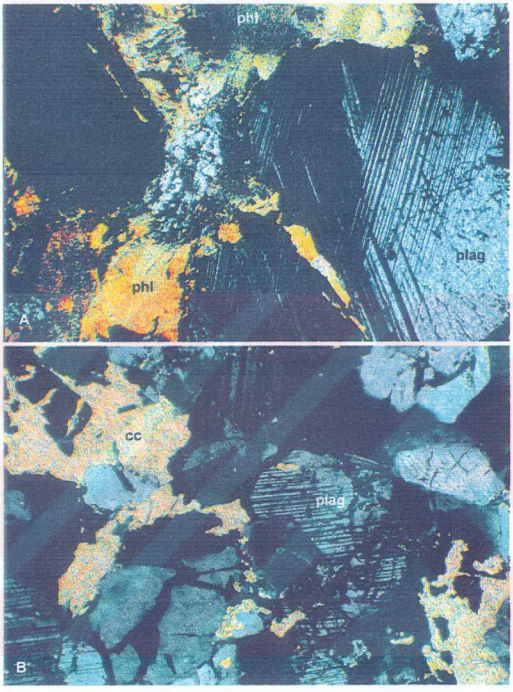

Figure 34. Photomicrographs showing plagioclase crystals. A: (XPL, x2.5), B: (XPL, x10) (phl: phlogopite, plag: plagioclase, cc: calcite).

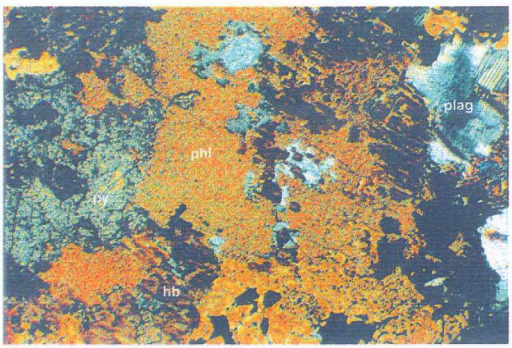

Figure 35. Photomicrograph showing albitized plagioclase (XPL, x2.5) (phl: phlogopite, py: pyroxene, hb: hornblende, plag: plagioclase).

The accessory mineral sphene has subhedral to euhedral form. It is found generally as inclusions in other minerals, especially in close association to pyroxene and phlogopite. It has strong pleochroism that is indication of high Ti-content of the mineral. Opaque minerals (usually magnetite with some hematite) are very common in all samples.

There is neither olivine nor orthopyroxene in the studied samples. The absence of these two minerals is a characteristic feature of the phlogopite-bearing Kurançalı Metagabbro.

The alteration products including albite, epidote, iron-oxide minerals, actinolite may indicate initial ocean floor hydrothermal alteration in spite of their very less amount. Yalınız et al. (1996) also indicated the presence of this type of alteration in gabbros and dolerites of the Sarıkaraman Ophiolite from the CAO. Presence of calcium may indicate the circulation of low temperature fluids as indicated by Yalınız et al. (1996). Tribuzio et al. (1997) also suggested that calcitization is due to infiltration of CO_2-bearing fluids at the latest stage of ocean floor metamorphism.

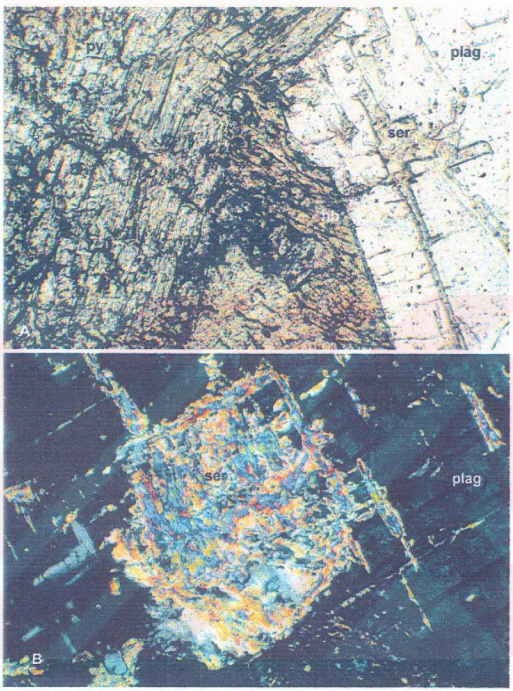

Figure 36. Photomicrograph showing alteration on plagioclase. A: (PPL, x10), B: (XPL, x10) (py: pyroxene, plag: plagioclase, hb: hornblende, ser: sericite).

3.3. Metamorphic Ophiolitic Complex

Four main groups are identified from studied thin sections of 20 metamorphic samples which were collected from the metamorphic ophiolitic complex in the Kurançalı area. The groups are; (A) calcsilicate rocks and interlayers of biotite-gneisses, (B) metacarbonate and calcsilicate metacarbonate rocks, (C) amphibolites and calcsilicate amphibolites, (D) metaserpentinites.

(A) Calcsilicate gneisses and interlayers of biotite-gneisses: Calcsilicate rocks having interlayers of biotite-gneiss are the most abundant rock types in the complex. This group essentially constitutes the mineral assemblage of calcite, diopside, epidote, plagioclase, biotite, quartz, hornblende (±), orthoclase (±), cordierite (±) and muscovite (±). The observed paragenesis are;

biotite-cordierite-quartz-orthoclase±tourmaline±sphene±chlorite

biotite-cordierite -muscovite-quartz-orthoclase

biotite-cordierite-quartz

calcite-epidote-diopside-orthoclase-quartz

diopside-biotite-quartz-epidote

The studied samples showed that as biotite increases calcite, epidote and diopside decrease while cordierite appears. Cordierite is essentially present in the biotite-gneisses of calcsilicate rocks.

Biotite flakes of variable sizes, subidiomorphic to xenomorphic, are deep brown to greenish brown in color. They are partly chloritized. Epidotes are characterized by fine-grained xenomorphs having pleochroism from yellowish green to green. Diopsides are colorless and xenomorphic with fine size. Cordierites are generally found as idiomorphic to subidiomorphic

porphyroblasts. They show well-developed exsolution lamellae and seritization in some samples. Quartz, which is found in all samples, is usually xenomorphic. Quartz occurs either as fractured porphyroblasts or as fine grained mylonitic crystals. They have characteristic undulatory extinction. K-feldspars are usually xenomorphic, and have perthitic texture and kaolinization due to alteration. Plagioclases are xenoblastic with polysynthetic twinning. They are partly seritized. Subidiomorphic calcite crystals are dominant where biotite and muscovite disappear or too less in amount. Muscovite flakes of variable sizes are also present in association with biotites. In addition to these minerals, in some samples, tourmaline, sphene, apatite exist. Opaques are common in these rocks.

All of the studied samples show strong foliation. The samples those are poor in biotite, rich in diopside and epidote, show well oriented small biotite flakes while aggregates of epidote and diopside xenomorphic crystals are common. Biotite crystals in biotite-rich calcsilicate gneisses and biotite-gneisses, display lepidoblastic texture with subidiomorphic to xenomorphic deep brown flakes. Quartz, K-feldspar and plagioclase of this group show inequigranular granoblastic texture with interlobate grain boundaries. In some samples, porphyroblasts and small grains of quartz and feldspars show lenticular-flaser texture indicating to a later cataclastic deformation. Cataclatic effects are abundant in the Sheared Zone.

(B) Calcsilicate metacarbonate rocks and pure metacarbonate interlayers: Carbonate rich calcsilicate rocks are essentially composed of quartz, calcite, diopside, biotite, cordierite in varying amounts with minor amounts of hornblende, plagioclase, accessory minerals of sphene and apatite while pure metacarbonate interlayers has only calcite and quartz.

The samples of this group are well-foliated and show some degree of cataclastic deformation. Lenticular-flaser texture of quartz porphyroblasts in calcsilicate carbonate rocks is the characteristic feature.

Xenomorphic quartz is found either as porphyroblasts or as fine grains with interlobate boundaries. Quartz grains are characterized by their strong undulatory extinction. Some porphyroblasts of this mineral have poikiloblastic character with inclusions of opaque minerals and biotite. It is found less than 10% in pure metacarbonate interlayers while it is more than 30-40% in other impure calcsilicate-marble samples. It is observed in pure metacarbonate rocks as filling material between the calcite crystals.

Calcite, the main mineral phase of pure carbonate interlayers within calcsilicate carbonate rocks with an amount of more than 85%, is found in varying amounts. In general, subidiomorphic calcite crystals have polygonal boundaries. They have well-developed cleavage and gliding lamellae.

Subidiomorphic to xenomorphic biotite crystals which is not present in pure metacarbonate interlayers, exist in varying amounts in calcsilicate carbonate rocks. Where calcite is present in high amount, biotite flakes are less and show mineral orientation rather than lepidoblastic texture. However, biotite flakes show lepidoblastic texture in biotite-rich calcite-poor samples. They are brown in color with pleochroism.

Xenomorphic diopside is present as fine grains and found either in calcite-rich biotite-poor or in calcite-poor biotite-rich calcsilicate carbonate rocks. They are colorless to pale green in color. They are replaced by amphiboles at rims.

Hornblendes, which are the main constituents of the amphibolites, are usually found in lesser amounts in calcsilicates carbonate rocks. They are subidiomorphic to idiomorphic and show are greenish brown to brown pleochroic colors.

Cordierite porphyroblasts are generally found in paragenesis with biotite in biotite-bearing rocks. They have xenomorphic grains showing well-developed exsolution lamellae.

In biotite-rich samples, xenomorphic muscovites are also present.

Xenomorphic plagioclases are fine to medium grained and found only in calcsilicate carbonate rocks, and not in pure metacarbonate rocks.

The observed paragenesis are;

quartz-calcite

quartz-calcite-biotite-diopside

quartz-biotite-diopside

quartz-biotite-hornblende-cordierite

quartz-biotite-muscovite-cordierite

In addition to the main minerals, accessory minerals of sphene, zircon, apatite and opaques are present.

(C) Amphibolites and calcsilicate amphibolites: Amphibolites are found as interlayers in calcsilicate gneissic rocks. They are well-foliated and characterized by nematoblastic texture.

Amphibolites are mainly composed of hornblende crystals (at least 65%) and high-Ca plagioclases, relict clinopyroxene with minor amount of epidote, chlorite, quartz and garnet.

The main mineral of the amphibolites is hornblende. Hornblendes are variable in size from fine grained to coarse grained. Hornblendes have ragged crystals with idiomorphic to xenomorphic form. There are also some long prismatic crystals. Hornblendes are represented by a calcic variety showing a green to greenish brown color. They have 56° cleavage and they are partly chloritized. After hornblende, xenomorphic plagioclase is the most common mineral of the amphibolites. They are high-calcic types which are represented by polysynthetic twinning. Plagioclases have poikiloblastic

texture due to inclusions of epidote. There are also some xenomorphic quartz in pure amphibolites. Quartz is characterized by undulatory extinction and is fine grained. Xenomorphic porphyroblasts of garnet with inclusions of quartz and chlorite are also present. Epidotes in plagioclase porphyroblasts are fine grained, yellowish green in color and show slight pleochroism. Diopside is also present as relicts between hornblende grains except for few samples. Other than these minerals, sphene and opaques are also present in accessory amounts.

The studied calcsilicate amphibolites differ from pure amphibolites interpreted above. The hornblende content of calcsilicate amphibolites is less than that of amphibolites. They further contain biotite and calcite those are not found in amphibolites. The quartz content of calcsilicate amphibolites is higher than that of amphibolite. Moreover, there is no garnet in calcsilicate amphibolites.

In amphibolites and calcsilicate amphibolites, with increasing amount of idiomorphic hornblende, the amount of plagioclase and garnet increase while biotite, calcite and quartz decrease.

It can be assumed that amphibolites are derived from basic rocks while calcsilicate amphibolites have sedimentary/volcanosedimentary origin.

(D) Metaserpentinites: Metaserpentinites are observed as lenses among the metamorphic slices in the field, especially in the Sheared Zone. Metaserpentinites show nematoblastic texture with poorly developed foliation. Metaserpentinites include serpentine minerals (antigorite, chrysotile), orthopyroxene and clinopyroxene. The relict orthopyroxenes are enstatitic and partly replaced by chrysotile with fibers perpendicular to fracture walls of pyroxenes or at rims. The replacement is of limited extend. Clinopyroxenes are diopsidic in composition. Secondary hornblendes around pyroxenes are also recognized.

3.4. Kurançalı Granitoid

The Kurançalı Granitoid is observed as thin leucocratic dykes in the Kurançalı area. Some representative samples are analysed by point counting method. The modes of the minerals included in dykes and the data to be plotted on QAP (quartz-alkali feldspar-plagioclase) diagram are given in Table 1. The modal compositions of the samples were plotted on the QAP ternary diagram of Streckeisen (1976) (Figure 37) to classify and to name the rock types. Plots on the QAP diagram showed that three subtypes of the granitoid are present in the study area: alkali-feldspar granite, quartz syenite and alkali-feldspar quartz syenite.

The major mineral content of the Kurançalı Granitoid is K-feldspar, quartz and plagioclase in different modes. The most abundant mineral of the granitic rocks is K-feldspar in the range of 62.05-73.88%. Quartz is present with varying amounts between 10.0% and 28.2%. The plagioclase is generally less than 6.9% except for two samples having greater than 17.0% plagioclase (Table 1). Other than these main phases, muscovite, biotite, amphibole, rarely clinopyroxene are present in few amount in some samples. The accessory minerals are sphene, zircon, apatite, and hematite-magnetite of opaques (Table 2). The alteration products are represented by sericite and kaoline in varying amounts, less intensely by chlorite and calcite, and very rarely by epidote and biotite.

The dykes are from fine to fairly medium grained with holocrystalline porphyritic texture except for one sample (FT-63/B) having equigranular texture. There is only minor textural variation in the samples. The crystals are generally interlocking to each other. They show foliation in different amounts except for an equigranular sample (FT-63/B) in which there is no lineation. FT-4 cutting the metamorphic ophiolitic complex is intensely affected by deformation. Around K-feldspar porphyroclasts, very fine anhedral grains of quartz and K-feldspar are present. However, other foliated samples have

Table 1. Modal compositions and QAP data (quartz-alkali feldspar-plagioclase) of the Kurançali Granitoid.

MINERALS / SAMPLES	FT-4 Quartz syenite	FT-28 Alkali feld. granite	FT-34 Alkali feld. granite	FT-49 Alkali feld. granite	FT-50/B Alkali feld. granite	FT-55 Alkali feld. quartz syenite	FT-57 Alkali feld. quartz syenite	FT-59/B Alkali feld. granite	FT-63/B Quartz syenite	FT-77 Alkali feld. quartz syenite	FT-400 Alkali feld. quartz syenite	FT-401 Alkali feld. quartz syenite	FT-405 Alkali feld. quartz syenite
Quartz	17.3	28.2	26.07	25.8	24.3	10.0	12.1	26.1	11.4	10.9	10.1	11.9	22.36
K-feldspar	62.05	68.75	69.36	67.6	68.1	69.1	66.2	66.9	66.2	69.2	68.4	67.1	73.88
Plagioclase	17.4	0.8	1.69	1.1	1.6	5.5	6.9	1.8	19.27	5.4	6.2	6.4	1.7
Muscovite	-	2.07	1.7	0.2	0.7	0.98	0.3	1	0.29	2.1	7.8	8.1	0.7
Biotite	0.1	-	-	4.6	3.5	0.9	1.1	3.8	-	7.8	0.9	1.4	1
Amphibole	2.55	-	0.4	0.1	0.8	10.05	11.8	0.1	2	4.1	3.1	2.7	0.1
Clinopyroxene	-	-	-	-	-	-	-	-	-	-	-	0.1	-
Accessories	0.2	0.06	0.08	0.1	0.2	0.07	0.2	0.1	0.03	0.1	0.1	0.2	0.06
Opaques	0.3	0.08	0.7	0.5	0.9	0.6	1.2	0.2	0.8	0.4	0.2	2.1	0.2
Quartz (Q)	17.87	28.9	26.85	27.30	25.85	11.82	14.18	27.53	11.76	12.73	11.92	13.93	22.86
Alkali feldspar (A)	64.15	70.07	71.4	71.53	72.45	81.68	77.73	70.57	68.32	80.96	80.76	78.57	75.41
Plagioclase (P)	17.97	0.82	1.75	1.16	1.7	6.5	8.09	1.9	19.92	6.31	7.32	7.50	1.73

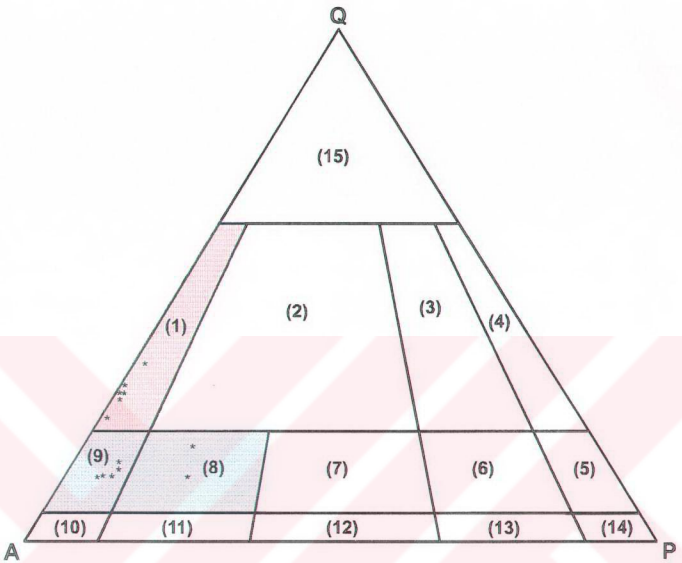

Figure 37. QAP ternary diagram of Streckeisen (1976) for modal classification of intrusive rocks on which modal values of felsic dykes from the study area are plotted. Where; A: Alkali-feldspar, Q: Quartz, P: Plagioclase, (1): alkali-feldspar granite, (2): granite, (3): granodiorite, (4): tonalite, (5): quartz-diorite, (6): quartz-monzodiorite, (7): quartz-monzonite, (8): quartz-syenite, (9): alkali-feldspar syenite, (10): alkali-feldspar syenite, (11): syenite, (12): monzonite, (13): monzodiorite, (14): diorite for An<50.

Table 2. Accessory minerals and alteration products observed in modally analysed samples of the Kurançali Granitoid.

	MINERALS / SAMPLES	FT-4 Quartz syenite	FT-28 Alkali feld. granite	FT-34 Alkali feld. granite	FT-49 Alkali feld. granite	FT-50/B Alkali feld. granite	FT-55 Alkali feld. quartz syenite	FT-57 Alkali feld. quartz syenite	FT-59/B Alkali feld. granite	FT-63/B Quartz syenite	FT-77 Alkali feld. quartz syenite	FT-400 Alkali feld. quartz syenite	FT-401 Alkali feld. quartz syenite	FT-405 Alkali feld. quartz syenite
Accessory	Sphene	+	+	-	-	+	+	+	+	-	+	-	-	-
	Apatite	+	+	+	+	-	-	-	+	+	+	+	+	+
	Zircon	+	-	-	+	-	-	+	+	-	+	-	+	-
	Opaque	+	+	+	+	+	+	+	+	+	+	+	+	+
Alteration Products	Sericite	+	+	+	+	+	+	+	+	+	+	+	+	+
	Kaoline	+	+	+	+	+	+	+	+	+	+	+	+	+
	Chlorite	+	-	-	+	+	+	+	+	-	+	+	+	-
	Calcite	-	-	+	+	-	+	+	+	-	+	+	+	-
	Epidote	+	+	-	-	-	-	-	-	-	-	-	-	-
	Biotite	+	-	-	-	+	+	-	-	-	-	-	-	-

relict porphyritic texture among very fine-grained crystals. They are highly mylonitized.

K-feldspar is generally found as anhedral phenocryst up to 0.5 cm surrounded by smaller grains. In coarse grains perthite formations are seen as bands and strains. Plagioclase grains are found in euhedral to anhedral. The pericline twinning, albite twinning and Carlsbad twinning together with few zoned crystals characterize plagioclases, that are very less than K-feldspar. Quartz crystals are usually intergrown with K-feldspar resulting in graphic texture. Fine grains and phenocrysts of quartz are also present as well as intergrown quartz with K-feldspar. Subhedral to anhedral hornblende recognized in few samples has sieve texture. Greenish brown biotites, generally, have subhedral to anhedral flakes with some degree of chloritization. Muscovites, which are observed in a few samples, are euhedral to subhedral. Colorless, anhedral clinopyroxene is recognized only in one sample.

Petrography of the Kurançalı Granitoid may be compared with the microgranites of the Cefalıkdağ region which was studied by Geven (1995) Porphyritic granites are further defined by Göncüoğlu and Türeli (1994) from the Ekecikdağ region, where they occur as thick leucocratic dykes. According to previous works, porphyritic-aphanetic texture, relatively small grain size and presence of quartz phenocrysts are distinctive features.

CHAPTER 4

MINERALOGY

4.1. Introduction

This chapter focuses on the mineralogical and morphological characteristics of the pyroxene, both primary and secondary hornblende, phlogopitic biotite and vermiculite that were distinguished by petrographical methods. Moreover, it is tried to detect the alteration sequence of pyroxene → secondary hornblende → secondary biotite → vermiculite and/or primary phlogopitic biotite → vermiculite in more detail.

4.2. Description of the Minerals

Brief descriptions of the constituent minerals, pyroxene, hornblende, phlogopitic biotite and vermiculite, which may be the products of successive replacements, are given to control the structural and chemical changes during vermiculitization process from the phlogopitic mica.

Pyroxene is the parent mineral of the alteration sequence based on the petrographical studies. Diopsidic augites of the studied samples are members of the clinopyroxene group and have the general formula: $Ca(Mg,Fe,Al)(SiAl)_2O_6$ (Klein and Hurlbut, 1985).

Based on the textural data, three groups of hornblende were described: igneous, alteration (uralitization), metamorphic. Primary hornblendes as product of primary crystallization, as well as secondary hornblendes are common ingradients of the Kurançalı Metagabbro. Secondary hornblende characteristically alters from pyroxene during the late magmatic stages of crystallization of igneous rocks due to action of hydrothermal solutions. Some of the hornblendes are actinolitic in composition and found as late stage fibrous crystals and patches at rims of pyroxenes and earlier stage hornblendes. The structural formula for the hornblende and actinolitic hornblende are given as $(Na,K)_{0-1}Ca_2(Mg,Fe,Al)_5(Si_{6-7}Al_{2-1}O_{22})(OH,F)_2$ (Deer et al., 1980) and $Ca_2(Mg,Fe^{2+})_5(Si_8O_{22})(OH,F)_2$ (Klein and Hurlbut, 1985), respectively.

Phlogopitic biotite having $K(Mg,Fe)_3(AlSi_3O_{10})(OH)_2$ structural formulae (Klein and Hurlbut, 1985) is a trioctahedral mica. The phlogopitic biotite has primary origin in the studied metagabbro and is found generally as irregular foliated masses and books. In addition to primary type of the mica, secondary biotite due to alteration of pyroxene and hornblende is found along cleavage and fracture surfaces.

Vermiculite is a monoclinic mica-like mineral with the structural formulae:

$$\overbrace{(Mg,Ca)_{0.7-0.1}Mg_{3.5-5.0}(Fe,Al)_{2.5-1.0}}^{6.0}\overbrace{Al_{2.0-2.5}Si_{6.0-5.5}}^{8.0}O_{20}(OH)_4(H_2O)_{7.0-9.9}$$

(Deer et al., 1980)

Vermiculite is expected to be the final alteration product in the recognized successive alteration sequence (pyroxene → secondary hornblende → secondary biotite → vermiculite) or to be directly altered from primary phlogopitic biotite. During this transformation, morphology and structure of vermiculite do not differ from parent micas while its chemistry is

different from that of the parent minerals. The recognized secondary sheet silicates (i.e., secondary biotite and vermiculite) are often linked with the transformational processes. These secondary sheet silicates develop due to gradual changes in the interlayer of the parent minerals (Nagasawa et al., 1974; Noack and Colin, 1986; Proust et al., 1986; Beaufort, 1987; de Kimpe et al., 1987; Buurman et al., 1988).

4.3. Scanning Electron Microscope – Energy Dispersive X-Ray Analyses

Thin section analyses of rock samples using polarizing microscope give only two-dimensional data about the bulk mineral composition, crystal fabric and texture. Therefore, scanning electron microscope (SEM) analyses were utilized to examine the actual three-dimensional crystal relationships and morphological changes on the petrographically studied 4 metagabbro samples. Energy dispersive x-ray analysis (EDS) was used to check semi-quantitatively the phase changes in minerals. This study especially focuses on the detection of successive replacement of pyroxene and/or transformation of phlogopite to vermiculite due to alteration. As the applied method is based on semi-quantitative data, it only gives a very general sight.

After all peaks on the EDS spectrum of the four measured samples were identified, the relative concentrations of the elements were compared with the crystal morphology and chemical formula of the suspected mineral. The peak heights of Si, Al, especially K and Ca were correlated with the chemical formulas because the peak heights are proportional to their concentrations.

In all the studied samples, it is observed that pyroxene crystals, started to be altered to biotite at edges and cleavage surfaces, are primary phases (Figures 38, 39). Although the secondary hornblende could not be noticed, the presence of primary hornblende was recognized in studied samples by SEM-EDS method (Figures 39, 40, 41). In Figure 40, the characteristic two edges of rhombic cleavage of the hornblende is partly recognizable in three

dimensions while at left of the microphotograph given in Figure 41, rhombic hornblende with micro flakes of mica is well preserved.

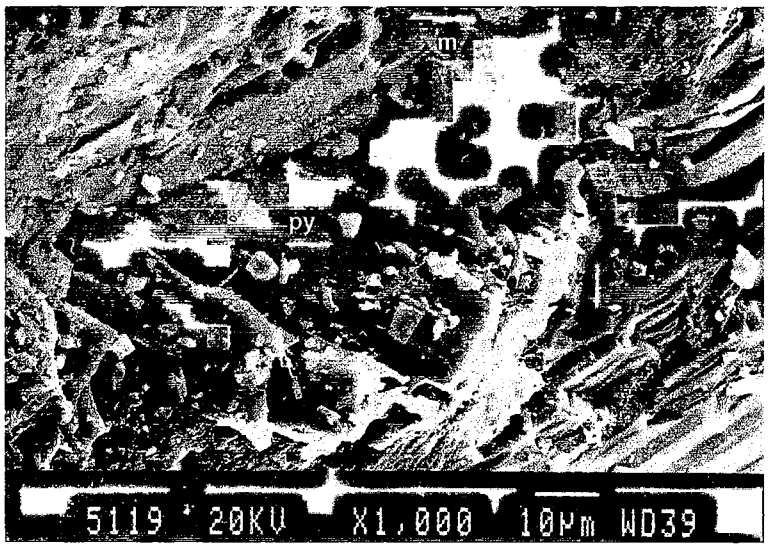

Figure 38. SEM photomicrograph showing the occurrence of primary diopsidic augite in three-dimensions (py: pyroxene, m: mica).

Mica flakes either primary or secondary are present almost in all samples in varying sizes (Figures 38, 40, 41). Primary mica books defined in hand specimens are also identifiable by SEM (Figure 42). Secondary biotite flakes developing along fractures of the pyroxene and hornblende are fine grained and form very thin books (Figure 43). Secondary biotite flakes developing from the surface of the pyroxene are recognizable by SEM (Figure 44). In Figure 44, vermiculite is also present in between the mica flakes but it is not detectable only by SEM method. EDS is needed to control semi-quantitatively the elemental changes.

From this surface study, it is understood that vermiculite and mica could not be differentiated only by SEM because of their similar platy morphologies

(Figure 44). Vermiculite could be differentiated from mica only by its partially expanded form (Figures 44, 45). Nevertheless, EDS analyses clearly show the difference between vermiculite and mica (Figure 39). The presence of Ca instead of K within the flakes between mica flakes was indicated by EDS. This verifies the presence of vermiculite among mica flakes. EDS spectrum at different points taken along a line on mica flakes with vermiculitized parts (Figure 46) show a close association between vermiculite and mica (Figure 47). This close relationship between vermiculite and mica has implications for models of mica transformation (Jackson, 1963; Barnhisel and Bertsch, 1989) which will be described in the following chapter.

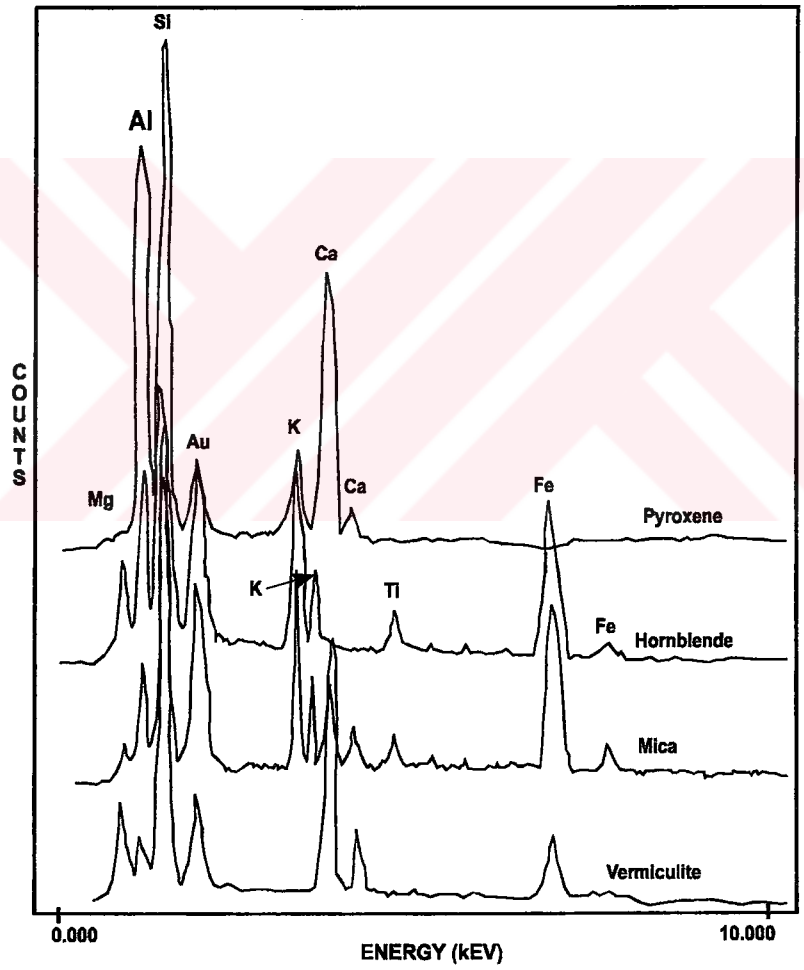

Figure 39. EDS spectra of minerals (pyroxene, hornblende and mica separates, and vermiculitized part of the mica crystal).

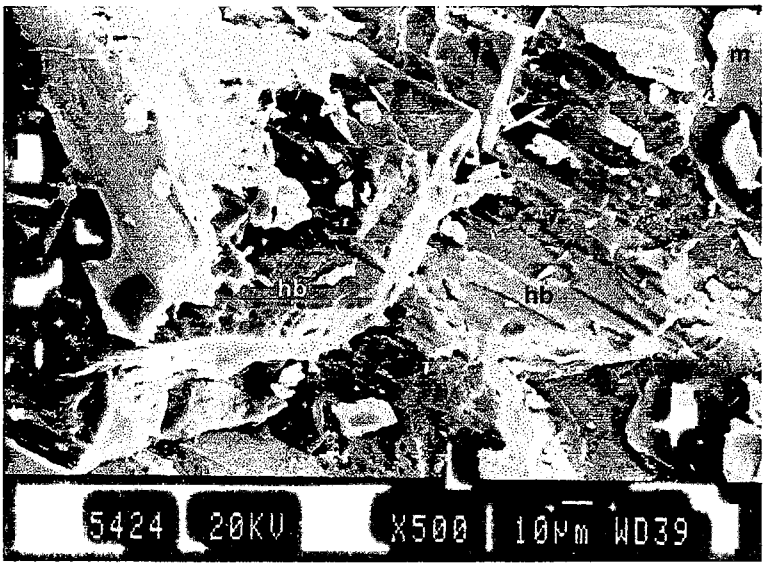

Figure 40. SEM photomicrograph showing two edges of rhombic cleavage of hornblende in three-dimensions (hb: hornblende, m: mica)

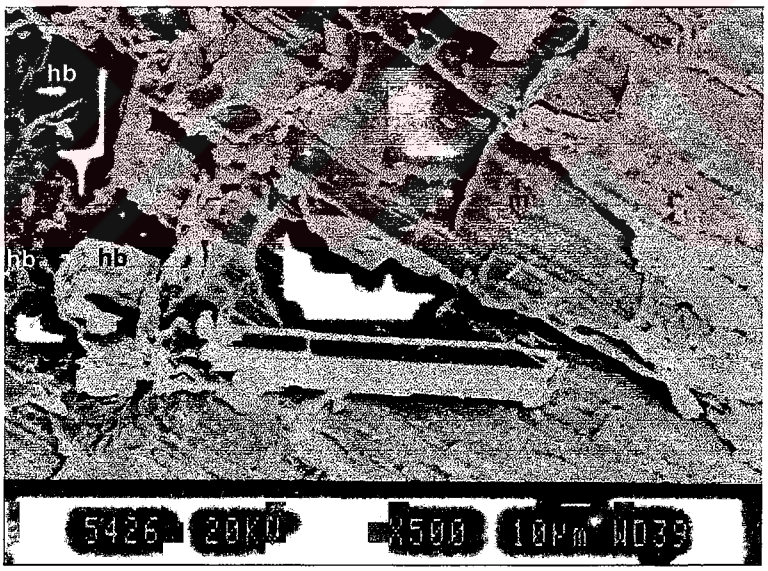

Figure 41. SEM photomicrograph showing rhombic cleavage of hornblende in three-dimensions (hb: hornblende, m: mica)

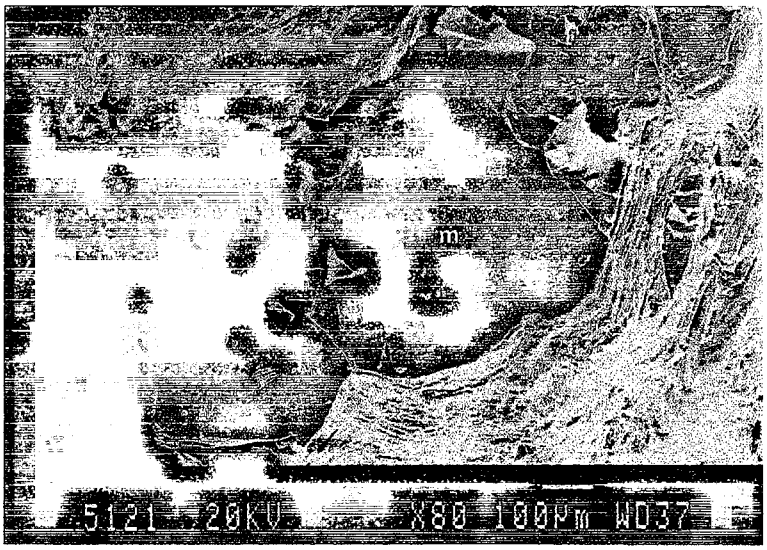

Figure 42. SEM photomicrograph showing primary mica book (m: mica)

Figure 43. SEM photomicrograph showing secondary mica development along fracture surface of pyroxene (py: pyroxene, m: mica)

Figure 44. SEM photomicrographs showing mica development from surface of pyroxene and vermiculite occurrence together with mica flakes in cavities (Lower photomicrograph is close up view of upper one) (m: mica, v: vermiculite, py: pyroxene).

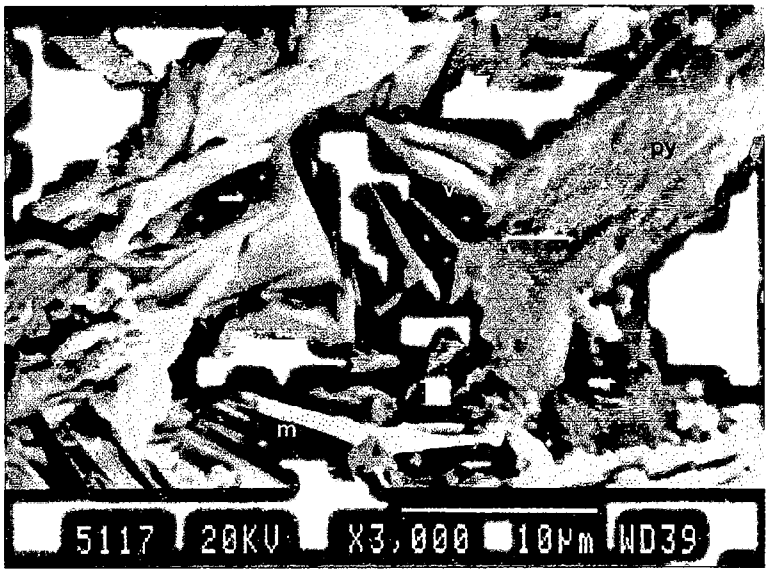

Figure 45. SEM photomicrograph showing vermiculite flakes with their expanded forms (v: vermiculite, py: pyroxene, m: mica)

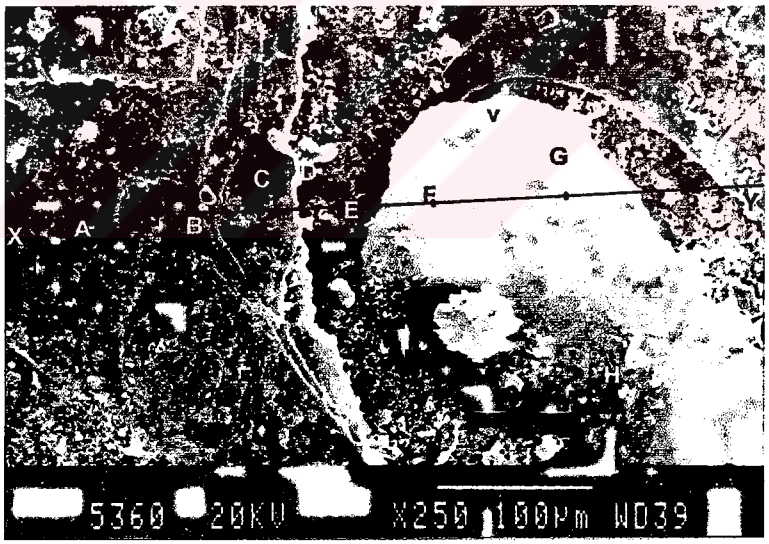

Figure 46. SEM photomicrograph showing vermiculitized mica.

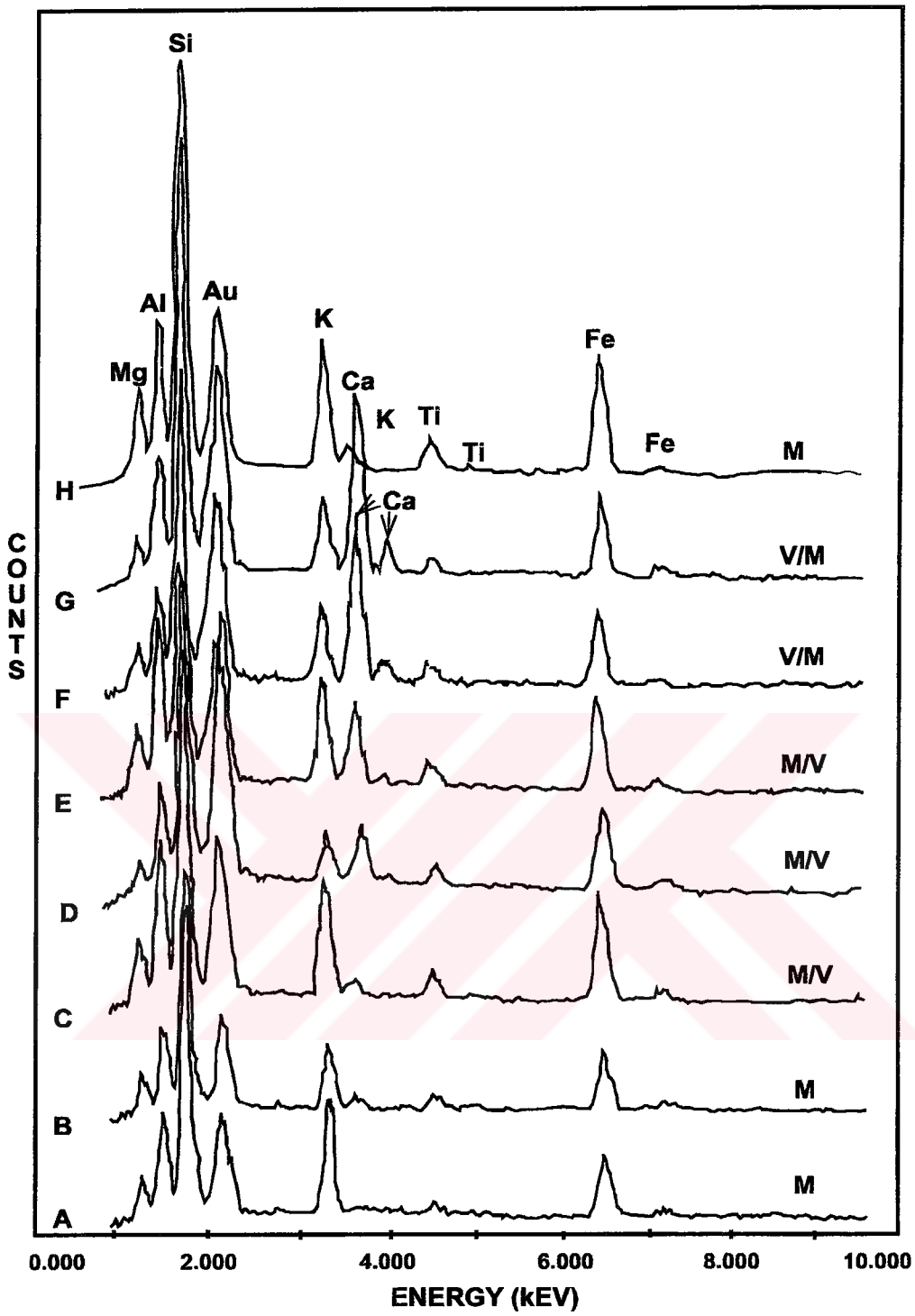

Figure 47. EDS spectra showing K-Ca relationship as the vermiculitization from mica proceeds, along a line (X-Y) on Figure 46. Vermiculitization increases from point A to point H with increasing Ca and decreasing K (M: mica, M/V: interstratified mica and vermiculite (higher amount of mica), V/M: interstratified vermiculite and mica (higher amount of vermiculite)).

SEM observations enabled two groups of samples to be distinguished: a) Samples containing large flakes of mica which are free from pyroxene and hornblende were observed. Taking into account the EDS analyses, these samples were tentatively identified to have mica and vermiculite. b) Samples consisting of small mica flakes at edges and cleavage surfaces of pyroxene and hornblende were detected.

The geochemical cycles of Si, Al, Fe, Ca and K in the investigated minerals show variability from one mineral to the next (Figure 39). Especially Ca and K show a range of mobilities during alteration of diopsidic clinopyroxene through secondary hornblende to mica to vermiculite, which is easily interpreted, from EDS of the minerals. Transformation to biotite from parent mineral is achieved by entrance of K into mineral structure and replacement of Ca by K. There are some uncertainties on the EDS diagrams (Figures 39, 47), that is the Mg peaks of the samples are too small. However, all the minerals have structural Mg in their octahedral sheets.

The morphological differences among pyroxene, hornblende and micaceous flakes are easily recognized although vermiculite and mica could not be morphologically differentiated by the SEM studies. SEM studies of the mica bearing samples suggest that the pyroxenes and hornblendes were altered and evolved into secondary biotite. On the other hand, it could not be detected that vermiculite is formed from the primary phlogopitic biotite or secondary biotite.

4.4. Semi-Quantitative Electron Microprobe Analyses

Electron microprobe analyses were carried out semi-quantitatively on polished and carbon coated thin section by using JEOL JXA-733 microprobe associated with a scanning electron microscope (SEM). The elements routinely analysed are Si, Al, Mg, Ca, Fe, Na, K and Ti. In this study, microphotographs of thin sections were taken using oblique and polarizing

lights in order to view the point which will be analysed at SEM, because the crystal boundaries and features of the minerals on polished sections are similar at both SEM and oblique light of the petrographical microscope (Figure 48a,b,c). The photograph of the image under polarizing microscope was taken to identify the minerals.

The contacts of the minerals were chosen to observe the elemental distributions, changes and transformational phases among the minerals. The contact to be studied, was chosen first on microphotographs taken under polarizing and oblique lights. It was then tried to find this contact with the same magnification at SEM. Finally the point was focused at SEM and the magnification was made higher to analyse the selected area.

To able to observe the elemental differences of secondary hornblende and pyroxene, sample FT-33 was analysed. A transition of contact between pyroxene to secondary hornblende was selected (Figure 48a,b,c,d). Considering the optical properties and theoretical formula of the minerals, assumptions were made for arial distributions of the elements and elemental changes along a profile. As seen from Figure 48(e,f), concentrations of Al and Si opposes, where Al is high, Si is low. From concentration differences of the elements, boundaries of the minerals could be easily drawn. Concentration of Mg is slightly higher where there is low Al but high Si at the first sight, there is not clear distinguishable difference in concentrations of Ca on both sides of the contact (Figure 48g). However, the Ca-concentration seems to be slightly higher at the right side where Al is low. Considering the microphotographs of the element concentrations, it can be suggested that where Al is high (left side), Mg and Si are lower, and the mineral is hornblende while at the other side (right one), the mineral is pyroxene where Mg and Si are higher than Al.

At the microphotograph taken at x72 magnification, the main phases are hornblende at left and pyroxene at right (Figure 48a,b). However, there are small size pyroxene relicts in the transitional zone, which is difficult to identify by at x72 magnification. At higher magnification, the point display very

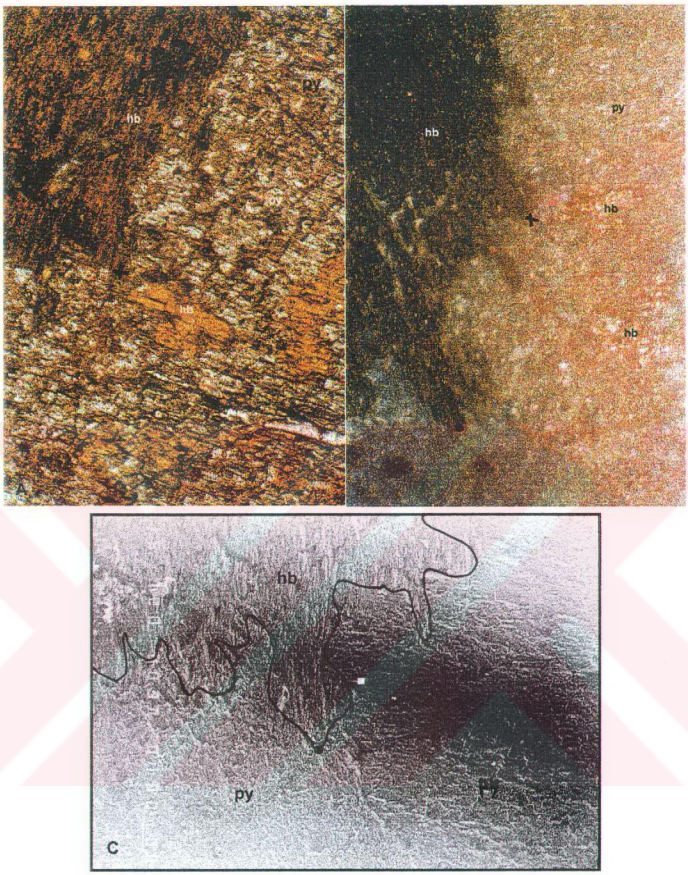

Figure 48. Photomicrographs showing elemental distributions and relationships between pyroxene and hornblende. Photomicrographs; A: taken under polarized light (x72), B: taken under oblique light (x72), C: taken from SEM (white rectangular indicating the analysed point, x72), D: taken from SEM showing analysed area (x400), E: Al-concentration, F: Si-concentration, G: Ca-concentration (py: pyroxene, hb: hornblende).

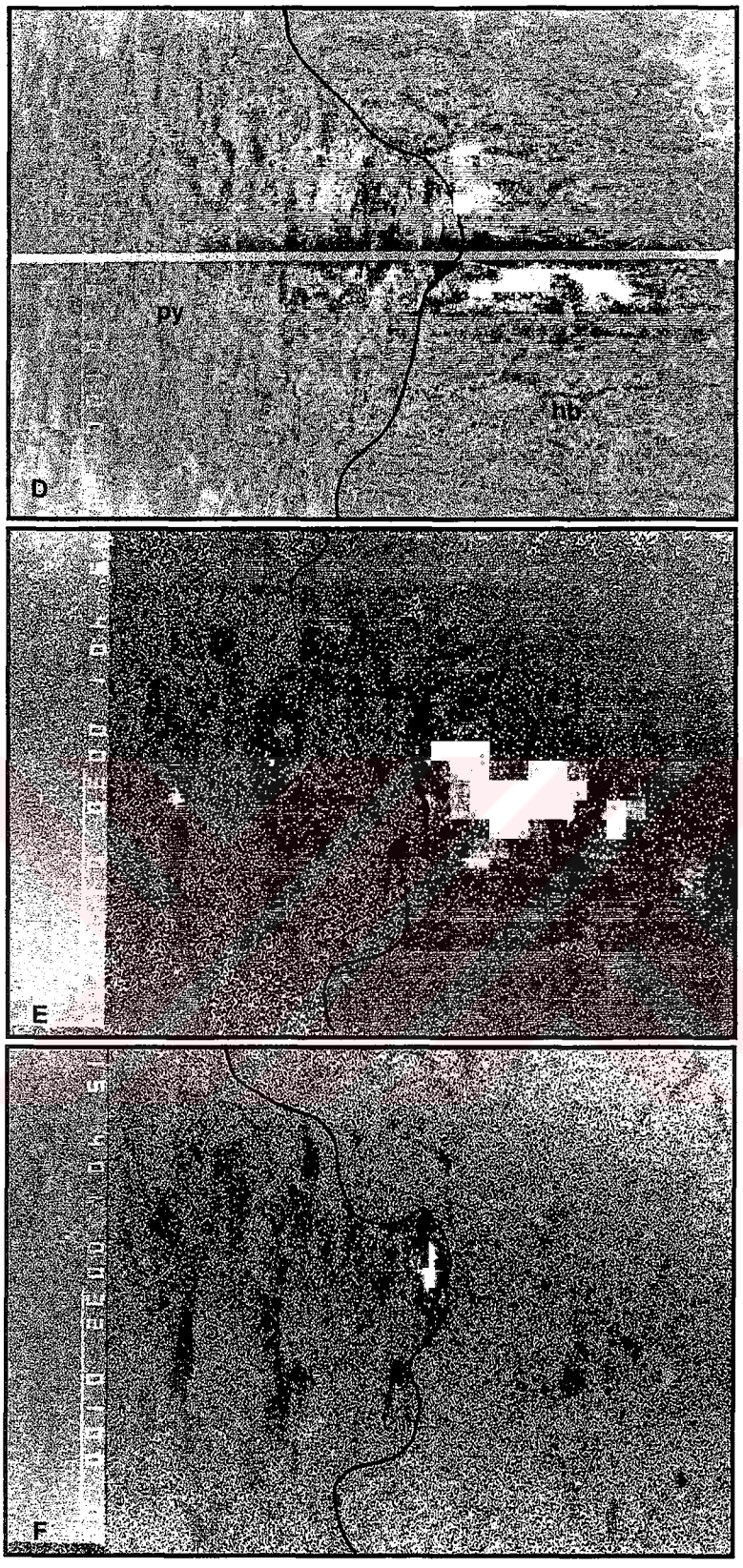

Figure 48 (continued).

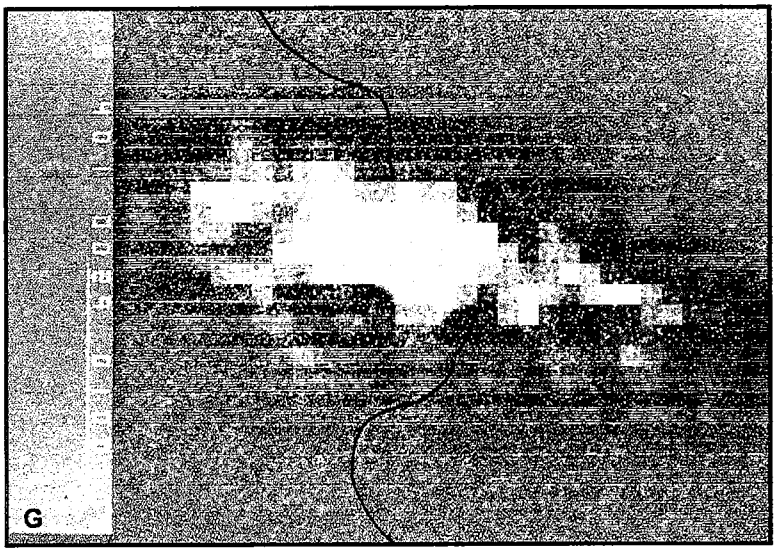

Figure 48 (continued).

fine grained relict pyroxene not observed at small magnification (Figure 48d) and secondary hornblende. That is to say, at high magnification the relict pyroxene at left and hornblende at right appear.

In a similar way, sample FT-69 was examined to observe the elemental changes among the phases hornblende, phlogopite and vermiculite. On microphotographs of polarized and oblique lights, a point where hornblende, phlogopite and vermiculite are present (Figure 49a,b) from left to right, was chosen. Using the microphotograph taken under the oblique light, the location of the studied point was chosen at x72 magnification of SEM (Figure 49c). Then the selected point was examined at x480 magnification (Figure 49d). When the elemental concentrations are viewed, it is seen that Al and Ca show opposing behavior (Figure 49e,f). That is to say, where Al is high in concentration, Ca is low. From the concentrations of these elements, boundary of the hornblende and phlogopite crystals could be easily drawn. Mg concentration is slightly higher in the mica zone than in the hornblende zone. However, using this method could not differentiate phlogopite and vermiculite. Phlogopite and vermiculite having approximately the same

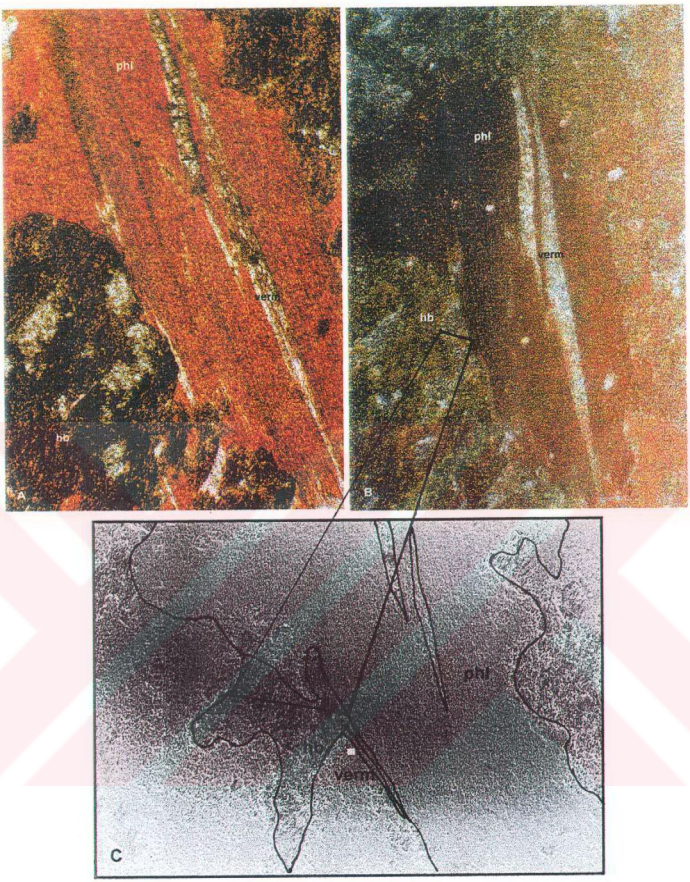

Figure 49. Photomicrographs showing elemental distributions and relationships among hornblende, phlogopite and vermiculite. Photomicrographs; A: taken under polarized light (x72), B: taken under oblique light (x72), C: taken from SEM (white rectangular indicating the analysed point, x72), D: taken from SEM showing analysed area (x480), E: Al-concentration, F: Ca-concentration, G: K-concentration, H: Si-concentration, I: Mg-concentration, J: K and Ca change along a line on (D) (hb: hornblende, phl: phlogopite, verm: vermiculite).

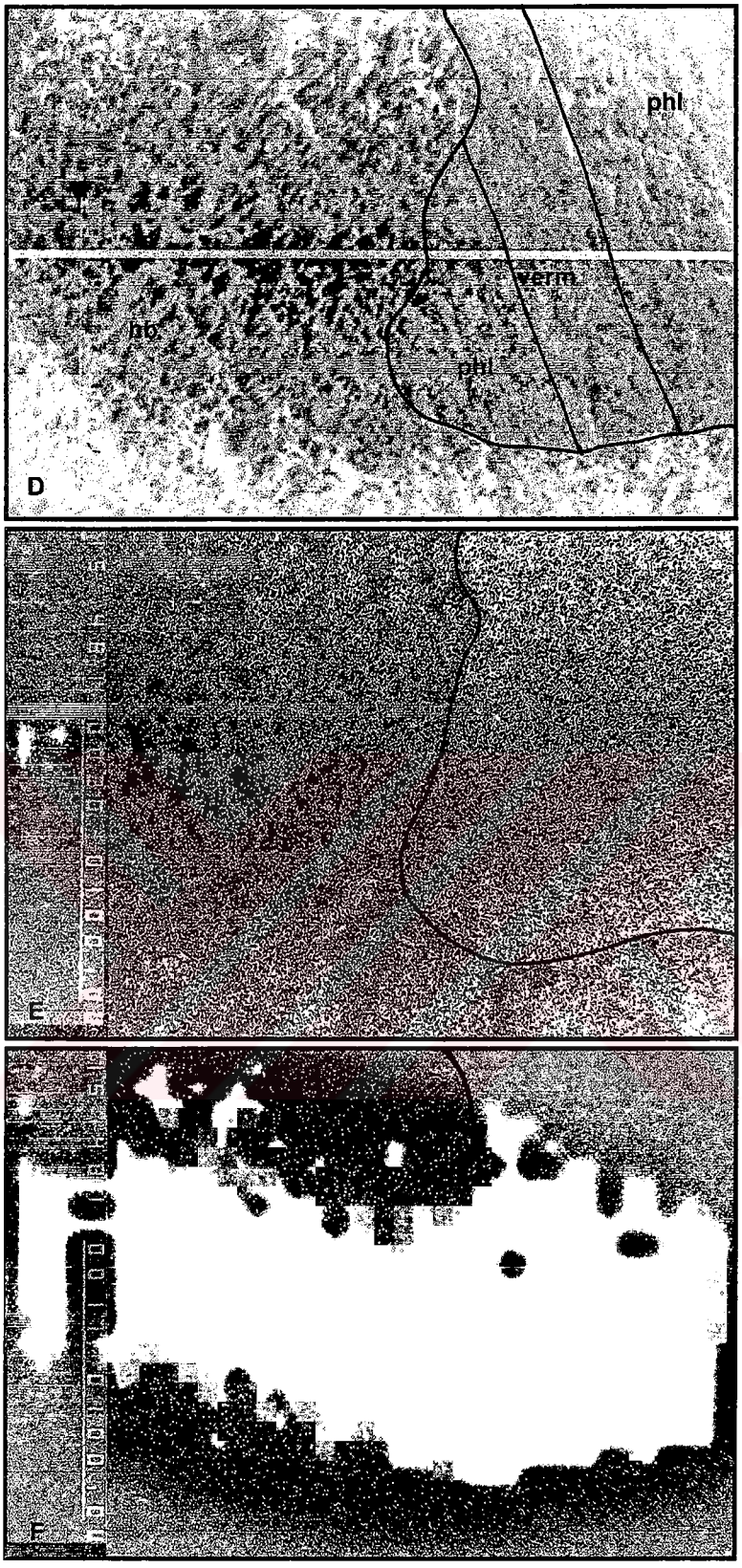

Figure 49 (continued).

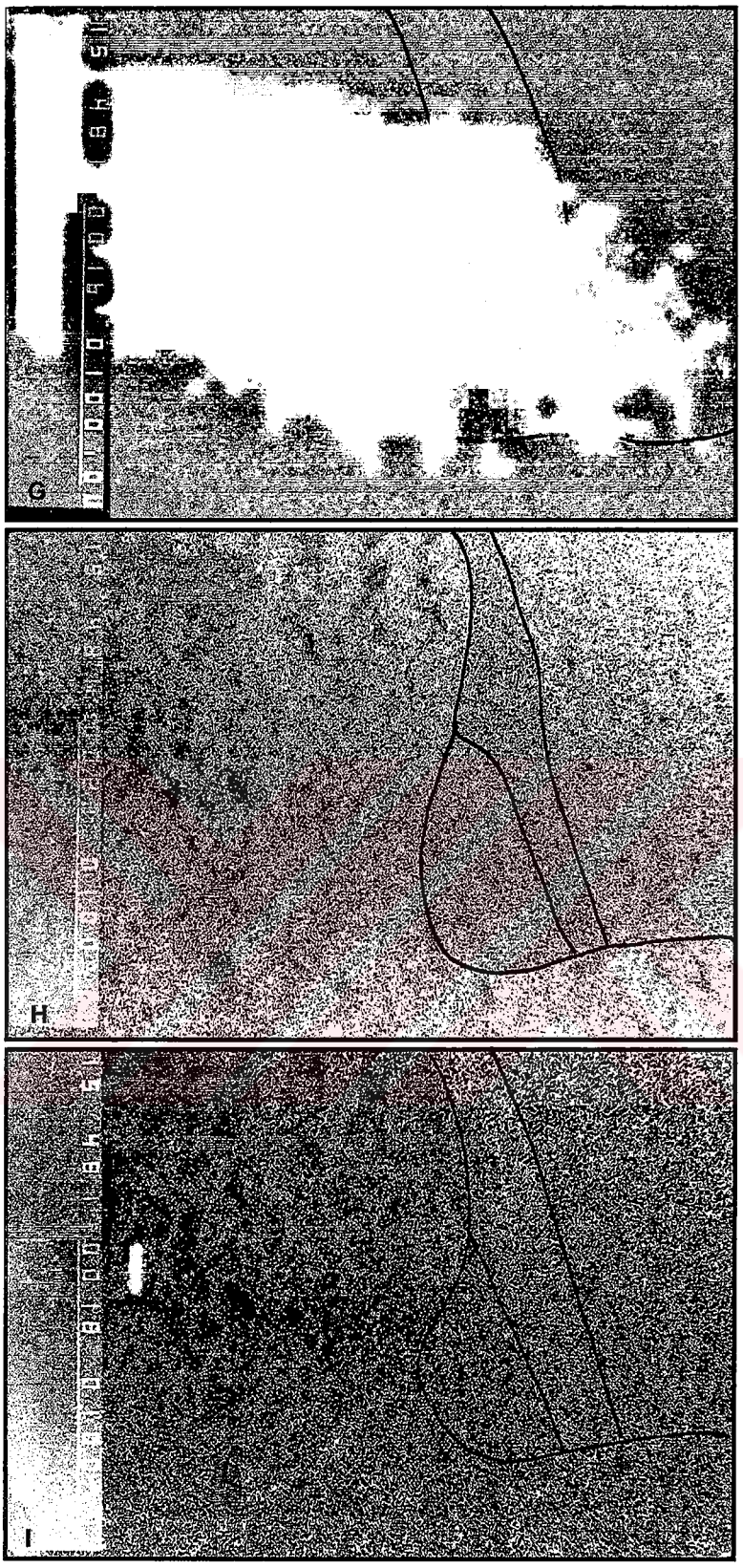

Figure 49 (continued).

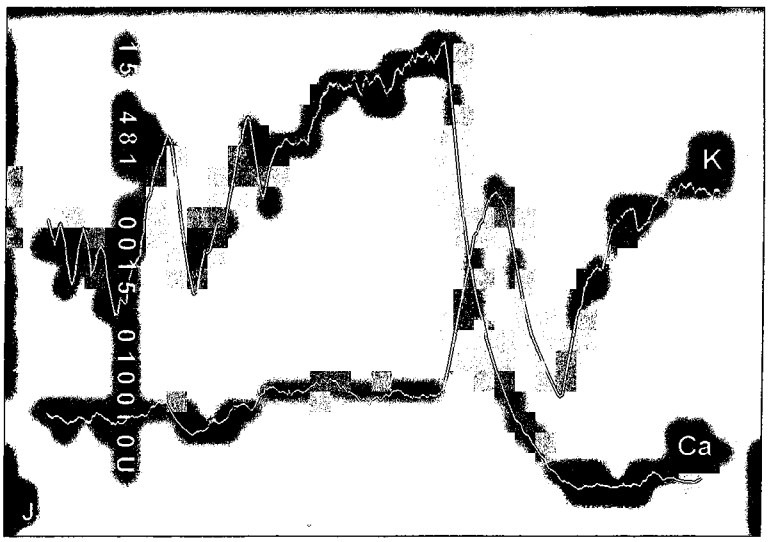

Figure 49 (continued).

concentrations of Ca and Al differ only in K- and Si-concentrations and slightly in Mg-concentration. In the phlogopite crystal, a zone crossing the phlogopite is lower in K and Si but higher in Mg-concentration (Figure 49g,h,i). This zone is assumed to be vermiculite considering their theoretical chemical formula given in Section 4.2. Because during the transformation of phlogopite to vermiculite, K is replaced by Mg while Si is replaced by Al. In the microphotograph given in Figure 49(j), it is seen that there is an elemental change in Ca and K along a profile on the microphotograph given in Figure 49. According to these observations, it is concluded that there is a sharp decrease in Ca-concentration along a line passing through hornblende to phlogopite and vermiculite while there is a sharp increase in K-concentration. Moreover, a decrease in K-concentration from phlogopite to vermiculite and an increase in K from vermiculite to phlogopite are recognizable.

The sample FT-72 was also examined to control the elemental changes in an area including pyroxene, hornblende, phlogopite and vermiculite (Figure 50a,b). In this sample at x400 magnification (Figure 50c), the concentration of the Al obviously differs in three zones (Figure 50d). Al concentration is the

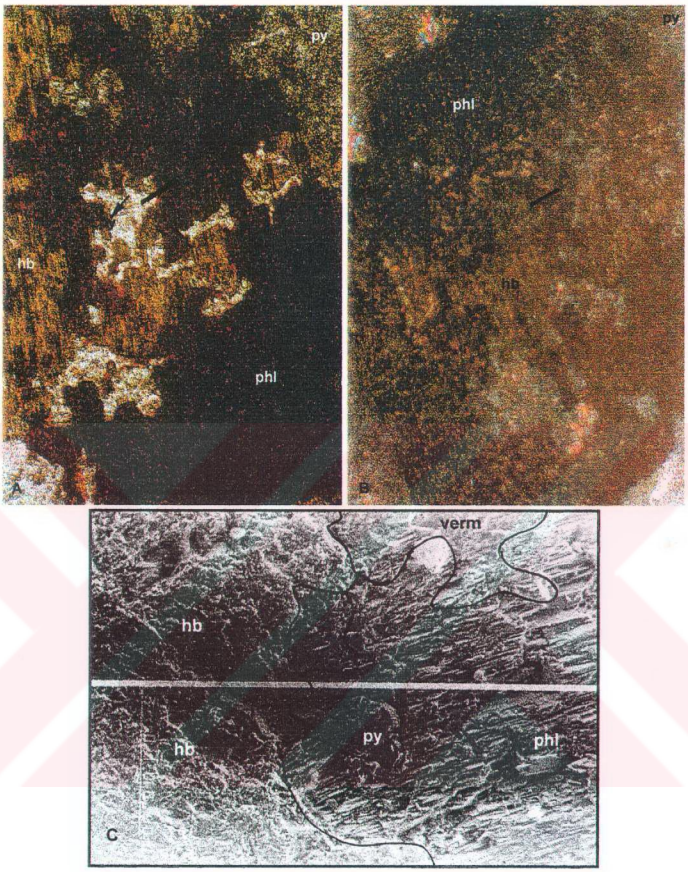

Figure 50. Photomicrographs showing elemental distributions and relationships among hornblende, pyroxene, phlogopite and vermiculite. Photomicrographs; A: taken under polarized light (x72), B: taken under oblique light (x72), C: taken from SEM showing analysed area (x480), D: Al-concentration, E: Mg-concentration, F: Fe-concentration (hb: hornblende, py: pyroxene, phl: phlogopite, verm: vermiculite).

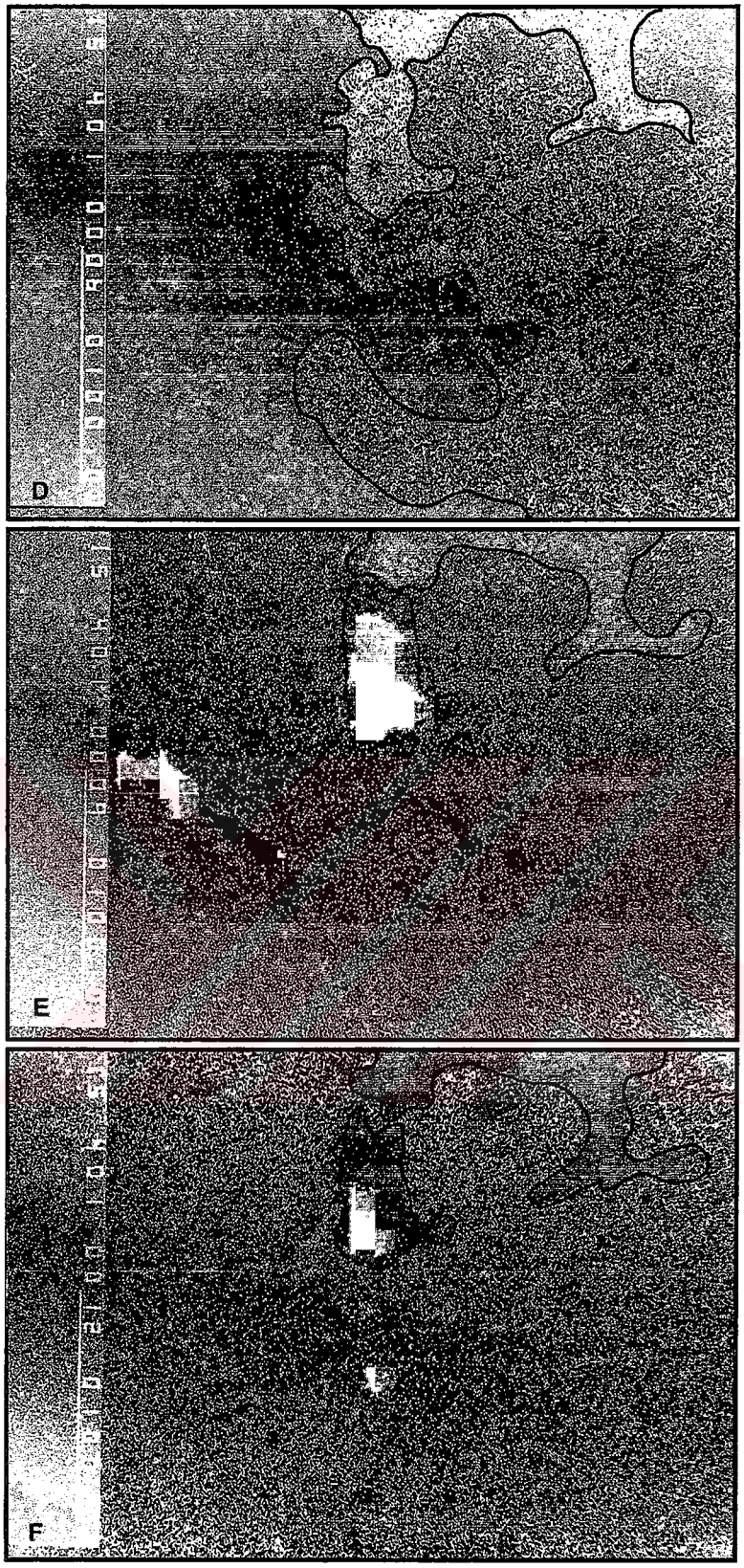

Figure 50 (continued).

lowest at the left side, medium at the middle and lower parts of the right side and the highest at the right upper part of the image. When concentrations of Mg and Fe were examined together with Al, it is seen that where Al has the highest concentration, Fe- and Mg-concentrations are the lowest (Figure 50e,f). However, in zones where Al has the lowest and medium concentrations, the Fe- and Mg-concentrations do not change. There is small zone where Al is the lowest, Fe is slightly lower while Mg remain the same. This small zon.e may represent pyroxene although it is not certain.

K-concentration is higher at medium Al zone, but it is lower where Al is the highest. The zone with the highest Al, lower K, the lowest Mg- and Fe-concentrations, is assumed to represent Al-rich vermiculite. The presence of the Al-vermiculite is also confirmed by XRD studies (see Section 4.5.). The zone showing medium Al as well as K-concentration is assumed to be phlogopite. The zone with the lowest Al-concentration, higher Mg- and Ca-concentrations and slightly higher Fe-concentration may represent the hornblende.

In sample FT-59/C, the elemental distribution of phlogopite and vermiculite were examined (Figure 51a,b,c,d). There is a clear distinction among concentrations of K, Ca and Mg. Where K is lower Ca and Mg are higher (Figure 51e,f,g). It is also observed that there is an increase in Al-concentration where Fe-concentration decreases (Figure 51h,i). However, the Al- and Fe-concentrations showing opposing behaviors do not display sharp boundaries between the examined minerals as observed in concentrations of K, Ca and Mg. There is a clear distinction in the concentrations of Al and Si to put the boundary between the two phases (Figure 51h,j), however their concentration behavior changes from place to place. There is no proportional change between them as seen in concentrations of K, Ca and Mg to put the boundary between phlogopite and vermiculite minerals. The elemental distributions of Al, Si and Fe not giving sharp mineral boundaries may indicate transitional phases between phlogopite and vermiculite, which are formed during the transformation of the phlogopite to vermiculite. It can be seen that

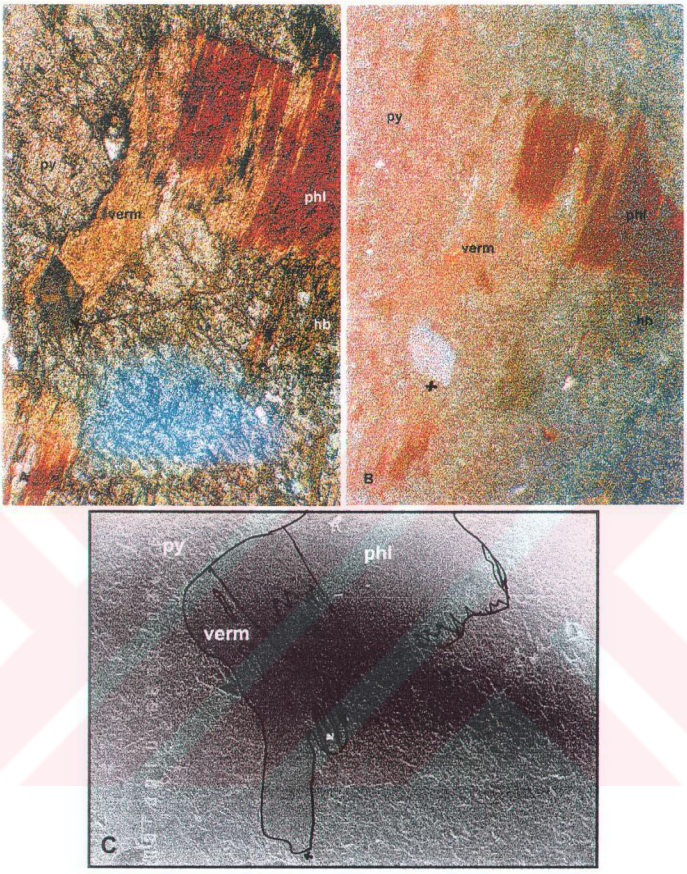

Figure 51. Photomicrographs showing elemental distributions and relationships between phlogopite and vermiculite. Photomicrographs; A: taken under polarized light (x72), B: taken under oblique light (x72), C: taken from SEM (white rectangular indicating the analysed point, x72), D: taken from SEM showing analysed area (x400), E: K-concentration, F: Ca-concentration, G: Mg-concentration, H: Al-concentration, I: Fe-concentration, J: Si-concentration (hb: hornblende, phl: phlogopite, verm: vermiculite).

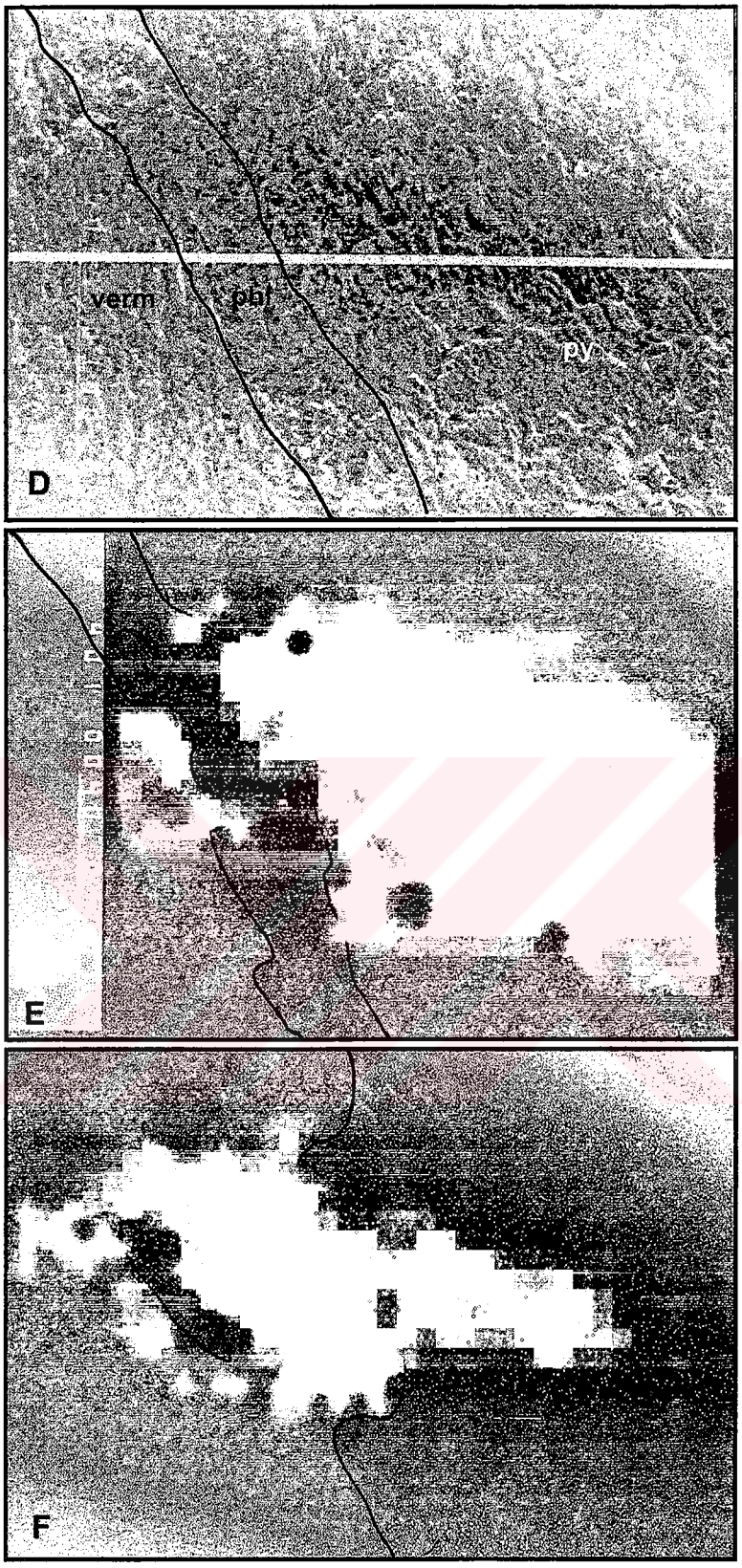

Figure 51 (continued).

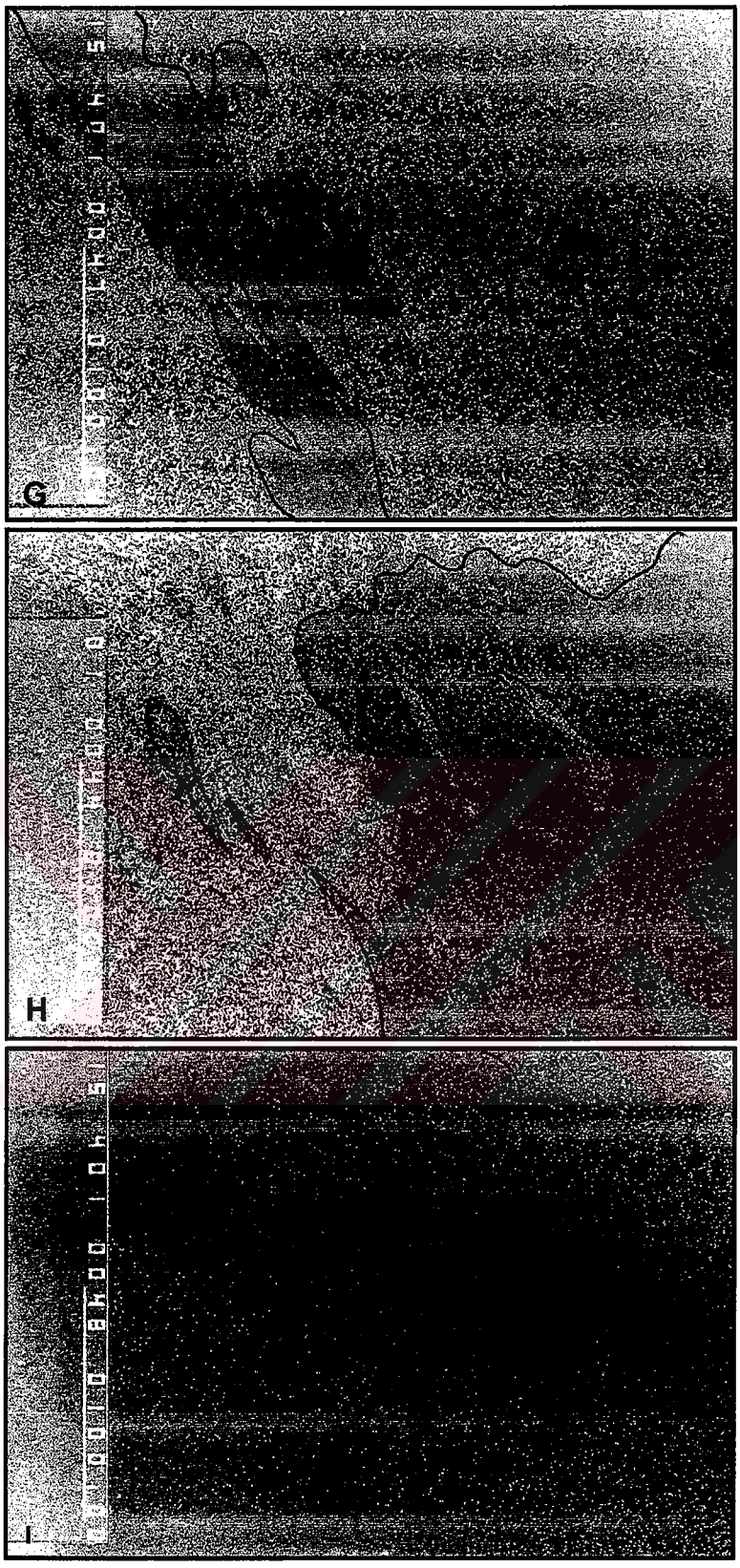

Figure 51 (continued).

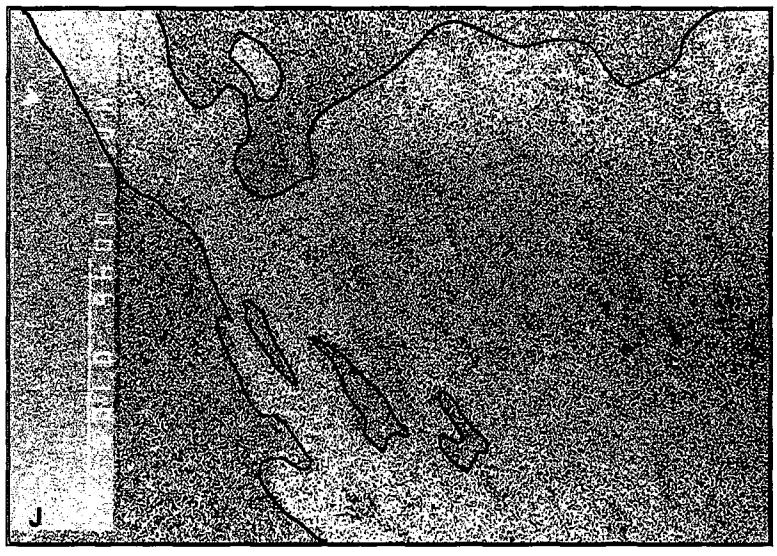

Figure 51 (continued).

where K is higher, Al, Fe and Mg is slightly higher while Si is slightly lower (Figure 51). This can be due to early transformation of phlogopite to vermiculite during early stage weathering. This assumption may be explained by Moon's et al. (1994) data. According to Moon et al. (1994), at the early stages the vermiculitization of phlogopite proceeds by means of a continuous decrease of Al for Si tetrahedral substitutions and progressive increase of Al for Fe and Mg. The observed vermiculitization process in this sample, is in good agreement with the currently accepted weathering mechanisms (e.g., Proust et al., 1986; Fordham, 1990; Moon et al., 1994).

It can be concluded from above assumptions that pyroxene has higher Si, Mg and Ca concentrations than hornblende while Fe in pyroxene is slightly lower than in hornblende. When the concentrations in hornblende and phlogopite are compared, it is seen that Ca in hornblende is much higher than in phlogopite while Al is lower. Mg of hornblende is slightly lower than that of phlogopite or same. Phlogopite and vermiculite mainly differ in concentrations of K and Mg and sometimes in Al. Concentration of K is low or absent while

Mg- and/or Al-concentrations are higher in vermiculite whereas it is the opposite in phlogopite (i.e., higher K).

All these results are assumptions based on the semi-quantitative concentrations of the elements in minerals, which were identified under petrographical microscope. Although they are assumptions, the observations by semi-quantitative microprobe analyses are confirmed by the wet chemical analysis (see Section 4.7.).

4.5. X-Ray Diffractometry Analyses

Petrographic and semi-quantitative SEM-EDS, EMP studies showed the presence of vermiculitized parts in the mica flakes. X-ray diffractometry (XRD) studies were mainly aimed to find out the mica type and the degree of alteration to vermiculite. It is further examined whether vermiculitization is complete or not. In this aim, not only the oriented air-dried specimens, the specimens saturated with ethylene glycol and glycerol, and the specimens heated to 170°C, 350°C, 600°C, but also the random specimens were examined for each of eight mica samples. The samples were first purified from pyroxene, hornblende, and plagioclase. Mica samples could not be separated from vermiculitized parts by Frantz isodynamic magnetic separator because of intergradient growth of vermiculite and/or interstratified phases, and similar behavior of mica and vermiculite on the magnetic separator.

XRD patterns of all of the analysed samples are similar to each other except for small differences (Figure 52). The oriented specimens as well as random ones, mainly have strong first order basal spacing of 10.1-10.2 Å and its rational peaks 5.04-5.09 Å, 3.35-3.39 Å and 2.51-2.52 Å. On random samples, since the randomness of the mica flakes could not be well provided, basal spacing of 10.1-10.2 Å and its rational peaks as well as nonbasal peaks are well-developed. During the identification of the 10.1 Å mineral, XRD pattern of sample FT-25 will be discussed due to the similarities of all the

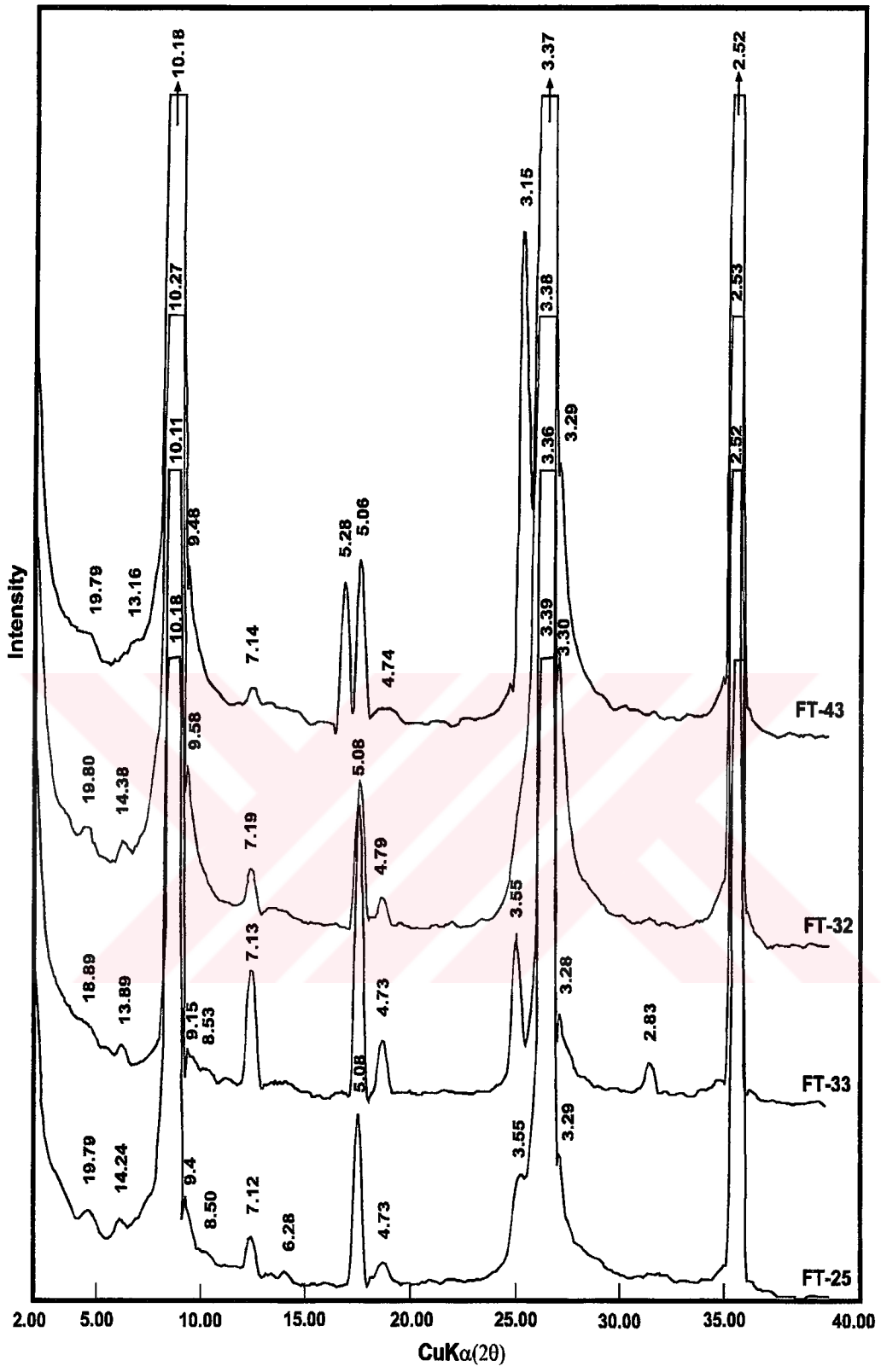

Figure 52. X-ray diffraction patterns of the oriented samples to show their similarities (air-dried patterns).

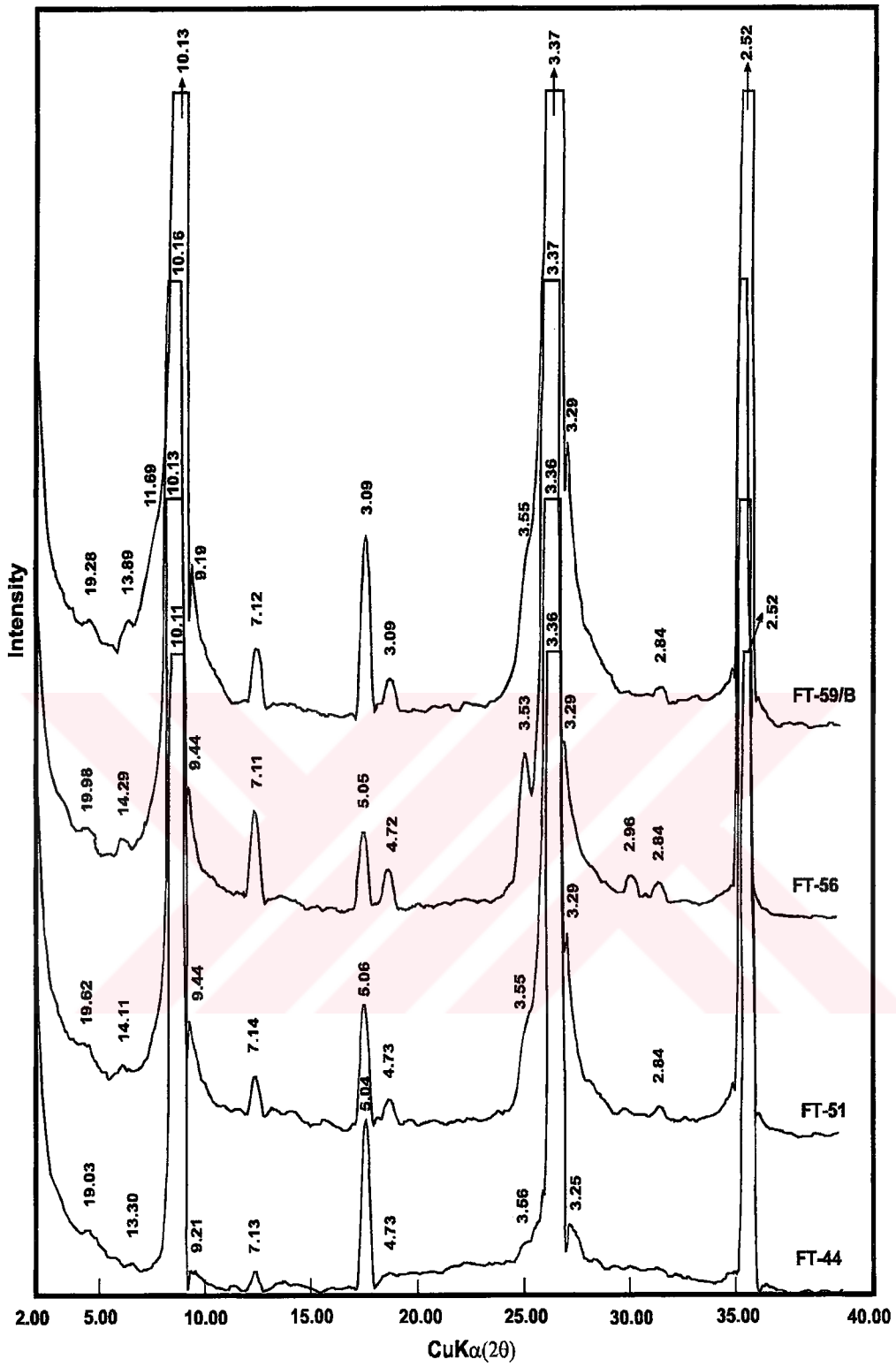

Figure 52 (continued).

samples (Figure 53). Table 3 shows the scheme that was followed during the identification of the analysed samples.

The sample FT-25 among the analysed specimens is chosen to be the representative sample, has a sharp and intense 10.17 Å peak when air-dried, and give 060 reflection of random slides 1.541 Å (Figure 53). These reflections were attributed to mica with trioctahedral type according to the data given by Chen (1977), Bonorino (1959), Nemecz (1981), Bailey (1980). To find out the type of the trioctahedral mica (given in Table 3) XRD patterns of oriented and random specimen were compared with the patterns in the literature (Table 4). Based on the comparison of the data given in Table 4, the specimens were attributed to $2M_1$ phlogopite of trioctahedral mica group having high Mg-content. The observed relatively intense 10.17 Å 001 peak and very weak 002 peak at 5.08 Å on the XRD patterns of the specimens were described as characteristics of the phlogopite by Fanning and Keramidas (1977) and Meunier and Velde (1979). These results were also confirmed by the wet chemical mineral analyses (see Section 4.7.). All of the characteristic peaks of the $2M_1$ phlogopite are present in the studied samples except for basal spacing of 008. The d(008) spacings of the samples are very intense while this spacing in the literature is represented by a very weak intensity (Table 4). This strong reflection may be due to very fine inclusions of anhydrous iron oxide (hematite) present in the phlogopite and could not be removed by magnetic separation. Hematite has also a reflection of 2.52 Å (Brindley and Brown, 1984), and this reflection overlaps with the 008 basal spacing of the phlogopite. XRD data of organic matter saturated and heated phlogopite specimens showed no change on basal reflections (Figure 53).

When the XRD patterns of the samples were examined, it was noticed that, phlogopite is not the pure phase, although it is the highest in amount. There are very small and broad peaks with basal spacings of 13.8-14.25 Å, 7.1-7.25 Å, 4.7-4.75 Å and 3.54-3.57 Å (Figures 52, 53). These peaks were well correlated with the vermiculite data of Barshad (1950), Bassett (1959), Roy and Romo (1957), Nemecz (1981), de la Calle and Suquet (1988),

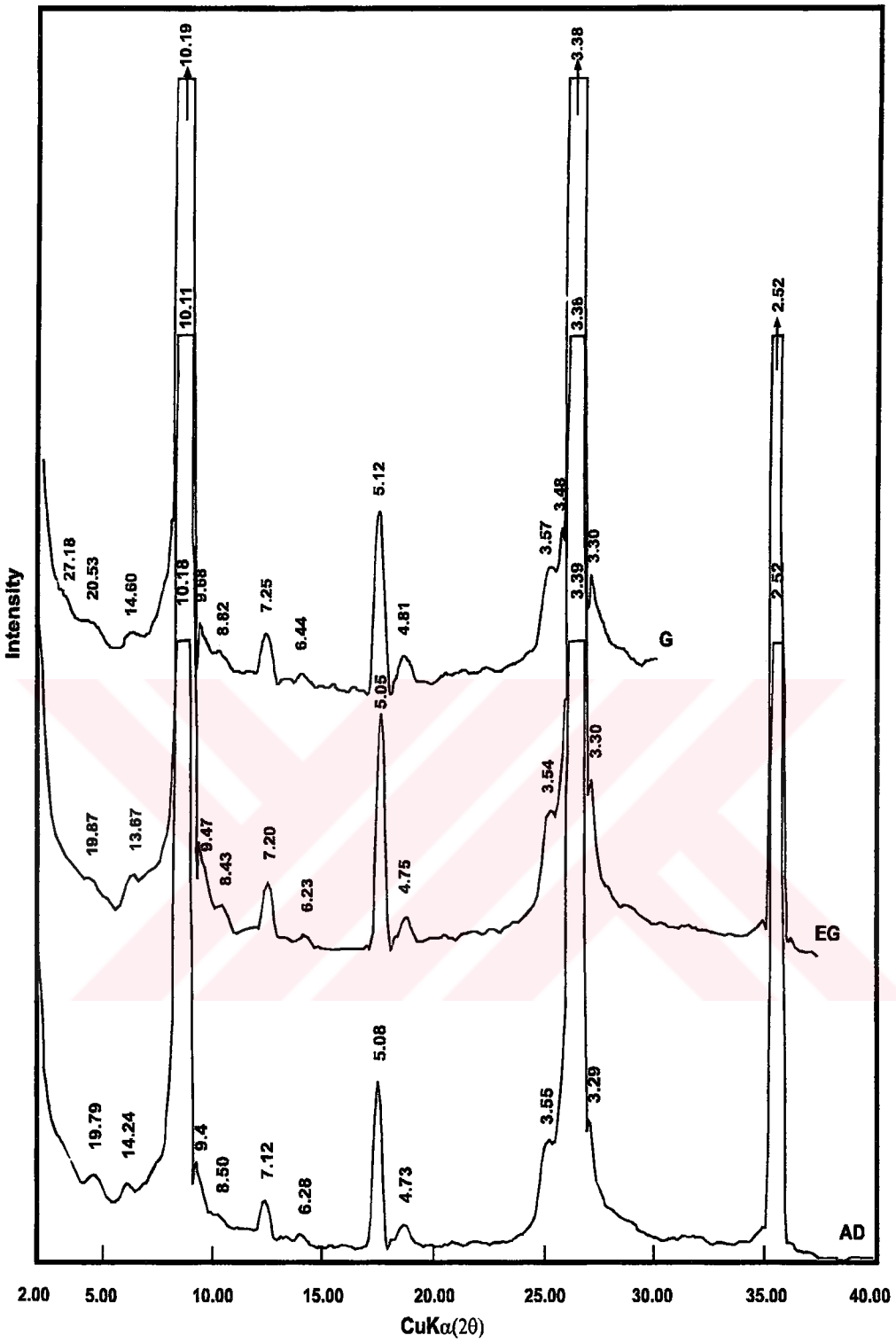

Figure 53. X-ray diffraction patterns of the oriented sample FT-25 representing all the analysed samples (AD: air-dry, EG: ethylene glycol, G: glycerol, heating to 170°C, 350°C and 600°C).

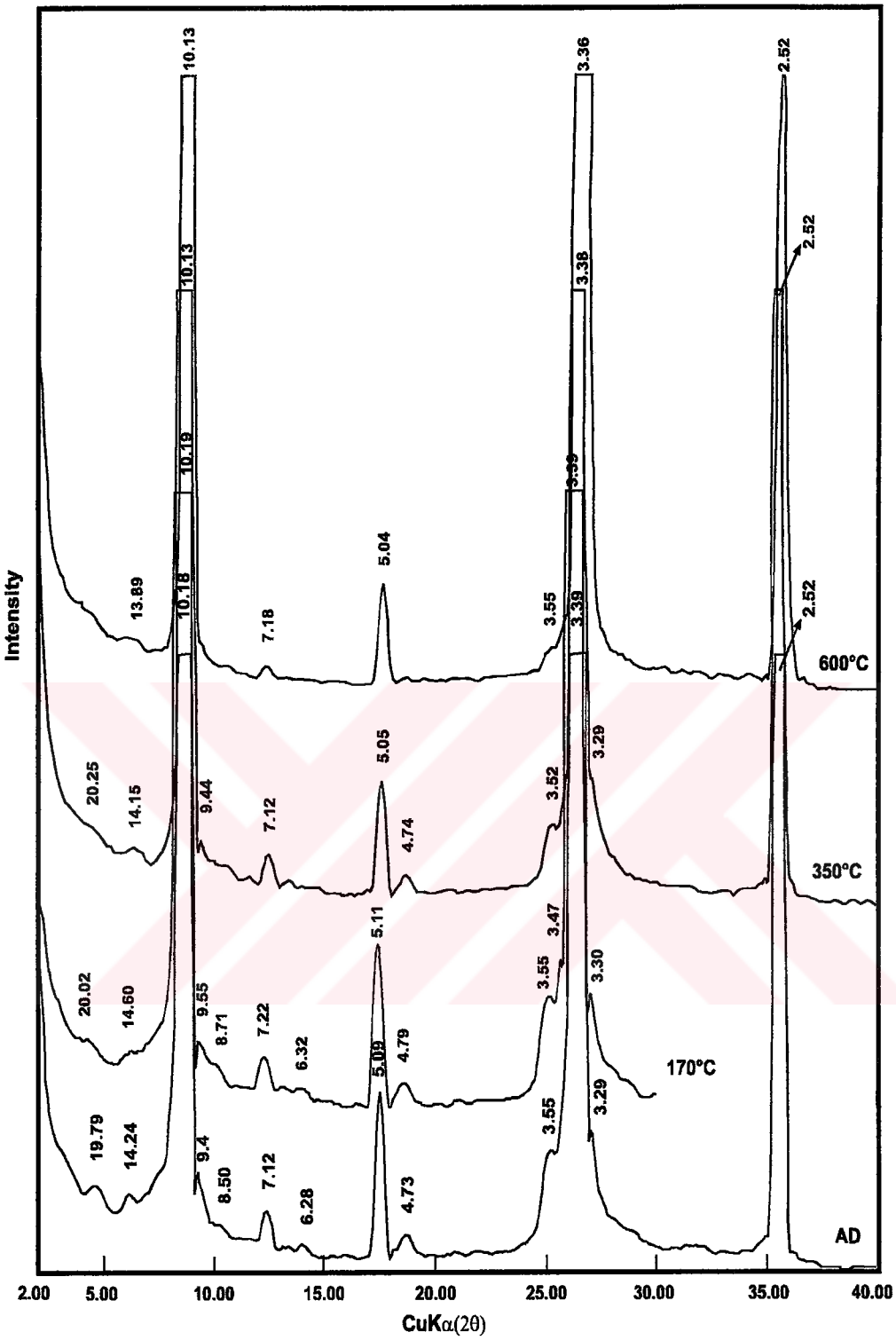

Figure 53 (continued).

Table 3. Identification of the 10 Å mineral (Modified from Nemecz, 1981).

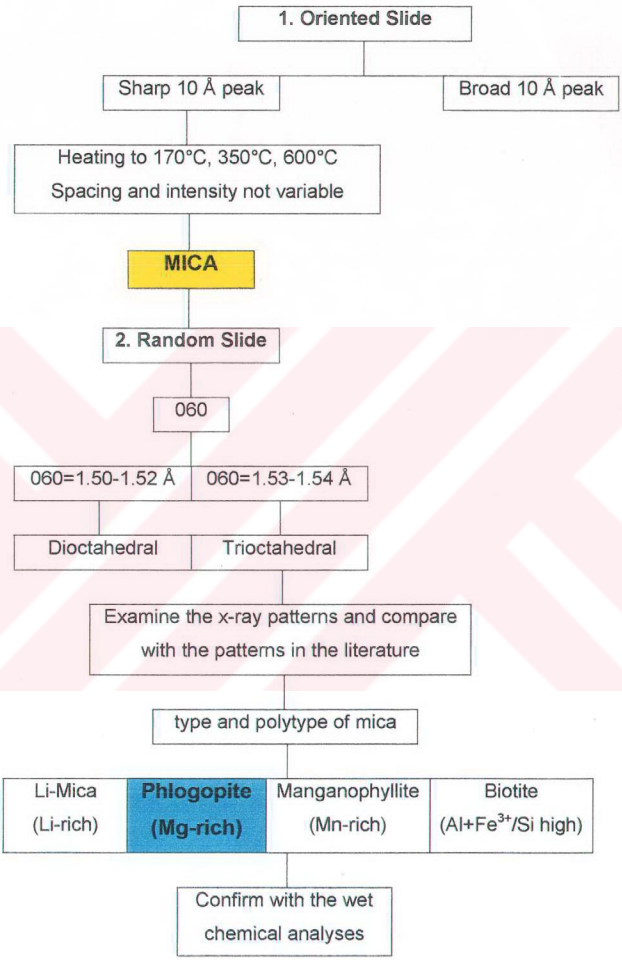

Table 4. XRD data for $2M_1$ phlogopite from literature and for the analysed mica samples from the Kurançalı Metagabbro.

	1		2		3		4		FT-25		FT-32		FT-33		FT-43		FT-44		FT-51		FT-56		FT-59/B	
hkl	d(Å)	I	d(Å)	I	d(Å)	I	d(Å)	I	d(Å)	I	d(Å)	I	d(Å)	I	d(Å)	I	d(Å)	I	d(Å)	I	d(Å)	I	d(Å)	I
002	10.1	100	10.13	vs	10.12	10	10.125	vs	10.18	vs	10.18	vs	10.27	vs	10.11	vs	10.11	vs	10.13	vs	10.13	vs	10.13	vs
004	5.056	20	5.06	w	5.06	2	5.034	w	5.08	w	5.06	w	5.075	w	5.04	w	5.04	w	5.057	w	5.057	w	5.057	w
11 $\bar{4}$	3.54	35	3.54	m	3.54	4	3.540	w	3.53	w	3.54	w	3.54	w	3.54	w	-	-	3.54	w	3.53	w	3.54	w
006	3.362	100	3.36	vs	3.36	10	3.361	m	3.39	m	3.37	m	3.38	m	3.36	m	3.36	m	3.37	m	3.37	m	3.37	m
114	3.283	40	3.28	m	3.283	4	3.282	w	-	-	3.23	w	-	-	-	-	-	-	-	-	3.24	w	3.25	w
11 $\bar{5}$	3.156	10	3.16	vw	3.16	1	3.155	vw	3.14	vw	3.15	vw	3.16	vw	-	-	3.12	vw	3.16	vw	-	-	3.14	vw
025	3.040	40	3.04	s	3.04	4	3.038	m	3.07	m	-	-	3.04	m	-	-	-	-	-	-	3.09	-	-	-
115	2.926	10	2.93	vw	2.93	1	2.923	vw	2.93	vw	2.93	vw	-	-	-	-	-	-	2.94	vw	2.94	vw	-	-
11 $\bar{6}$	2.818	20	2.82	w	2.818	2	2.817	w	2.82	w	-	-	-	-	2.84	w	-	-	-	-	2.82	w	-	-
116	2.624	100	2.62	vs	2.624	8	2.624	vs	2.63	vs	2.63	vs	2.63	vs	2.63	vs	2.64	vs	2.62	vs	2.63	vs	2.63	vs
008	2.522	30	2.52	vw	2.522	4	2.519	vw	2.52	s	2.52	s	2.53	s	2.52	s	2.52	s	2.52	s	2.52	s	2.52	s
133	2.439	40	-	-	-	-	2.437	m	2.44	m	2.44	m	2.45	m	2.44	m	2.45	m	2.44	m	2.44	m	2.44	m
13 $\bar{5}$	2.270	10	-	-	-	-	2.272	vw	2.28	vw	2.27	vw	2.27	vw	-	vw	2.28	vw	2.29	vw	2.27	vw	2.7	vw
135	2.180	10	-	-	-	-	2.181	m	2.18	m	2.18	m	2.18	m	2.18	m	2.18	m	2.18	m	-	-	2.18	m
0010	2. 17	65	-	-	-	-	-	-	-	-	-	-	-	-	-	-	-	-	-	-	-	-	-	-
060	1.538	50	-	-	-	-	1.538	m	1.541	m	1.542	m	1.544	m	1.540	m	1.542	m	1.541	m	1.542	m	1.544	m

1. $2M_1$ phlogopite (Smith and Yoder, 1954 in Fuji et al., 1993)
2. $2M_1$ phlogopite (Smith and Yoder, 1956)
3. $2M_1$ phlogopite (Chen, 1977)
4. $2M_1$ phlogopite (Bailey, 1984)

FT-25, FT-32, FT-33, FT-43, FT-44, FT-51, FT-56, FT-59/B : Studied samples

vs = very strong; w = weak; m = medium; vw = very weak

Suquet et al. (1984), etc. However, their intensities and shapes are not typical of data given in the literature. They may reflect the low order and low amount of vermiculite. In addition to this, a mineral with reflections of around 9.4 Å, 6.2 Å and 3.2 Å having small intensities are also found. This mineral may be attributed to anhydrous vermiculite (i.e., no water layer in its interlayer) when it is compared with the data of Barshad (1950), Walker (1956), Suquet et al. (1984), de la Calle and Suquet (1988), Vali and Hesse (1992), etc. That is to say, two types of vermiculite (two-layer hydrate with 14 Å reflection and anhydrous type with 9.4 Å reflection) are assumed to be present in the studied samples. Some reflections of the vermiculite especially 9.4 Å and 3.29 Å of anhydrous vermiculite and 3.55 Å of two-layer hydrate vermiculite are found on shoulders of the phlogopite reflections causing asymmetry (Figures 52, 53). Tailing of the asymmetrical X-ray reflections is tentatively identified as a mixture of more than one layer silicate (Meunier and Velde, 1979). These tailings are observed as separate peaks where alteration degree of phlogopite is higher (Figure 54). The interstratification is not obvious on the first basal spacing although it is more easily seen around 3.36 Å peak of the phlogopite. In addition to these tailings, there is also a very weak 19.78 Å basal reflection displaying random interstratification of the 10.18 Å of the phlogopite and 9.4 Å of anhydrous vermiculite (Figure 53). The phlogopite samples, FT-32 and FT-43, with the lowest and the highest amount of vermiculitized parts among the studied samples are given Figure 54. XRD patterns of the vermiculites and interstratification of phlogopite and anhydrous vermiculite show negligible expansion on the ethylene glycol and glycerol (Figure 53). Contraction behavior of the two-hydrate vermiculite and anhydrous vermiculite were also examined by heating to 170°C, 350° and 600°C (Figure 53). They do not fully contract although intensities of 3.55 Å and 3.29 Å reflections, especially found on shoulders of 3.39 Å reflection of phlogopite, become less and less. Moreover, 9.4 Å reflection of anhydrous vermiculite also persists to be on shoulder of 10.18 Å reflection of phlogopite.

The best procedure to distinguish the trioctahedral from dioctahedral varieties is to use the position of 060 reflection (Moore and Reynolds, 1989).

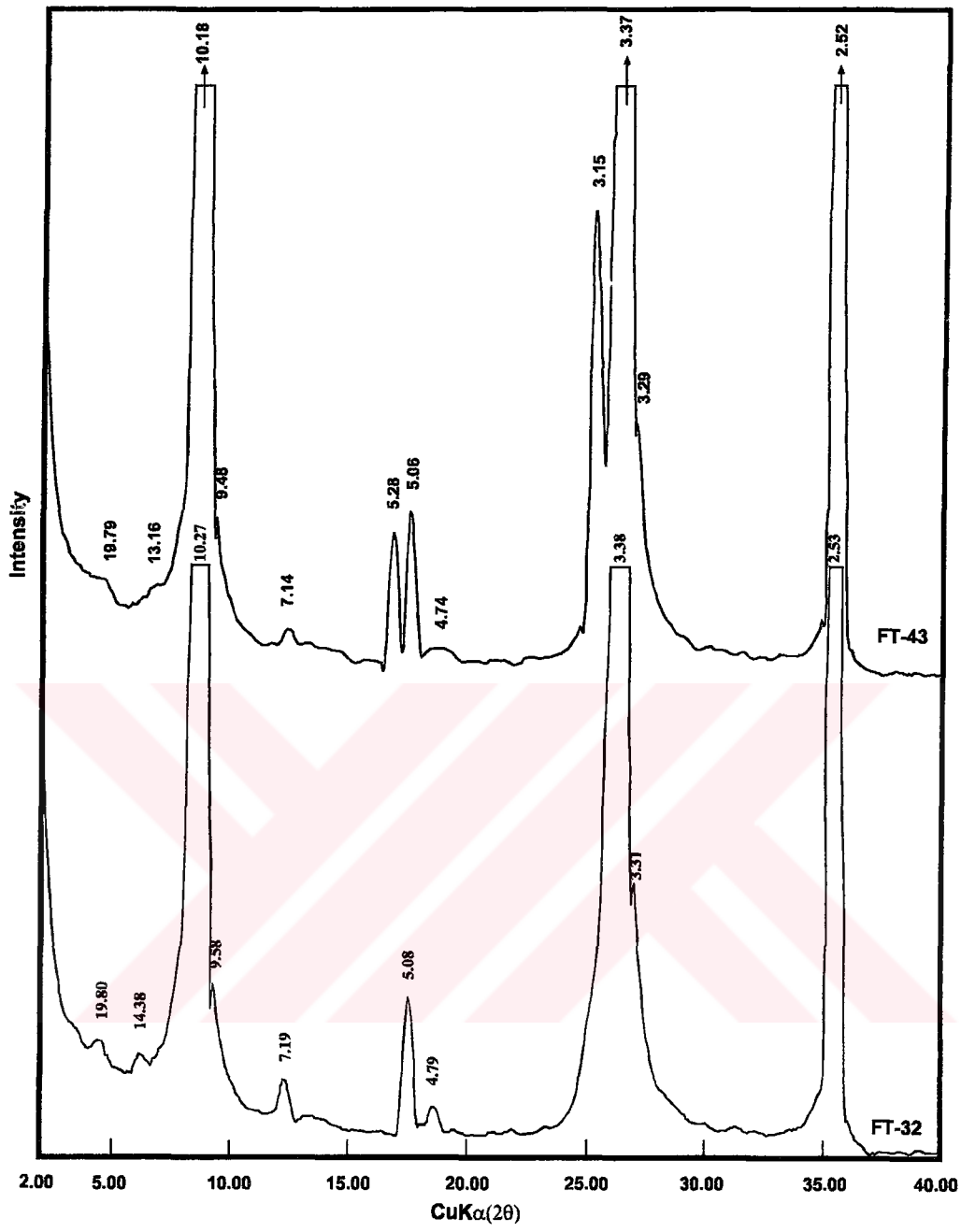

Figure 54. X-ray diffraction patterns of phlogopite samples (FT-43, FT-32, with the highest and the lowest amount of altered parts, respectively) showing different intensities of interstratified phlogopite/vermiculite and vermiculite.

060 reflection of the assumed vermiculites on random XRD patterns is around 1.50-1.52 Å which obeys to 060 reflection of dioctahedral vermiculite in the literature (e.g., Nemecz, 1981; Carroll, 1970; Chen, 1977; Moore and Reynolds, 1989; etc.). That is to say, the assumed vermiculite, although it is low in amount, is dioctahedral type.

Expansion of vermiculite depends on the type of interlayer cation and hydration conditions (e.g., Barshad, 1950; Vali and Hesse, 1992) (Table 5). Anhydrous type of vermiculites does not expand by organic matter saturation (Table 5). The partial and negligible expansion of basal spacing 14 Å with ethylene glycol and glycerol and incomplete contraction on heating in vermiculite, is very probably due to the fact that the studied mineral is a hydroxy-Al (Douglas, 1977; Buurman et al., 1988; April and Newton, 1983; Argast, 1991; Barnhisel, 1977). This interpretation is also in accordance with the SEM-EDS and EMP data.

Although the behaviors of assumed vermiculites and interstratified phlogopite/vermiculite on organic matter saturated and heated specimens were suggested to be due to their hydroxy-Al and anhydrous characters, these behaviors may be also due to their very low amount in the phlogopite-rich samples. That is to say, the true characteristics of the studied vermiculitic material in very low amount may not be accurately represented by XRD method.

The samples suggested to have the highest and the lowest vermiculitized parts among the studied samples are also confirmed by the thermal analyses.

4.6. Thermal Analyses

The thermogravimetric (TGA) and the differential thermal (DTA) measurements were carried out simultaneously with a Rigaru thermal

Table 5. Basal reflections d(002) for vermiculite saturated with various cations as related to ionic radius and charge of ion before and after immersion in water and glycerol (Modified from Barshad, 1950).

Saturating cation		Mg	Ca	Ba	H	Li	Na	K	NH_4	Rb	Cs
Ionic radius (Å)		0.65	0.99	1.35	0.30[Y]	0.60	0.95	1.33	1.48	1.48	1.69
Charge of ion		2	2	2	1	1	1	1	1	1	1
Basal reflection d(002)Å	Before immersion in water	14.33	15.07	12.56	14.33	12.56	12.56	10.42	11.24	11.24	11.97
	After immersion in water	14.47	15.41	15.41	-	15.07	14.76	10.57	11.22	11.22	11.97
	After immersion in glycerol	14.33	14.18	14.33	-	14.33	14.33	10.64	11.22	11.22	11.97

[Y] Covalent radius

instrument using calcined Al_2O_3 as reference for mica specimens from the Kurançalı Metagabbro. The mica samples having interstratifications of phlogopite and vermiculite are purified from pyroxene, hornblende and plagioclase by Frantz isodynamic magnetic separator. Vermiculite could not be separated from mica therefore micas with vermiculitized parts were thermally analysed together from room temperature to 1100°C.

Before interpreting the DTA-TGA curves of the analysed samples, thermal behaviours of the natural vermiculite and phlogopitic end-member of biotite will be explained. On the diffrential thermal analysis curve of vermiculite, loss of either H_2O or OH^- is indicated as an endothermic reaction in literature (e.g., Grim, 1968; Symkatz-Kloss, 1974; Todor, 1976; Nemecz, 1981; de la Calle and Suquet, 1988). The H_2O is held in the lattice by its polarity, while the OH^- is held by ionic bonding, therefore there is a large difference in the temperature at which each compound is driven off. Physically adsorbed water, H_2O, is lost from interlayer position of the vermiculite lattice in two stages with a pair of endothermic peaks at temperatures in the range of 100°C to 300°C (Barshad, 1950; Walker, 1951; Grim, 1968; Roy and Romo, 1957; Mackenzie, 1957; Bassett, 1958; Symkatz-Kloss, 1974; Todor, 1976; Nemecz, 1981; Justo et al., 1987; de la Calle and Suquet, 1988; etc.) (Figure 55). The first stage of dehydration is represented with a peak at around 100°C referring to loss of water molecules not in contact with Mg ions. The second stage represents the loss of a residual monomolecular layer of H_2O in contact with Mg ions and gives an endothermic peak in between 200°C and 300°C. However, vermiculite loses structural OH^- from its lattice and decomposes in the vicinity of 800°C giving an endothermic reaction. According to these authors (op.cit.), there is no reaction or dehydration for vermiculite at a temperature range of 300°C and 800°C. Therefore, in this temperature range the DTA curve is observed as a straight line. However, Suquet et al. (1984) observed the oxidation of ferrous to ferric iron and then progressive dehydration with the appearance of a non-swelling phase -a biopyribole- formed by an enstatite in epitaxial growth on the 010 plane of a non-swelling vermiculite (Figure 56). de la Calle and

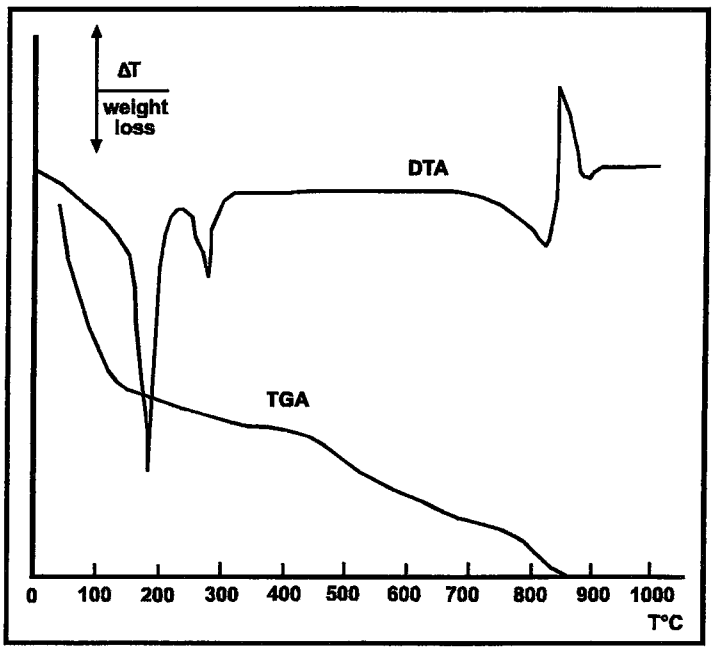

Figure 55. DTA-TGA curves of natural vermiculite (After Nutting, 1943; Grim, 1968).

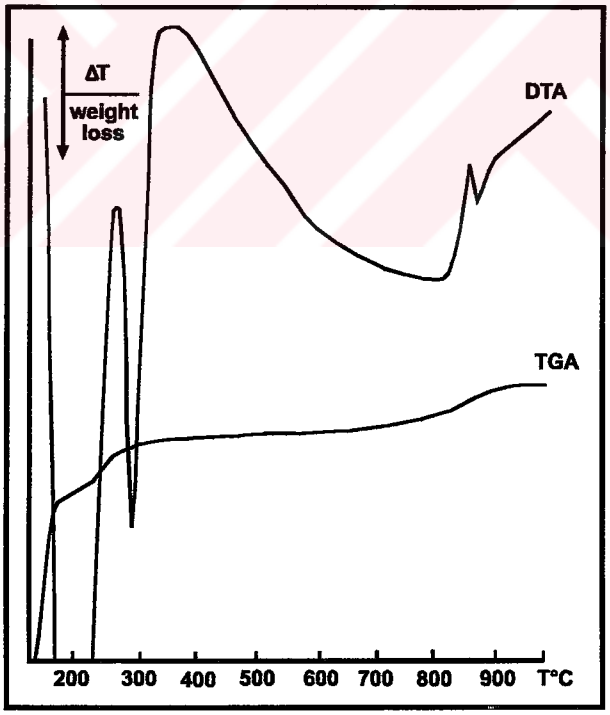

Figure 56. DTA-TGA curves of natural vermiculite (After Suquet et al., 1984).

Suquet (1988) assumed that enstatite must be formed from the hydroxyls linked to trivalent cations, because the dehydration temperature follows the order: Fe^{2+} < Fe^{3+} < Al < Mg (Sarasota and San, 1985). The transformation of biopyribole to oxides (enstatite, cristobalite, forsterite, olivine, etc.) is shown in DTA by the endothermic peaks (800°C and 900°C) separated by an exothermic peak (850°C). Suquet et al. (1984) assigned that; (i) the first endothermic peak at 830°C to the dehydration of the part of the vermiculite which becomes enstatite; (ii) the exothermic peak at 845°C to the crystallization of the enstatite or of a type of mullite (Symkatz-Kloss, 1974); (iii) the endothermic peak at 875°C to the dehydration of the non-swelling phyllosilicate. The intensity of these peaks varies according to the sample, its texture, and the nature of the interlayer cations (Barshad, 1950; Walker and Cole, 1957; Andre, 1972 in de la Calle and Suquet, 1988).

Differential thermal analyses of phlogopitic biotite yield a curve without any pronounced deflections up to 1000°C, indicating the absence of any abrupt dehydration in this temperature range (Grim and Bradley, 1951) (Figure 57). Thermogravimetric curves of biotite and phlogopite in Figure 57 show that phlogopite has a slow, relatively gradual loss of water up to about 800°C without any restricted interval of large water loss while biotite loses water gradually up to about 400°C; it shows very little loss between about 400 and 850°C and considerable loss between 850°C and 1000°C (Roy, 1949). Walker (1949) also presented a dehydration curve for biotite, and, unlike Roy's curve (Figure 57) it shows an almost uniform rate of water loss up to about 850°C, where the dehydration is essentially complete.

The obtained DTA and TG curves for the samples of the Kurançalı Metagabbro do not correspond with data given neither for phlogopite nor for vermiculite in the literature. None of the specimens taken from the Kurançalı Metagabbro, give endothermic peaks of DTA curve at low temperature which are characteristic for vermiculite in the literature (Figure 58). The specimens are steady up to 300°C. The steady behaviour on the DTA curve is characteristic of phlogopite and not of vermiculite may indicate that the

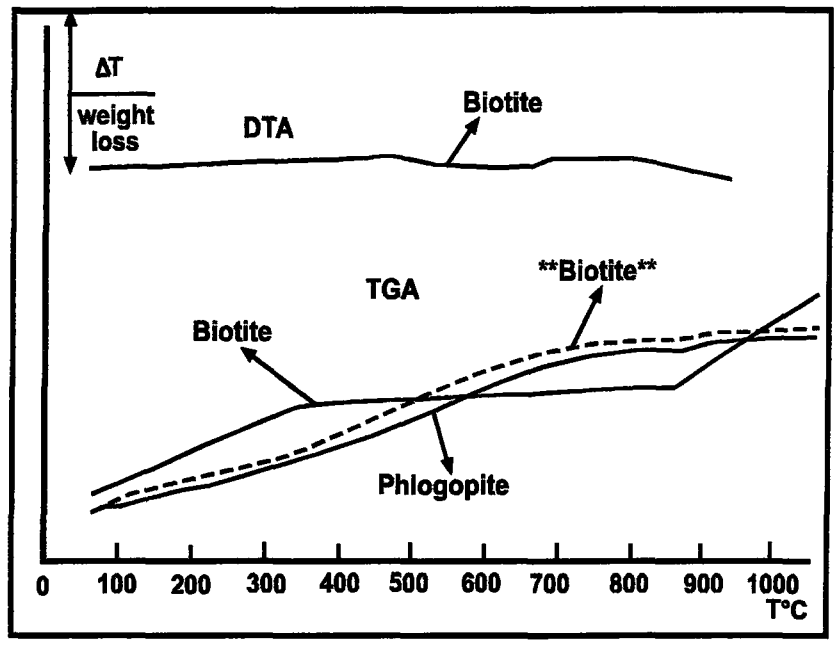

Figure 57. DTA-TGA curves of biotite and phlogopite (After Roy, 1949; ** Walker, 1949; Grim, 1968).

amount of phlogopite is much higher than the amount of vermiculite. There is a too broad and too shallow endothermic reaction taking place in a wide range of temperatures from about 300°C to about 750-800°C. This slight endothermic reaction is assumed to be due to very slow dehydroxlylation of the vermiculitized parts of the phlogopite. The broad, very shallow endothermic effect between 300° and 600°C was preferred to represent the gradual release of strongly held interlayer water in the vermiculitized material (Zhelyaskova-Panayotova et al., 1992). The studied specimens show small broad exothermic peak at about 900°C. As mentioned in the literature reviews of the vermiculite and phlogopite, this exothermic reaction at about 900°C is a characteristic feature of vermiculite and not of phlogopite and represents the crystallization of new oxides. That means, it is caused by the vermiculitized parts of the parent mineral, phlogopite. When the DTA curves of the samples were examined, it was noticed that as the slope of the dehydration curve at temperatures between 300°C and 750-800°C becomes lower (i.e., close to be

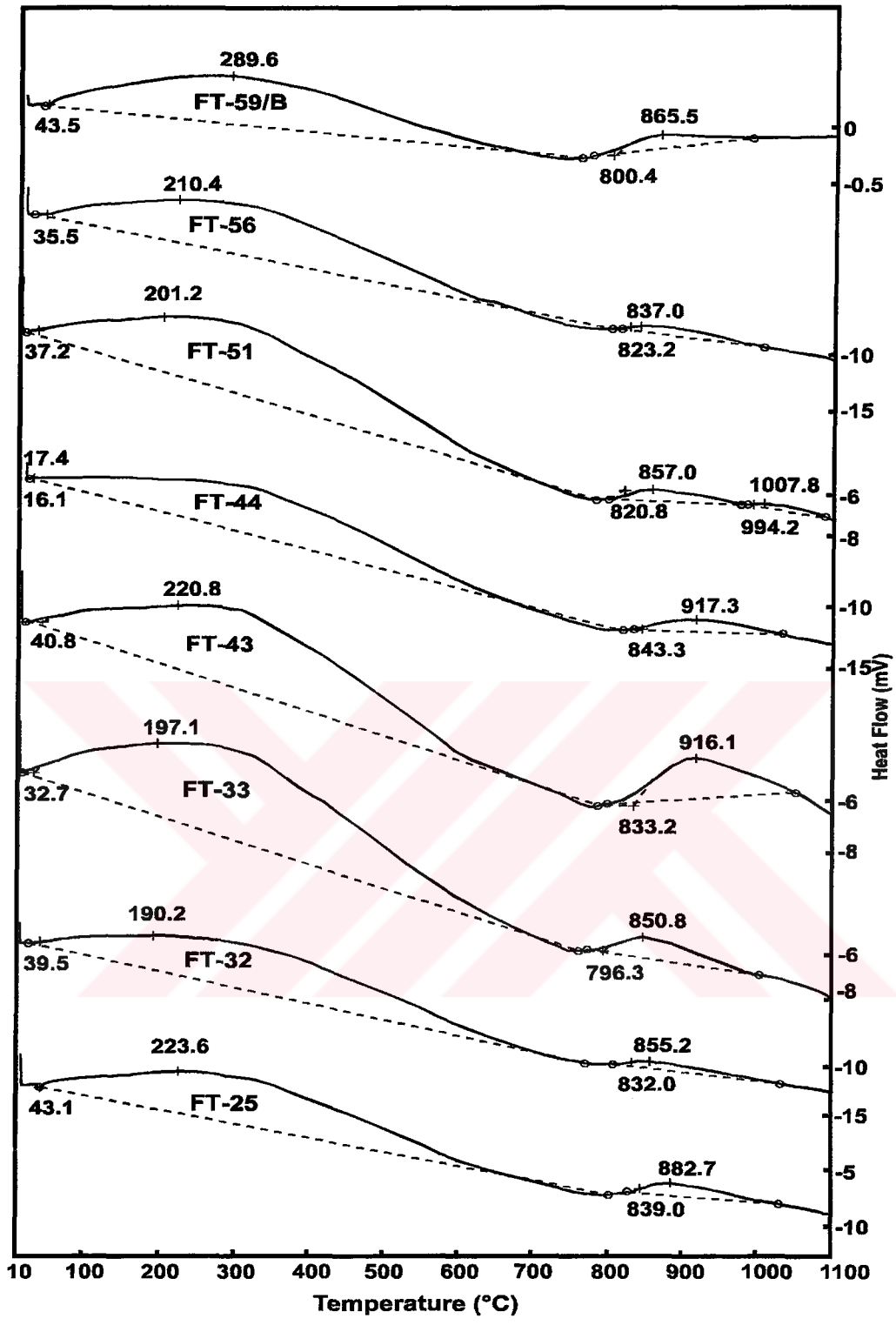

Figure 58. DTA curves of the studied mica samples (FT-25 to FT-59/B: sample numbers).

steady) the height of the exothermic curve becomes smaller. This observation may indicate that this type of specimens have lower amount of vermiculitized parts.

The very slow dehydration observed on the DTA is accompanied by small inflections in the weight loss curve (i.e., TGA curve) (Figure 59). The samples FT-43 and FT-51 show continuous weight loss from about 10°C to 1100°C while others display stepwise weight losses. The weight losses of the samples vary from 0.7% to 2.5%.

The simultaneous DTA-TGA measurements resulted in that all mica samples from Kurançalı Metagabbro have phlogopite with varying amounts of vermiculite or interstratified phlogopite/vermiculite phases. The vermiculite or randomly interstratified phases replacing phlogopitic mica is few which was also detected by XRD (see Section 4.5.). Figure 60 shows the associated DTA-TGA curves of the analysed samples, FT-32 and FT-43, with the highest and the lowest alteration products.

4.7. Inductively Coupled Plasma Spectrometry Analyses

Chemical analyses were carried out on mineral separates (pyroxene, hornblende and phlogopite) from the Kurançalı Metagabbro by inductively coupled plasma spectrometry (ICP). The results are expressed in oxide form and the total iron was given in Fe_2O_3 form. To allocate the ICP total iron values to Fe^{2+} and Fe^{3+}, same samples were decomposed in an orthophenanthroline complex and Fe^{2+} was measured colormetrically by a spectrophotometry. The compositions and unit cell contents of the representative minerals are given in Tables 6, 7 and 8. The compositional changes among the analysed mineral separates are summarized in Figure 61. According to this graph (major oxides vs. weight %) it is easily seen that there is a continuous depletion in SiO_2 and CaO from pyroxene through amphibole to dark mica while K_2O increases. However, Al_2O_3, TiO_2, MgO, K_2O and H_2O contents of the dark mica are strongly higher than those of

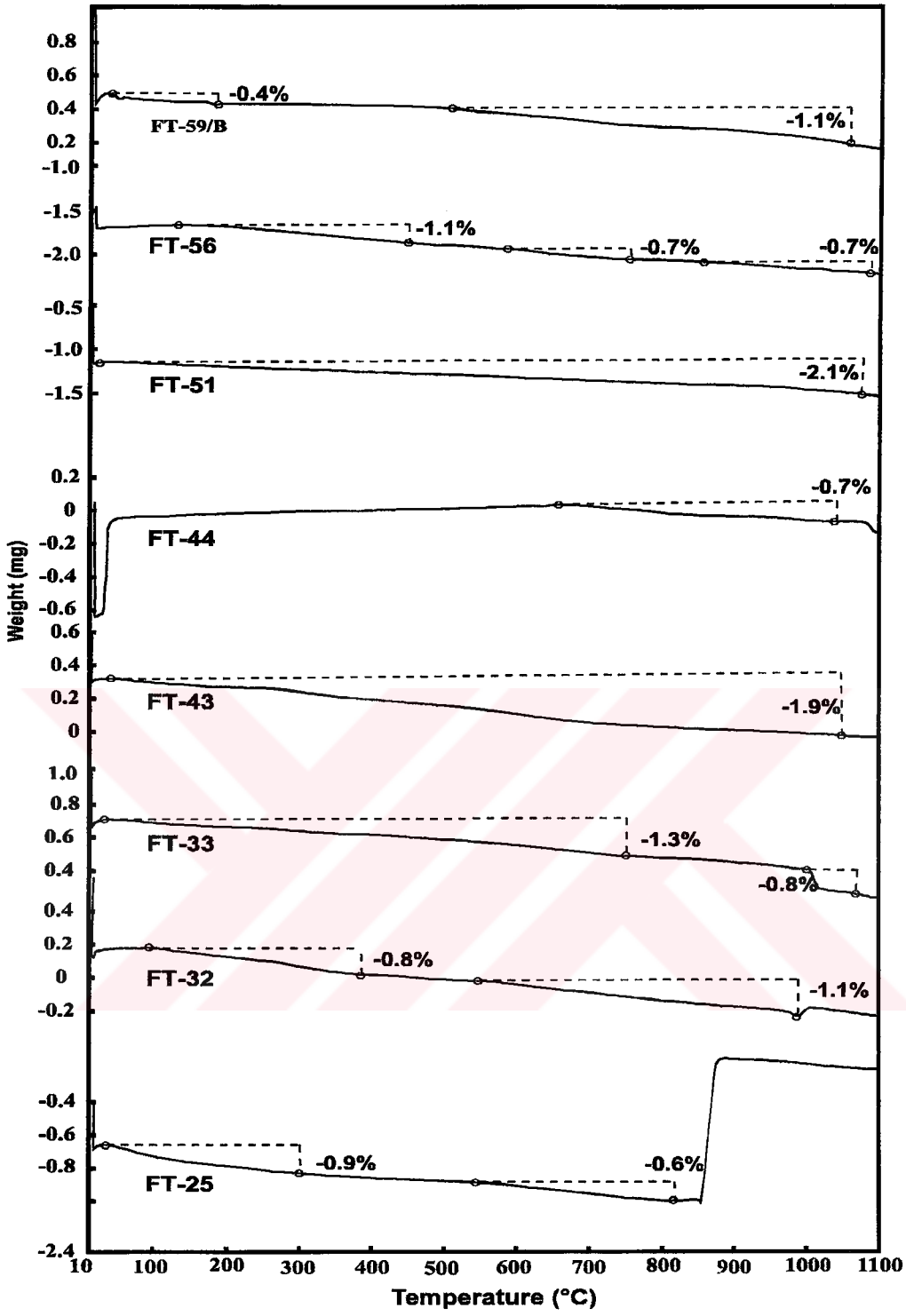

Figure 59. TGA curves of the studied mica samples (FT-25 to FT-59/B: sample numbers).

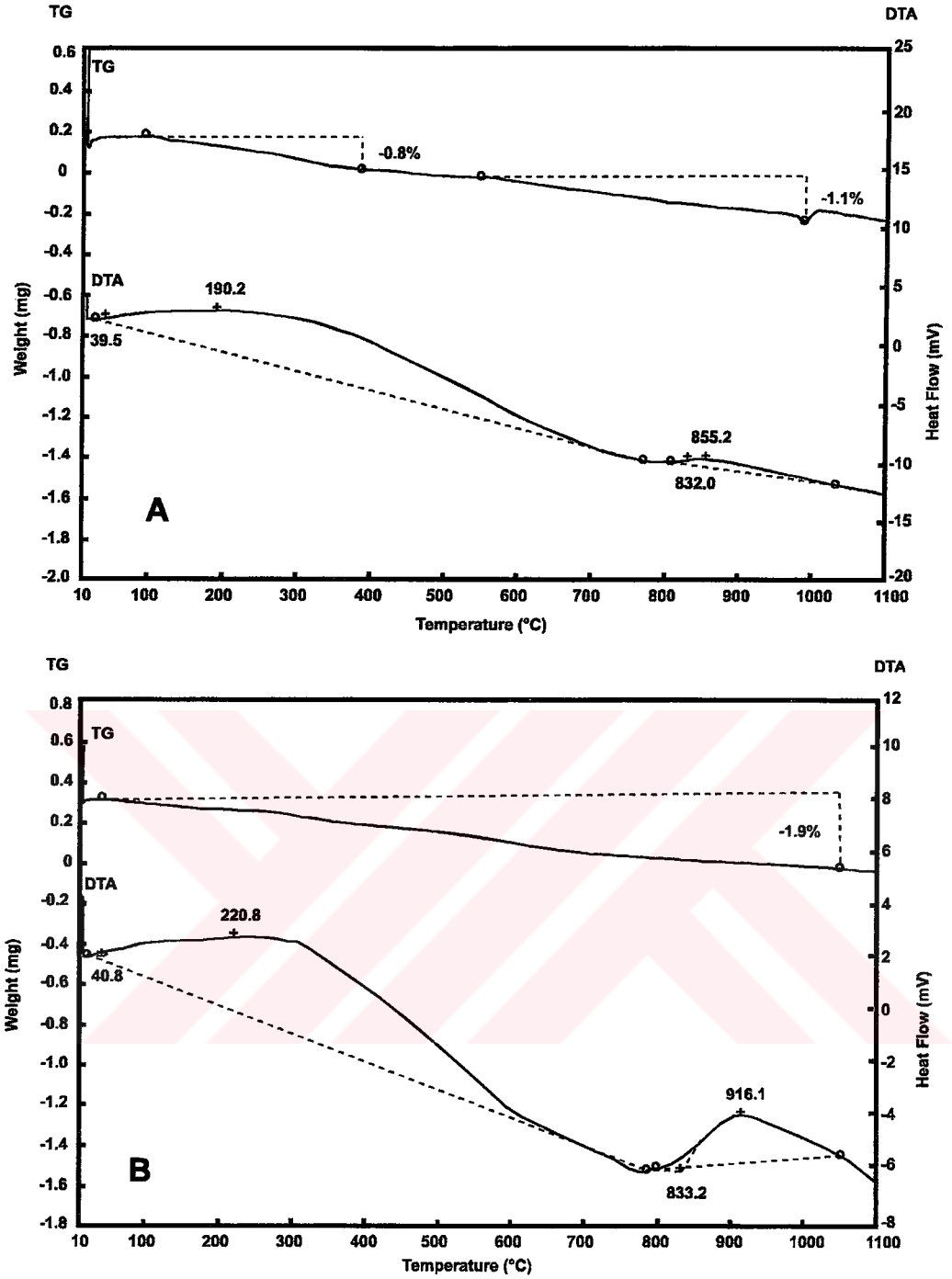

Figure 60. DTA-TGA curves of two mica samples having both the least (A: FT-32) and the highest (B: FT-43) vermiculite interstratification.

Table 6. Compositions and structural formula of representative pyroxene samples.

Major oxides \ Samples	FT-26	FT-111
SiO_2	48.65	47.90
Al_2O_3	7.73	8.16
TiO_2	0.9	0.99
FeO	10.1	9.8
Fe_2O_3	1.2	0.7
MgO	9.89	10.42
CaO	20.91	20.57
Na_2O	0.52	0.40
K_2O	0.09	0.11
LOI*	0.23	0.15
Total	100.22	99.2
Si	1.832	1.811
Al	0.330	0.363
Ti	0.026	0.028
Fe^{2+}	0.318	0.310
Fe^{3+}	0.034	0.020
Mg	0.555	0.587
Ca	0.844	0.833
Na	0.038	0.030
K	0.005	0.006
En	32.33	33.93
Fs	18.53	17.91
Wo	49.14	48.16
Fe:Mg	0.3643	0.3456

FT-26, FT-111 : samples from pyroxene gabbro
*: Loss on ignition, $Fe:Mg=Fe^{2+}/(Fe^{2+}+Mg^{2+})$
$En=100xMg/(Mg+Fe^{2+}+Ca)$; $Fs=100xFe^{2+}/(Mg+Fe^{2+}+Ca)$;
$Wo=100xMg/(Mg+Fe^{2+}+Ca)$

Table 7. Compositions and structural formula of representative amphibole samples.

Major oxides \ Samples	FT-66	FT-410
SiO_2	44.27	44.08
Al_2O_3	12.97	12.01
TiO_2	1.87	1.89
FeO	9.86	11.63
Fe_2O_3	6.0	6.14
MgO	9.21	8.84
CaO	11.32	11.93
Na_2O	1.45	1.22
K_2O	1.64	1.21
LOI*	0.78	0.27
Total	99.37	99.22
Si	6.453	6.465
Al^{IV}	1.547	1.535
Al^{VI}	0.682	0.541
Ti	0.205	0.209
Fe^{2+}	1.202	1.427
Fe^{3+}	0.675	0.679
Mg	2.000	1.932
Ca	1.769	1.874
Na	0.410	0.347
K	0.305	0.227
$(Ca+Na)_B$	2	2
Na_B	0.2314	0.1256
$(Na+K)_A$	0.4834	0.449
$Mg/(Mg+Fe^{2+})$	0.62	0.58

FT-66, FT-410 : samples from hornblende gabbro
*: Loss on ignition
$(Ca+Na)_B$, Na_B and $(Na+K)_A$: Numbers in B and A sites of the standard formula given by Leake (1978) $(A_{0-1}B_2C^{VI}_5T^{IV}_8O_{22}(OH,F,Cl)_2)$.

Table 8. Compositions and structural formula of representative mica samples.

Major oxides / Samples	FT-32	FT-43	FT-59/B
SiO_2	41.11	39.10	38.35
Al_2O_3	13.89	15.89	15.86
TiO_2	2.81	2.63	2.86
FeO	11.23	13.67	10.62
Fe_2O_3	5.9	6.02	5.92
MgO	12.50	10.34	13.82
CaO	0.23	0.44	0.20
Na_2O	0.25	0.22	0.27
K_2O	8.91	8.39	8.77
LOI*	2.65	2.67	2.80
Total	99.48	99.37	99.47
Si	5.955	5.826	5.693
Al^{IV}	2.045	2.174	2.307
Al^{VI}	0.327	0.206	0.433
Ti	0.306	0.506	0.315
Fe^{2+}	0.644	0.653	0.653
Fe^{3+}	1.361	1.662	1.302
Mg	2.698	2.239	3.019
Ca	0.036	0.069	0.032
Na	0.070	0.063	0.078
K	1.647	1.556	1.640
Fe:Mg	0.3352	0.4260	0.3013
f_{com}	64.82	71.32	54.48

FT-32, FT-43, FT-59/B : samples from phlogopite-gabbro
*: Loss on ignition
$Fe:Mg=Fe^{2+}/(Fe^{2+}+Mg^{2+})$
$f_{com}=((2Fe_2O_3+FeO)x(2Fe_2O_3+FeO+MgO)^{-1})x100$

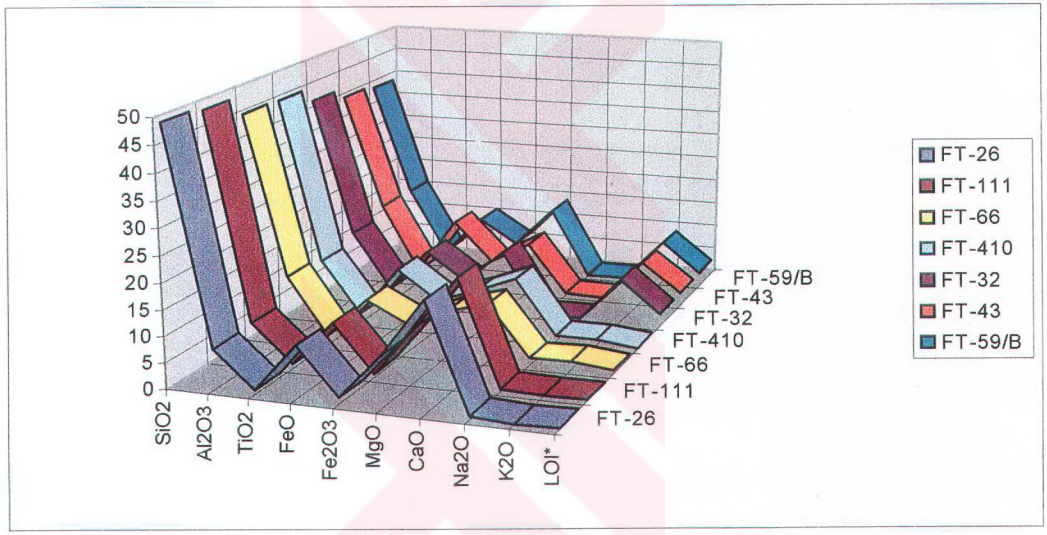

Figure 61. Graph showing the compositional change in the separate minerals.

pyroxene. This observation supports the data obtained semi-quantitatively by EMP.

Structural formula for the minerals were calculated using the method described by Deer et al. (1980) which is given in Appendix C. The structural formula were calculated assuming anhydrous form on the basis 23 oxygens for amphiboles, 22 oxygens for micas and 6 oxygens for pyroxenes. Anydrous basis was taken to care because the measured H_2O^+ may be erroneous and F, Cl were not measured during analyses. The cell contents of the minerals converted from major oxides for structural formula are given in Tables 6, 7 and 8. The calculated unit cell contents are real only for fractions that contain well-defined minerals.The presence of contaminants which could not be separated by Frantz isodynamic magnetic separator may cause erronenous results, although the purification of the minerals was provided more than 95% for pyroxene and hornblende, and 98% for mica. In additon, the minor alteration products (vermiculite in mica, secondary amphibole in pyroxene, secondary mica in hornblende) in spite of their low amount may cause erroneous results.

The obtained unit cell contents were used for the nomenclature of the minerals. The results for pyroxene were plotted on Wo-En-Fs diagram prepared by Morimoto et al. (1988) (Figure 62). According to these plots, analysed pyroxene are defined to be diopsidic ($En_{32.33}Fs_{18.53}Wo_{49.14}$-$En_{34.93}Fs_{17.91}Wo_{48.16}$) in composition which were interpreted as diopsidic augite by petrographic and semi-quantitative SEM-EDS, EMP studies.

The amphibole samples were interpreted and named using the classification and nomenclature given by Leake (1978). The calculations were made on the basis of the Leake's standard formula definition ($A_{0\text{-}1}B_2C^{VI}{}_5T^{IV}{}_8O_{22}(OH,F,Cl)_2$) given in Appendix D. The values obtained fit well with calcic amphibole group having $(Ca+Na)_B \geq 1.34$ and $Na_B < 0.67$. The studied samples plots on the tschermakitic hornblende area of the calcic amphiboles (Figure 63).

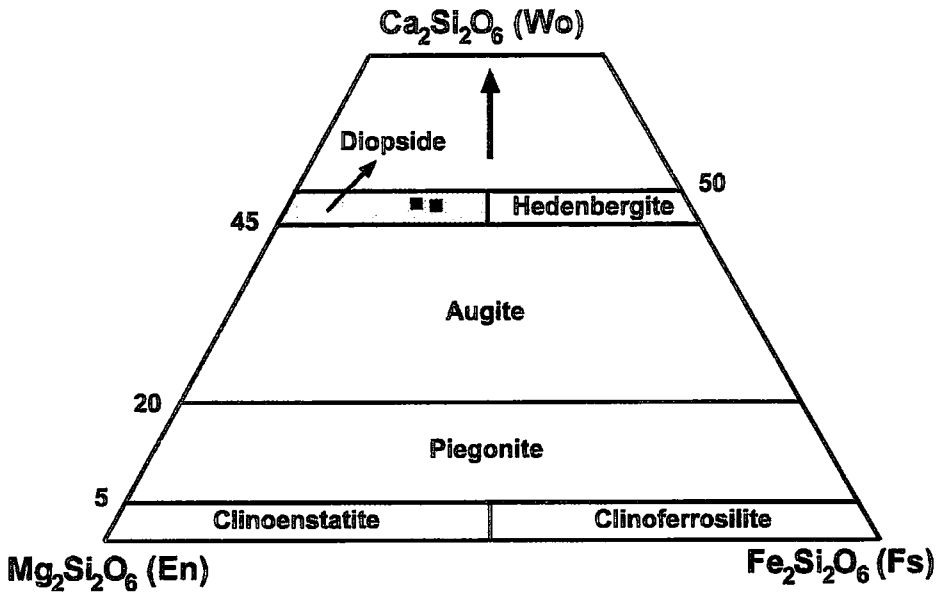

Figure 62. Plots of clinopyroxenes from the pyroxene-gabbro samples on the pyroxene quadrilateral diagram (After Morimoto et al., 1988).

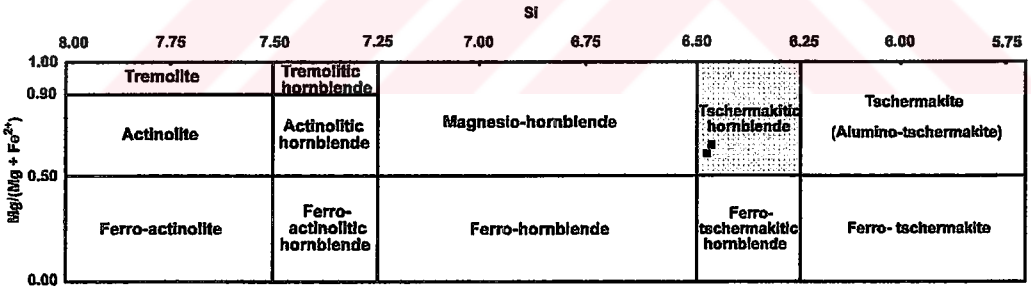

Figure 63. Plots of amphibole samples on the Si and Mg/(Mg+Fe^{2+}) diagram for $(Ca+Na)_B \geq 1.34$, $Na_B < 0.67$, $(Na+K) < 0.50$ and $Ti < 0.50$ (After Leake, 1978).

The structural formula of the analysed hornblende separates are $(Na,K)_{0.4834}(Ca,Na)_2(Al^{VI},Ti,Fe^{3+},Mg,Fe^{2+})_{4.764}(Si,Al)_8O_{22}(OH,F,Cl)_2$ - $(Na,K)_{0.449}(Ca,Na)_2(Al^{VI},Ti,Fe^{3+},Mg,Fe^{2+})_{4.80}(Si,Al)_8O_{22}(OH,F,Cl)_2$.

Reddish brown, purplish greenish mica is classified as Mg-biotite (phlogopitic) by plotting the analytical data given in Table 3 on the Mg-$Fe^{2+}(Mn^{2+})$-$R^{3+}(Al,Fe^{3+},Ti)$ diagram described for trioctahedral micas by Forster (1960) (Figure 64). For nomenclature, the data is also plotted onto the phlogopite-annite-siderophyllite-eastonite rectangle of Deer et al. (1980). According to these plots, one of the dark micas displays Mg-rich biotite composition (close to the phlogopite area) while two of them plot on phlogopite area within the range of $phlogopite_{(69.87-57.40)}$ - $annite_{(30.13-42.60)}$ (Figure 65). This data is in good accordance with the results of petrographic, XRD, and thermal analyses.

The Fe-common ($f_{com}=(2Fe_2O_3+FeO)x(2Fe_2O_3+FeO+MgO)^{-1})x100$) of phlogopite which is used for the classification vermiculite deposits by Lvova (1974) is very high for the studied samples. It is within the range of 54.48 and 71.32. According to Lvova (1974), the associated rocks and the geodynamic conditions of their formation, properties of the parent mica (structure, f_{com}, F quantity, etc.) which depend on the host rock, are the main controlling factors of the vermiculite formation under exogenous conditions (i.e., weathering crusts of sialilic type). The phlogopitic micas in the study area may be classified in the Group B Type 4 of Lvova's (1974) classification. In this class, the magmatic (cumulate) sequence of ophiolite complexes (peridotites, pyroxenites and gabbros) are host rocks and they occur as ophiolitic boudens within the highly crystalline basement rocks (consisting of gneisses, amphibolites, mica-schists and marbles) as is the case in the study area. Their f_{com} values are rather high (20-40). But calculated f_{com} values of the studied samples are higher than this range (Table 8). This high iron content in the phlogopitic mica may be caused by the submicroscopic iron-oxide inclusions that were identified by thin section investigations but could not be removed from the purified samples.

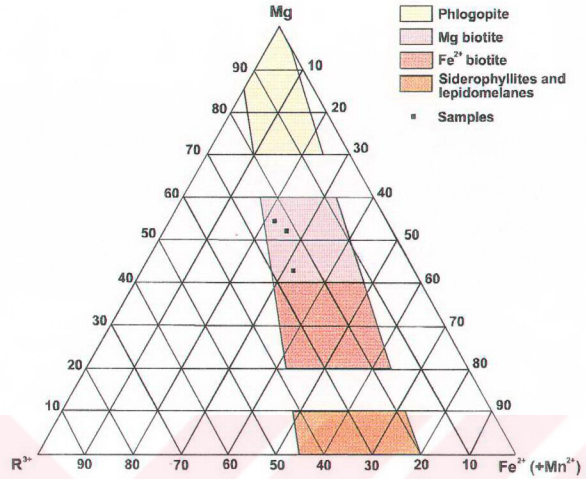

Figure 64. Plots of dark mica samples on the triangular diagram showing relation between Mg, Fe^{2+} (Mn^{2+}), and R^{3+} (Al, Fe^{3+}, and Ti) in trioctahedral micas (After Foster, 1960).

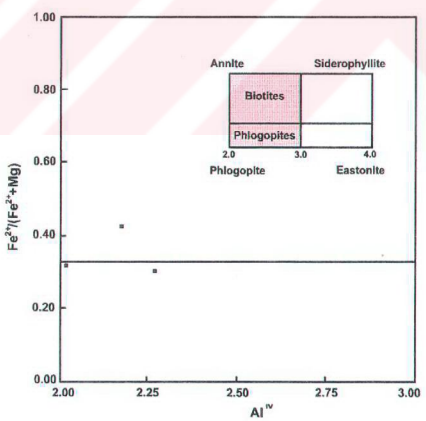

Figure 65. Plots of dark mica samples on the phlogopite-annite-eastonite-siderophyllite quadrilateral showing $Fe^{2+}/(Fe^{2+}+Mg)$ and Al^{IV} relation (After Deer et al., 1980).

CHAPTER 5

DISCUSSION

The metagabbro from Kurançalı (Kırşehir) was interpreted in terms of geology, petrography and mineralogy in the previous chapters. The metamorphic rocks underlying the metagabbro in the study area were also geologically and petrographically defined. In this chapter, the geological and petrogenetical implications of new findings will be discussed. However, the main emphasis will be on the vermiculite formation.

The Kurançalı Metagabbro and the underlying metamorphic ophiolitic complex from Kurançalı area (northwest of Kırşehir) are observed to be thrusted onto Aşıgediği Formation of CAM (Göncüoğlu, 1977; Göncüoğlu et al., 1991, 1992, 1993a) or Aşıgediği Metamorphics of Göncüoğlu et al. (1998). This metagabbro together with the underlying metamorphic ophiolitic rocks were, however, called as Hacıselimli formation by Kara and Dönmez (1990). According to these authors, the metagabbro is a stock and the amphibolites are dykes and sills that intruded the sedimentary units during the syn- and/or post-sedimentational period. They were then metamorphosed and deformed together with the host sedimentary rocks. Kara and Dönmez also correlated these units with the basic intrusive rocks of Ketin (1955) and Ayan (1963), Sineksizyayla metagabbros of Göncüoğlu (1977), and gabbros existing in the Ortaköy granitoid of Atabey et al. (1987).

Later, Göncüoğlu et al. (1992), Yalınız (1996), Yalınız and Göncüoğlu (1998) interpreted the Kurançalı Metagabbro as a part of the CAO which is in

thrust contact with the underlying metamorphic ophiolitic rocks. This suggestion is confirmed in this study. However, Göncüoğlu et al. (1992) put forward that the Kurançalı Metagabbro is overthrusting the Gümüşler Formation of the CAM (Göncüoğlu, 1977, 1981; Göncüoğlu et al., 1991, 1992) considering the amphibolites underlying the metagabbro as equivalents of the those in the Gümüşler Formation. In a recent work, Yalınız and Göncüoğlu (1998) noticed that the metagabbro is thrusted onto the subophiolitic metamorphics. In this study, the metamorphic rocks including calcsilicate amphibolites, calcsilicate cherty marbles with lenses and blocks of metaserpentinites and amphibolites were interpreted to be equivalents of the metamorphic ophiolitic complex of Göncüoğlu et al. (1991, 1998) but neither of amphibolites of Gümüşler Formation nor of the subophiolitic metamorphics. The Kurançalı Metagabbro and the metamorphic ophiolitic complex are separated with a sheared zone comprising boudens of metagabbro, metaserpentinite and amphibolite. The Kurançalı Metagabbro and underlying metamorphic ophiolitic units were altogether thrusted onto massif marbles of the Aşıgediği Formation of the CAM along a steep contact and not onto the Gümüşler Formation as suggested by Göncüoğlu et al. (1992).

The felsic dykes that are alkali-feldspar granite, alkali-feldspar quartz syenite and quartz syenite in composition, are called as the Kurançalı Granitoid in the study area. The Kurançalı Granitoid is a part of the CAG of Göncüoğlu et al. (1991, 1992). The dykes intrude the metagabbro, sheared zone and metamorphic ophiolitic complex. However, Yalınız's (1996) interpretation that the Kurançalı Metagabbro was cut by plagiogranites of CAO, could not be confirmed.

The Kurançalı Metagabbro shows a distinct magmatic layering. However, this magmatic layering was misidentified by Kara and Dönmez (1990) that the layering is caused by metamorphism. The metagabbro is variable in size from microscopic to pegmatitic and heterogeneous in composition. It is mainly composed of varying amounts of clinopyroxene,

primary and secondary amphibole, primary and secondary dark mica (phlogopite and biotite, respectively), and plagioclase. According to the mineralogical composition, the individual layers have been described as phlogopite gabbro, pyroxene-phlogopite gabbro, pyroxene gabbro (pyroxenite), pyroxene-hornblende gabbro, pyroxene-plagioclase gabbro, hornblende gabbro, hornblende-plagioclase gabbro, plagioclase-hornblende pegmatitic gabbro, hornblende pegmatitic gabbro.

The phlogopite observed in the studied samples was assumed to be of primary origin while secondary biotite was suggested to be the alteration product from pyroxene and amphibole which is resulted from the effects of K-rich solutions rising with the intruding K-feldspar rich granitic dykes. Biotite and amphibole having secondary origin were also investigated by Bayhan (1986) from gabbros intruded by Çelebi granitoid and by Önen (1985), Önen and Unan (1988) from gabbros around Kaman region.

The most characteristic feature of the Kurançalı Metagabbro is the presence of the primary phlogopite. In terms of the phlogopite-annite series of biotite, phlogopite from the Kurançalı Metagabbro display remarkably low $Fe^{2+}/(Fe^{2+}+Mg)$ (i.e., Fe:Mg) ratio of 30-40. The atomic ratio of $[Fe^{2+}/(Fe^{2+}+Mg)]x100$ has been related to the temperature and f_{O_2} which prevailed during biotite crystallization (Wones and Eugster, 1965). According to Wones and Eugster (1965), the phlogopitic trend with low $Fe^{2+}/(Fe^{2+}+Mg)$ represents constant or slightly increasing f_{O_2}, H_2O saturation in the melt during crystallization and cooling. Later studies showed that the crystallization paths of biotite from various igneous complexes (Czamanske and Wones, 1973; Haslam, 1968; Lalonde and Martin, 1983) display variable degrees of decreasing $Fe^{2+}/(Fe^{2+}+Mg)$ with the differentiation, which is believed to result from increasing or constant f_{O_2} during crystallization. However, biotites interpreted by Nash and Wilkinson (1970) display an opposite trend with increasing $Fe^{2+}/(Fe^{2+}+Mg)$ which was explained with increasing f_{O_2} during its primary crystallization. Rowins et al. (1991) assumed that these low $Fe^{2+}/(Fe^{2+}+Mg)$ ratios in biotite (phlogopitic) are not the result

of modification by an overprint of late stage fluid as was interpreted to have caused similarly uniform $Fe^{2+}/(Fe^{2+}+Mg)$ ratios in biotite in several felsic plutons (e.g., Dodge and Moore, 1968; Mahmood, 1983). The low $Fe^{2+}/(Fe^{2+}+Mg)$ is also reflected in coexisting clinopyroxenes to a slightly lesser degree (34-36) representing oxidizing magmatic conditions. According Rowins et al. (1991), these compositional trends with low $Fe^{2+}/(Fe^{2+}+Mg)$ in biotite is unmistakably magmatic although the minor development of hydrous replacement minerals indicate the limited extent of late- to post-magmatic fluid alteration.

Absence of olivine and orthopyroxene is a characteristic feature of the phlogopite-bearing Kurançalı Metagabbro. Absence of these two minerals and presence of phlogopite may be explained by suggestions given by Hewitt and Wones (1984). According to Hewitt and Wones (1984), siliceous liquids rising into a peridotitic mantle cause precipitated zones of phlogopite. The ultra-potassic magmas are generated from the phlogopite rich portions of the mantle. Phlogopite-bearing peridotite react to produce higher silica content at low pressures and lower silica contents at high pressures. Phlogopites can directly crystallize from the melt, or by a reaction with olivine and orthopyroxene at crustal levels. Drops in temperature while maintaining H_2O pressure and total pressure would lead olivine and/or orthopyroxene with a potassic liquid to form phlogopite.

The amphibole samples from the Kurançalı Metagabbro having high-Ti values (1.87-1.89 wt%) may have an importance for the assumption of the primary phlogopite. Because Johnson et al. (1996) assumed that high Ti-amphiboles (0.82-3.66 wt%) generally have high K_2O suggesting a transition to K-rich environment where phlogopite might occur with amphibole. High-Ti (>1.5 wt%) is also characteristic of interaction between magma and peridotite resulting in the formation of hydrous upper mantle (Johnson et al., 1996). Phlogopite and high-K amphibole can be stabilized in the subduction environment at depths >110 km (Sudo and Tatsumi, 1990; Thompson, 1992; Davies, 1994). Therefore, in areas of ancient convergence, a subduction-

derived fluid component could be preserved and recycled by, e.g., a later episode of magmatism related to rifting. The agent that produces mica is presumed to be a high-K melt (see references in Johnson et al., 1996). In brief, the occurrence of phlogopite and Ti-rich amphibole may indicate the preservation of ancient subduction characteristics that have been overprinted by a rifting (see references in Johnson et al., 1996). Therefore, phlogopite occurrence in the study area, which is studied for the first time, may have important petrologic implications, such as a hybridization of magmas above subducted oceanic crust. This very general approach is in good accordance with the interpretation of Göncüoğlu and Türeli (1993), Yalınız et al. (1996) and Yalınız and Göncüoğlu (1998) that the CAO are of supra-subduction type and related to a fore-arc extension within the İzmir-Ankara-Erzincan oceanic crust. Thus, the studied phlogopite-bearing gabbro of the CAO having the unusual wholerock composition (Kenan Yalınız, written communication) must be investigated in detail in terms of petrology, which is not the subject of this Master's Thesis study.

One of the most characteristic features of the phlogopite bearing Kurançalı Metagabbro and the main topic of this thesis is the vermiculitization of phlogopite. Based on the XRD data, two types of vermiculite are present in the studied samples, hydroxy-Al and anhydrous vermiculites. Douglas (1977) studied the similar type vermiculites showing no expansion on organic matter saturation or contraction on heating in one of the largest vermiculite mines in the United States, near Libby, Montana. He found out that, vermiculite formation in an augite pyroxenite body does not follow the normal path of occurrence. The type of vermiculite seems to indicate that there are some hydroxy-cation complexes (not developed into complete sheets) rather than hydrated cations in the interlayer space. Because it remains almost steady on heating and/or organic matter saturation. According to Douglas, the resulted vermiculite was hydroxy-Al variety of dioctahedral vermiculite.

Although the transformation of phlogopite to vermiculite is not fully understood, the occurrence of interstratified mica/vermiculite observed in this

study, have been generally accepted to form during transformation of mica to vermiculite (e.g., Jackson, 1963; Barshad, 1949; Walker, 1949; Fanning and Keramidas, 1977). As recognized on the studied samples, the transformation of phlogopite to vermiculite requires a structural change from trioctahedral to dioctahedral hydroxy-Al and anhydrous types which is induced by chemical changes. The most commonly observed reaction for the transformation of phlogopite to vermiculite involves loss of interlayer K and introduction of a hydrated Mg-Fe-Al interlayer (Barshad, 1950; Roy and Romo, 1957; Fanning and Keramidas, 1977; Banfield and Eggleton, 1988; Moon et al., 1994). This mechanism proceed releasing K, Si, Ti, and requiring a small amount of Mg, Fe or Al besides water and oxygen, and oxidation of ferrous to ferric iron. The conversion of phlogopite to vermiculite is initiated as $K=H_3O^-$ exchange, which opened up the interlayer spaces and promoted access of oxygen required for the oxidation of octahedral Fe (Banfield and Eggleton, 1988). Oxidation is apparently compensated by redistribution of some octahedral Al (replacing Si in the tetrahedral sheet) and loss of octahedral cations. The loss of octahedral cations of phlogopite during weathering in an acidic environment may result in their replacement by Al and tend to favor the development of hydroxy-Al interlayers in the vermiculites from the surface (Garrels and Christ, 1965; Douglas, 1977; May et al., 1979; Moon et al., 1994) forming the aluminous dioctahedral vermiculite. According to Moon et al. (1994), the early stage vermiculitization of phlogopite proceeds by means of a continuous decrease of Al-for-Si tetrahedral substitutions and a progressive increase of Al-for-(Mg-Fe^{2+}) octahedral substitutions with weathering. The excess Al is assumed to be used in the interlayer spaces. Vicente et al. (1977), Holdren and Berner (1979), Argast (1991) also suggested that source of the Al for the hydroxy-Al interlayers can be precipitated from an aqueous species derived from the simultaneous weathering and dissolution of associated feldspar as well as it derivation from the phlogopite.

In addition to necessity of hydroxy-Al vermiculite for weathering in acidic environment, the presence of anhydrous vermiculite could be also explained by early stage alteration according to Vali and Hesse (1992).

The elemental changes from phlogopite to vermiculite (K-depletion, slight decrease in Si, Al-enrichment) were observed by semi-quantitative electron microprobe analyses although these changes could not be detected by wet chemical analyses because of the limited amount of vermiculite in phlogopite.

The origin of the trioctahedral variety of vermiculite is still discussed while the dioctahedral variety is unquestionably accepted as the product of low temperature surface weathering in the literature (e.g., Gruner, 1934, 1939; Hendricks and Jefferson, 1938a,b; Brown, 1953; Hattaway, 1955; Walker, 1957; Deer et al., 1980; Barshad and Kishk, 1969; Graham et al., 1989; Moon et al., 1994; April et al., 1986). The occurrence of the trioctahedral variety is assumed to be due to hydrothermal solutions (Varley, 1948; Hadley, 1949; Hagner, 1944; Morel, 1955) or due to supergene solutions (e.g., Gevers, 1948; Kulp and Brobst, 1954; Clabaugh and Barnes, 1959; Justo et al., 1986; de la Calle and Suquet, 1988; Lvova, 1974), or combination of two (Palabora Mining Co. Staff, 1976; Bassett, 1959; Zhelyaskova-Panayotova, 1989; Zhelyaskova-Panayotova et al., 1992, 1993). Experimental studies done in this purpose resulted in that vermiculite is alteration product of micas due to effects of solutions having low alkali content (e.g., Barshad, 1948; Bassett, 1959; Roy and Romo, 1957; Komarneni and Roy; 1981). Some field evidences suggest the hydrothermal fluids effects such as; association of vermiculite with high temperature minerals and rocks, its presence at depths over 200 ft, the presence of vermiculite in proximity to pegmatites and felsic dykes while some other field evidences indicate supergene formation such as; the increase in the proportion of biotite and phlogopite with depth, the presence of unaltered biotite in the interior of pyroxenite. In the study area, vermiculitized phlogopite is present either in close proximity to the K-feldspar rich granitic dykes and/or

away from the dykes. In addition, according to experimental studies, alkali content of the solutions forming vermiculite must be low. That is to say, K-rich solutions rising together with the granitic dykes are not responsible for the formation of vermiculite but they are responsible for secondary biotite formation. During the petrographic studies, vermiculite from secondary biotite could not be recognized in the studied samples. Probably K-rich solutions prevent the vermiculite formation from secondary biotite.

Discussions on previous studies and petrographical-mineralogical data obtained in this study indicate that the dioctahedral hydroxy-Al and anhydrous vermiculite from primary phlogopite unquestionably represent early stage weathering.

In the initiation of this study, our assumption was that there is a continuous alteration of clinopyroxene → secondary hornblende → secondary biotite → vermiculite. Detailed petrographic works on textures and mineralogical studies have shown that clinopyroxene, hornblende and phlogopite were formed as primary magmatic phases. The formation of secondary amphibole in clinopyroxene (uralitization) is very probably a late stage hydrothermal event (autometasomatism). The formation the green-brown biotite (both in pyroxene, hornblende and phlogopitic biotite) is interpreted to be the result of K-metasomatism, related to the intrusion of K-rich granitic dykes of the CAG. The formation of vermiculite, on the other hand, is found to be a reaction that only involved in primary phlogopite.

Vermiculite occurrence observed in the phlogopite-bearing Kurançalı Metagabbro is found in only few locations in the CACC.

CHAPTER 6

CONCLUSIONS AND RECOMMENDATIONS

1. The Kurançalı Metagabbro is a part of the Central Anatolian Ophiolites.

2. The Kurançalı Metagabbro is thrusted onto the rock units of metamorphic ophiolitic complex of the CACC along a steep contact that in turn is thrusted on the Aşıgediği Metamorphics of the CAM. There is a mega shear zone between the Kurançalı Metagabbro and the metamorphic ophiolitic complex. The shear zone includes highly deformed rocks of both slivers.

3. Both the Kurançalı Metagabbro and the underlying metamorphic ophiolitic complex are cut by the Kurançalı Granitoid. It intrudes the host as irregular, thin dykes of alkali-feldspar granite, alkali-feldspar quartz syenite and quartz syenite composition. The dykes display well-developed mylonitic textures.

4. The Kurançalı Metagabbro is characterized by its layering either in composition or in grain size. Individual bands are described as phlogopite gabbro, pyroxene-phlogopite gabbro, pyroxene gabbro (pyroxenite), pyroxene-hornblende gabbro, pyroxene-plagioclase gabbro, hornblende gabbro, hornblende-plagioclase gabbro, plagioclase-hornblende pegmatitic gabbro, hornblende pegmatitic gabbro.

5. The Kurançalı Metagabbro is petrographically composed of varying amount of diopsidic augite, hornblende, phlogopite and plagioclase, and shows cumulate textures. The accessory minerals are sphene, magnetite and hematite. The alteration minerals are secondary hornblende, actinolitic hornblende, secondary biotite, vermiculite, albite, calcite, sericite and epidote.

6. The metagabbro is characterized by the absence of olivine and orthopyroxene.

7. The metamorphic ophiolitic complex mainly comprises calcsilicate rocks with interlayers of biotite-gneiss, metacarbonates, calcsilicate carbonate rocks and blocks of amphibolites, calcsilicate amphibolites and metaserpentinites. From the petrographic study, the protoliths of metamorphic rocks can be suggested as clastic and carbonate rocks for calcsilicate, calcsilicate carbonate, calcsilicate amphibolite and metacarbonate rocks while basic magmatic rocks are suggested for amphibolites.

8. The Kurançalı Granitoid is variable in composition. Majority of constituent minerals is represented by K-feldspar and partly by quartz. Plagioclase, hornblende, biotite, clinopyroxene, muscovite are also present in minor amount. Apatite, zircon, sphene are the accessory minerals. Hematite and magnetite are opaques.

9. Mineral ICP data on purified samples of the Kurançalı Metagabbro showed that the pyroxenes are diopsidic ($En_{32.33}Fs_{18.53}Wo_{49.14}$ - $En_{34.93}Fs_{17.91}Wo_{48.16}$), amphiboles are thschermakitic hornblende ($(Na,K)_{0.4834}(Ca,Na)_2(Al^{VI},Ti,Fe^{3+},Mg,Fe^{2+})_{4.764}(Si,Al)_8O_{22}(OH,F,Cl)_2$ - $(Na,K)_{0.449}(Ca,Na)_2(Al^{VI},Ti,Fe^{3+},Mg,Fe^{2+})_{4.80}(Si,Al)_8O_{22}(OH,F,Cl)_2$) and the dark micas are Fe-rich phlogopitic ($phlogopite_{(69.87-57.40)}$ - $annite_{(30.13-42.60)}$) in composition. It is shown that the most characteristic feature of the Kurançalı Metagabbro is the dominance of the primary phlogopitic mica. The unusual wholerock chemistry of these metagabbros may be used to discuss a petrogenetic model for the Central Anatolian Ophiolites.

10. It is suggested that the formation of vermiculite is not the product of a continuous reaction from clinopyroxene → secondary hornblende → secondary biotite → vermiculite but involves phlogopitic biotite → vermiculite.

11. The transformation of trioctahedral phlogopite to dioctahedral vermiculite is discussed. It is concluded that vermiculites, hydroxy-Al and anhydrous varieties, seem to represent an earlier stage of weathering in acidic environment.

12. The variations of Al^{IV}, Al^{VI}, Fe^{2+}, Fe^{3+}, Mg, Al contents showing the trends of compositional changes during transformation of phlogopite to vermiculite at the early stage of weathering, could not be observed step by step because detailed EMP analyses were not available for this study. Analyses by quantitative electron microprobe, infra-red and transmission electron microscope are needed for a detailed study on vermiculitization process.

13. It is recommended for future work that the investigated primary phlogopite-bearing metagabbro of the CAO in the Kurançalı area must be studied in detail in terms of petrology.

REFERENCES

Akıman, O., Erler, A., Göncüoğlu, M.C., Güleç, N., Geven, A., Türeli, K., and Kadıoğlu, Y.K., 1993. Geochemical characteristics of granitoids along the western margin of the Central Anatolian Crystalline Complex and their tectonic implications. Geological Journal, 28, 371-382.

April, R.H., and Newton, R.M., 1983. Mineralogy and chemistry of some Adirondack Spodosols. Soil Science, 135, 301-307.

April, R.H., Hluchy, M.M., and Newton, R.M., 1986. The nature of vermiculite in Adirondack soils and till. Clays and Clay Minerals, 34(5), 549-556.

Argast, S., 1991. Chlorite vermiculitization and pyroxene etching in an aeolian periglacial sand dune, Allen county, Indiana. Clays and Clay Minerals, 39(6), 622-633.

Atabey, E., Tarhan, N., Papak, İ., Akarsu, B., and Taşkıran, A., 1987. Ortaköy, Tuzköy (Nevşehir) – Kesikköprü (Kırşehir) yöresinin jeolojisi: MTA Rapor No: 8156, Ankara (unpublished).

Ayan, M., 1963. Contribution a l'etude petrographique de la region situee au Nord-Est de Kaman. MTA Yayını, Ankara, 115, 1-332.

Bailey, S.W., 1980. Structures of layer silicates. In: Brindley, G.W., and Brown, G. (eds.), Crystal Structures of Clay Minerals and their X-Ray Identification, Monograph No. 5, Mineralogical Society, London, 1-123.

Bailey, B.K., 1982. Mantle metasomatism – continuing chemical change within the earth. Nature, 296, 525-530.

Bailey, S.W., 1984. Review of cation ordering in micas. Clays and Clay Minerals, 32(2), 81-92.

Bailey, S.W., 1985. Classification and structures of micas. In: Bailey, S.W. (ed.), Micas, Mineralogical Reviews, 13, Washington, D.C., Mineralogical Society of America, 1-13.

Banfield, J.F., and Eggleton, R.A., 1988. Transmission electron microscope study of biotite weathering. Clays and Clay Minerals, 36, 382-403.

Barnhisel, R.I., 1977. Chlorites and hydroxy interlayered vermiculite and smectite. In: Dixon, J.B., and Weed, S.B. (eds.), Minerals in Soil Environments, Soil Sci. Soc. Amer., Madison, Wisconsin, 331-356.

Barnhisel, R.I., and Bertsch, P.M., 1989. Chlorites and hydoxy-interlayered vermiculite and smectite. In: Dixon, J.B., and Weed, S.B. (eds.), Minerals in Soil Environment, Soil Sci. Soc. Amer., Madison, Wisconsin, 729-788.

Barshad, I., 1948. Vermiculite and its relation to bioite as revealed by base exchange reactions: X-ray analyses, diffethermal curves, and water content. American Mineralogist, 33, 655-678.

Barshad, I., 1949. The nature of lattice expansion and its relation to hydration in montmorillonite and vermiculite. American Mineralogist, 34, 675-684.

Barshad, I., 1950. The effect of interlayer cations on the expansion of the mica type crystal lattice. American Mineralogist, 35, 225-238.

Barshad, I., 1952. Factors affecting the interlayer expansion of vermiculite and montmorillonite with organic substances. Soil Sci. Soc. Apl. Proc., 16, 176-182.

Barshad, I., 1954a. Cation exchange in micaceous minerals: I. Replaceability of the interlayer cations of vermiculites with ammonium and potassium ions. Soil Science, 77, 463-472.

Barshad, I., 1954b. Cation exchange in micaceous minerals. II. Replaceability of the interlayer cations of vermiculites with ammonium and potassium from vermiculite, biotite and montmorillonite. Soil Science, 78, 57-76.

Barshad, I., and Kishk, F.M., 1969. Chemical composition of soil vermiculite as related to their genesis. Contrib. Mineral. Petrol., 24, 136-155.

Bassett, W.A., 1958. Copper vermiculites from Northern Rhodesia. American Mineralogist, 43, 1112-1133.

Bassett, W.A., 1959. The origin of vermiculite deposit at Libby, Montana. American Mineralogist, 44, 282-299.

Bassett, W.A., 1960. Role of hydroxyl orientation in mica alteration. Bull. Geol. Soc. Amer., 71, 449-456.

Bassett, W.A., 1963. The geology of vermiculite occurrence. Clays and Clays Minerals, 10, 61-69.

Bayhan, H., 1986. İç Anadolu granitoyid kuşağındaki Çelebi sokulumunun jeokimyası ve kökensel yorumu. Jeoloji Mühendisliği, 29, 27-36.

Bayhan, H., 1990. Ortaköy granitoyidinin (Tuz Gölü doğusu) mineralojik, petrografik ve jeokimyasal incelenmesi. TÜBİTAK, Proje No. TBAG-841, 68 p. (unpublished).

Beaufort, D., 1987. Interstratified chlorite/smectite ("metamorphic vermiculite") in the upper Precambrian greywackes of Rouez, Sarthe, France. In: Schultz, L.G., van Oplhen, H., and Mumpton, F.A. (eds.), The Clay Mineral Society, Bloomington, Indiana, 59-65.

Black, P.M., 1975. Mineralogy of New Caledonian metamorphic rocks, IV. sheet silicates from Onegoa district. Contrib. Mineral. Petrol., 49, 269-284.

Bonorino, F.G., 1959. Hydrothermal alteration in the Front Range mineral belt, Colorado. Bull. Geol. Soc. Amer., 70, 53-90.

Brindley, G.W., and Brown, G., 1984. Crystal Structure of Clay Minerals and their X-ray Identification. Mineralogical Society, Monograph No. 5, London, 495 p.

Brown, G., 1953. The dioctahedral analoque of vermiculite. Clay Min. Bull., 6, 195-210.

Buchardt, W.S., 1954. Geology of Central Anatolia. MTA Rapor No: 2675, Ankara (unpublished).

Bush, A.L., 1976. Vermiculite in the United States. In: Rooney, L.F., and Berg, R.B. (eds.), Proceeding of Eleventh Forum on the Geology of Industrial Minerals Montana Bur. Mines and Geol. Sp. Pub. 74, pp. 145-155.

Buurman, P., Meijer, E.L., and van Wijck, J.H., 1988. Weathering of chlorite and vermiculite in ultramafic rocks of Cabo Ortegal, Northwestern Spain. Clay and Clay Minerals, 36, 263-269.

de la Calle, C., and Suquet, H., 1988. Vermiculite. In: Bailey, S.W. (ed.), Hydrous Phyllosilicates (Exclusive of Micas), Reviews in Mineralogy, v. 19, Min. Soc. Amer., Washington, D.C., 455-496.

de la Calle, C., Dubernat, J., Suquet, H., Pezerat, H., Gaultier, J.P., and Mamy, J., 1976. Crystal structure of two layer Mg-vermiculites and Na, Ca-vermiculites. In: Bailey, S.W. (ed.), Proc. Int'l Clay Conf., Mexico, 1975, Applied Publishing Ltd., Illinois, 201-209.

Carroll, D., 1970. Clay Minerals: A Guide to Their X-ray Identification. Geol. Soc. Amer., Special Paper 126, United States, 80 p.

Cerny, P., and Burt, D.M., 1984. Paragenesis, crystallochemical characteristics, and geochemical evolution of micas in granite pegmatites. In: Bailey, S.W. (ed.), Micas, Reviews in Mineralogy, Mineral. Soc. Amer., BookCrafters Inc., Michigan, 257-297.

Chen, P.-Y., 1977. Table of key lines in the x-ray powder diffraction patterns of minerals in clays and associated rocks. Department of Natural Resources, Geological Survey Occasional Paper 21, Authority of the State of Indiana, Bloomington, Indiana, 67 p.

Clabaugh, S.E., and Barnes, V.E., 1959. Vermiculite in Central Texas. Texas Univ., Bur. Econ. Geol. Rept. Invest. 40-45.

Crowley, M.S., and Roy, R., 1964. Crystalline solubility in the muscovite and phlogopite groups. American Mineralogist, 49, 348-363.

Czamanske, G.K., and Wones, D.R., 1973. Oxidation during magmatic differentiation, Finnmarka Complex, Oslo area, Norway. Part II: the mafic silicates. Journal of Petrology, 14, 349-380.

Davies, J.H., 1994. Lateral water transport across a dynamic mantle wedge: a model for subduction zone magmatism. In: Ryan, M.P. (ed.), Magmatic Systems, Academic Press, 197-221.

Deer, W.A., Howie, R.A. and Zussman, J., 1980. An Introduction to Rock Forming Minerals. 12th Ed. Longman, London, 528 p.

Dodge, F.C.W., and Moore, J.G., 1968. Occurrence and composition of biotites from the Cartridge Pass pluton of the Sierra Nevada batholith, California. U.S. Geol. Surv. Prof. Paper 600-B, B6-B10.

Douglas, L.A., 1977. Vermiculites. In: Dixon, J.B., and Weed, S.B. (eds.), Minerals in Soil Environments, Soil Sci. Soc. Amer., Madison, Wisconsin, 259-292.

Eriksson, S.C., and Wones, D.R., 1983. The Parks Pond pluton, eastern Maine: evidence for cratonization or orogenic activity. Geol. Soc. Amer. Abstr. With Programs 15, 18.

Erkan, Y., 1975. Orta Anadolu Masifi güneybatısında (Kırşehir bölgesinde) etkili rejyonel metamorfizmasının petrolojik incelemesi. H.Ü. Ph.D. Thesis, 147 p.

Erkan, Y., and Ataman, G., 1981. Orta Anadolu Masifi (Kırşehir yöresi) metamorfizma yaşı üzerine K/Ar yöntemi ile bir inceleme: H.U. Yerbilimleri Dergisi, 8, 27-30.

Erler, A., Akıman, O., Unan, C., Dalkılıç, F., Dalkılıç, B., Geven, A., and Önen, P., 1991. Kaman (Kırşehir) ve Yozgat yörelerinde Kırşehir Masifi magmatik kayaçlarının petrolojisi ve jeokimyası. Doğa-Tr. J. of Engineering and Environmental Sciences, 15, 76-100.

Fanning, D.S., and Keramidas, V.Z., 1977. Micas. In: Dixon, J.B., and Weed, S.B. (eds.), Minerals in Soil Environment, Soil Sci. Soc. Amer., Madison, Wisconsin, 195-195-258.

Farmer, V.C., Russell, J.D., McHardy, W.J., Newman, A.C.D., Ahlrichs, J.L., and Rimsaite, J.Y.H., 1971. Evidence of loss of protons and octahedral iron from oxidised biotites and vermiculites. Mineralogical Magazine, 38, 121-137.

Flinter, B.H., 1959. The magnetic separation of alluvial minerals in Malaya. American Mineralogist, 44, 738-751.

Floyd, P.A., Yalınız, M.K., and Göncüoğlu, M.C., 1998. Geochemistry and petrogenesis of intrusive and extrusive ophiolitic plagiogranites, Central Anatolian Crystalline Complex, Turkey. Lithos, 42, 225-241.

Fordham, A.W., 1990. Treatment of microanalyses of intimately mixed products of mica weathering. Clays and Clay Minerals , 38, 179-186.

Foster, M.D., 1960. Interpretation of the composition of trioctahedral micas. U.S. Geol. Surv. Prof. Paper, 354-B, 11-49.

Foster, M.D., 1963. Interpretation of the composition of vermiculites and biotites. In: Swineford, A. (ed.), Proceedings of the Tenth National Conference, Clays and Clays Minerals, New York, 70-89.

Fuji, N., Sayın, A., İçöz, S., 1993. Selected JCPDS (ASTM) cards for common minerals. MTA Yayını, Ankara, 52 p.

Garrels, R.M., and Christ, C.L., 1965. Solutions, Minerals, and Equilibria. Freeman, Cooper and Co., San Fransico, 450 p.

Geven, A., 1995. Petrography and geochemistry of Cefalıkdağ granitoid (Western part of Central Antolian Crystalline Complex): H.U. Yerbilimleri Dergisi, 17, 1-16.

Gevers, T.W., 1948. Vermiculite at Loolekop, Palabora, North East Transvaal. Trans. Geol. Soc. S. Africa, 133-173.

Göncüoğlu, M.C., 1977, Geologie des Westlichen Nigde Massivs: Univ. of Bonn, Ph.D. Thesis (unpublished).

Göncüoğlu, M.C., 1981, Niğde Masifinin jeolojisi. İç Anadolu'nun Jeoloji Simpozyumu: Türkiye Jeol. Kur. Bült., 16-19.

Göncüoğlu, M.C., 1985. Niğde Masifi batı yarısının jeolojisi. MTA Rapor No: 7856, 156 p.

Göncüoğlu, M.C., 1986. Geochronological data from the southern part (Niğde Area) of Central Anatolian Massif. MTA Dergisi, 105/106, 83-96.

Göncüoğlu, M.C., and Türeli, K., 1993. Petrology and geodynamic interpretation of plagiogranites from Central Anatolian ophiolites (Aksaray-Türkiye). Doğa - Türk Yerbilimleri Dergisi, 2, 195-203.

Göncüoğlu, M.C., and Türeli, K., 1994. Alpine collisional-type granitoids from western Central Anatolian Crystalline Complex, Turkey. Journal of Kocaeli University, 1, 39-46.

Göncüoğlu, M.C., Yalınız, K., and Tekeli, O., 1993b. Orta Anadolu ofiolitlerinin petrolojik özellikleri ve yapısal konumları. Hacettepe Üniversitesinde Yerbilimlerinin 25. Yılı Sempozyumu bildiri özetleri, 17-18.

Göncüoğlu, M.C., Erler, A., Dirik, K., and Yalınız K., 1994. Sivas Baseninin batısının jeolojisi. ODTÜ-AGuDoS Raporu, 80 p.

Göncüoğlu, M.C., Yalınız, M.K., Özgül, L., and Toksoy, F., 1998. Orta Anadolu Ofiyolitlerinin Petrojenezi: İzmir-Ankara-Erzincan Okyanus kolunun evrimine bir yaklaşım: TÜBİTAK Raporu, 61 p.

Göncüoğlu, M.C., Toprak, G.M.V., Kuşçu, İ., Erler, A., Olgun, E., 1991. Orta Anadolu Masifinin Batı Bölümünün Jeolojisi Bölüm II: Güney Kesim. TPAO Rapor No: 2909, 140 p.

Göncüoğlu, M.C., Erler, A., Toprak, V., Yalınız, K., Olgun, E., and Rojay, B., 1992. Orta Anadolu Masifinin Batı Kesiminin jeolojisi, Bölüm II: Orta Kesim. TPAO Rapor No. 3155, 76 pp.

Göncüoğlu, M.C., Erler, A., Toprak, V., Olgun, E., Yalınız, K., Kuşçu, İ., Köksal, S., and Dirik, K., 1993a. Orta Anadolu Masifinin Orta Bölümünün jeolojisi, Bölüm III: Orta Kızılırmak Tersiyer Baseninin Jeolojik Evrimi. TPAO Rapor No: 3313, 104 p.

Graham, R.C., Weed, S.B., Bowen, L.H., Amarasiriwardena, D.D., and Buol, S.W., 1989. Weathering of iron-bearing minerals in soils and saprolite on the North Carolina Blue Ridge Front: II. Clay mineralogy. Clays and Clay Minerals, 37(1), 29-40.

Grim, R.E., 1968. Clay Mineralogy. 2nd Ed., McGraw-Hill, New York, 596 p.

Grim, R.E., and Bradley, W.F., 1951. The mica minerals in X-ray Identification and Structures of Clay Minerals, Mineralogical Society of Great Britain Monograph, 138-172.

Gruner, J.W., 1934. Structures of vermiculites and their collapse by dehydration. American Mineralogist, 19, 557-575.

Gruner, J.W., 1939. Ammonium mica synthetised from vermiculite. American Mineralogist, 24, 428-435.

Güleç, N., 1994. Rb-Sr isotope data from the Ağaçören granitoid (east of Tuz gölü): geochronological and genetical implications. Türkiye Yerbilimleri Dergisi (TÜBİTAK), 3(1), 39-43.

Hadley, J.B., 1949. Preliminary report on corundum deposits in Buck Creek peridotite, Clay Country, North Carolina. U.S. Geol. Surv. Bull., 948-E, 103-128.

Hagner, A.F., 1944. Wyoming vermiculite deposits. Univ. of Wyoming Geol. Surv. Bull., 34, 47 p.

Haslam, H.W., 1968. The crystallization of intermediate and acid magmas at Ben Nevis, Scotland. Journal of Petrology, 9, 84-104.

Hattaway, J.C., 1955. Studies of some vermiculite type clay minerals. Clays and Clays Minerals, 74-86.

Hazen, R.M., and Burnham, C.W., 1973. The crystal structure of one-layer phlogopite and annite. American Mineralogist, 58, 889-900.

Hazen, R.M., and Wones, D.R., 1972. The effect of cation substitutions on the physical properties of trioctahedral micas. American Mineralogist, 57, 103-129.

Heincrich, E.W., 1946. Studies on mica group: the biotite-phlogopite series. Amer. Jour. Sci., 244, 836-848.

Hendrick, S.B., and Jefferson, M.E., 1938a. Crystal structure of vermiculites and mixed vermiculite-chlorites. American Mineralogist, 23, 851-863.

Hendrick, S.B., and Jefferson, M.E., 1938b. Structures of kaolin and talc-pyrophyl hydrates and their bearing on water sorption of the clays. American Mineralogist, 863-875.

Hewitt, D.A., and Wones, D.R., 1984. Experimental phase relations of the micas. In: Bailey, S.W. (ed.), Micas, Reviews in Mineralogy, Min. Soc. Amer., BookCrafters Inc., Michigan, 201-256.

Hindman, J.R., 1994. Vermiculite. In: Carr, D.D. (ed.), Industrial Minerals and Rocks, 6th ed., SME, Littleton, CO, 1103-1111.

Holdren, G.R., Jr., and Berner, R.A., 1979. Mechanisms of feldspar weathering – I. Experimental studies. Geochim. et Cosmochim. Acta, 43, 1161-1171.

Jackson, M.L., 1963. Interlayering of expansible layer silicates in soils by chemical weathering. Clays and Clay Minerals, 11, 29-46.

Jackson, M.L., Hzeung, Y., Corey, R.B., Evans, E.J., and Vanden Heuvel, R.C., 1952. Weathering sequence of clay-size minerals in soils and sediments: II. Chemical weathering of layer silicates. Proc. Soil. Amer., 6, 3-6.

Jelitto, J., Dubinska, E., Wiewiora, A., and Bylina, P., 1993. Layer silicates from serpentinite-pegmatite contact (Wiry, Lower Silesia, Poland). Clays and Clay Minerals, 41(6), 693-701.

Johnson, K.E., Davis, A.M., and Brynzia, L.T., 1996. Constracting sysles of hydrous metasomatism in the upper mantle: An ion microprobe investigation. Geochim. et Cosmochim. Acta, 60, 1367-1385.

Justo, A., Maqueda, C., and Perez Rodriguez, J.L., 1986. Estudio quimico de vermiculitas de Andalicia y Badajoz. Bol. Soc. Espafiola Mineral, 9, 123-129.

Justo, A., Maquea, C., Perez-Rodriguez, J.L., and Lagaly, G., 1987. An unusually expandable low-charge vermiculite. Clay Minerals, 22, 319-327.

Kadıoğlu, Y.K., 1991. Geology, petrography and geochemistry of Ağaçöeren (Aksaray) magmatic rocks. Ms.Sci. Thesis in Geological Engineering, Middle East Technical University, Ankara, 141 p (unpublished).

Kadıoğlu, Y.K., Ateş, A., and Güleç, N., 1998. Structural interpretation of gabbroic rocks in Ağaçören Granitoid, central Turkey: field observations and aeromagnetic data. Geological Magazine, 135(2), 245-254.

Kara, H., and Dönmez, M., 1990. 1:100 000 ölçekli açınsama nitelikli Türkiye jeoloji haritaları serisi, No: 34, Kırşehir G-17 paftası. MTA Yayını, 17 p.

Ketin, İ., 1955. Yozgat bölgesinin jeolojisi ve Orta Anadolu Masifinin tektonik durumu. Türkiye Jeol. Kur. Bült., 6, 1-40.

Ketin, İ., 1963. 1:500 000 ölçekli Türkiye jeoloji haritası, Kayseri paftası izahnamesi. MTA Yayını, Ankara, 83 p.

de Kimpe, C.R., Miles, N., Kodama, H., and Dejou, J., 1987. Alteration of phlogopite to corrensite at Sharbot Lake, Ontario. Clay and Clay Minerals, 35, 150-158.

Klein, C. and Hurlbut, C.S., 1985. Manual of Mineralogy, John Wiley and Sons, New York, 596 p.

Komarneni, S., and Roy, R., 1981. Hydrothermal transformations in candidate overpack materials and their effects on Cesium and strontium sorption. Nucl. Technol., 54, 118-122.

Köksal, S., 1996. The geological and petrological characteristics of the İdiş Dağı – Avanos (Nevşehir – Central Anatolia). M.Sc. Thesis in Geological Engineering, Middle East Technical University, Ankara, 140 p. (unpublished).

Kulp, J.L., and Brobst, D.A., 1954. Notes on the dunite and the geochemistry of vermiculite at the Day Book dunite deposit, Yancey Country, North Carolina. Economic Geology, 49, 211-220.

Lalonde, A.E., and Martin, R.F., 1983. The Baie-des-Moutons syenitic complex, La Tabatiere, Quebec. Part II. The ferromagnesian minerals. Can. Mineral., 21, 81-91.

Leake, B.E., 1978. Nomenclature of amphiboles. American Mineralogists, 63, 1023-1052.

Levinson, A.A., and Heinrich, E.Wh., 1954. Studies in the mica group, single crystal data on phlogopites, biotites and manganophyllites. American Mineralogist, 39, 937-945.

Lvova, I.A., 1974. Vermiculite Deposits in the USSR (Formation Types and Distribution Regularities), Nedra, Leningrad, 231p.

Maaloe, S., and Wyllie, P.J., 1978. Water content of a granite magma deduced from the sequence of crystallization determined experimentally with water-undersaturated conditions. Contrib. Mineral. Petrol., 52, 175-191.

MacEvan, D.M.C., 1948. The identification and estimation of montmorillonite group of minerals, with special reference to soil clays. Jour. Soc. Chem. Indus., 65, 298-304.

Mackenzie, R.C., 1957. Thermal methods in the Differential Thermal Investigations of Clays, Mineralogical Society, London, 1-22.

Mahmood, A., 1983. Chemistry of biotites from a zoned granitic pluton in Morocco. Mineralogical Magazine, 47, 364-369.

May, H., Helmke, P., and Jackson, M., 1979. Gibbiste solubility and thermodynamic properties of hyroxy-aluminum ions in aqueous solution at 25°C. Geochim. et Cosmochim. Acta, 43, 861-868.

McDowell, S.D. and Elders, W.A., 1980. Authigenic layer silicate minerals in Borehole Elmore I, Salton Sea geothermal field, California, U.S.A. Contrib. Mineral. Petrol., 74, 293-310.

Meunier, A., and Velde, B., 1979. Biotite weathering in granites of Western France. In: Mortland, M.M., and Farmer, V.C. (eds.), Developments in Sedimentology, v. 27, Elsevier Scientific Publishing Company, New York, 405-412.

Moon, H.S., Song, Y., and Lee, S.Y., 1994. Supergene vermiculitization of phlogopite and biotite in ultramafic and mafic rocks, Central Korea. Clays and Clay Minerals, 42(3), 259-268.

Moore, D.M., and Reynolds, R.C., Jr., 1989. X-ray Diffraction and the Identification and Analysis of Clay Minerals, Oxford University Press, Oxford, New York, 332 p.

Morel, S.W., 1955. Biotite in the basement complex of Southern Nyasaland. Geological Magazine, 92 (3), 241-255.

Morimoto, N., Fabries, J., Ferguson, A.K., Ginzburg, I.V., Ross, M., Seifert, F.A., Zussman, J., Aoki, K., and Gottardi, G., 1988. Nomenclature of pyroxenes. American Mineralogist, 73, 1123-1133.

Nagasawa, K., Brown, G., and Newman, A.C.D., 1974. Artificial alteration of biotite into a 14Å-layer silicate with hydroxy-aluminium interlayers. Clays and Clay Minerals, 22, 241-252.

Naney, M.T., 1983. Phase equilibria of rock forming ferromagnesian silicates in granitic systems. Amer. Jour. Sci., 223, 993-1033.

Nash, W.P., and Wilkinson, J.F.G., 1970. Shonkin Sag laccolith, Montana. Part I. Mafic minerals and estimates of temperature, pressure, oxygen fugacity and silica activity. Contrib. Mineral. Petrol., 25, 241-269.

Nemecz, E., 1981. Clay Minerals, Akademiai Kiado, Budapest, Hungary, 547 p.

Noack, Y., and Colin, F., 1986. Chlorites and chloritic mixed layer minerals in profiles on ultrabasic rocks from Moyango (Ivory Coast) and Antiquino (Brazil). Clay Minerals, 21, 171-182.

Nockolds, S.R., 1947. The relation between chemical composition and paragenesis in the biotite micas of igneous rocks. Amer. Jour. Sci., 245, 401-420.

Norrish, K., 1973. Factors in the weathering of mica to vermiculite. Proc. Int'l. Clay Conf. 1972., Madrid, 417-432.

Nutting, P.G., 1943. Some standard thermal dehydration curves of Minerals. U.S. Geol. Surv. Prof. Paper, 197E, 197-216.

Oktay, F.Y., 1981. Savcılıbüyükoba (Kaman) çevresinde Orta Anadolu Masifi tortul örtüsünün jeolojisi ve sedimentolojisi: İTÜ, Doçentlik Tezi, 175 p. (unpublished).

Önen, A.P., 1985. Mineralogy, Petrography and geochemistry of gabbros from northeast of Kaman region (Kırşehir). Ms.Sci. Thesis in Geological Engineering, Middle East Technical University, Ankara, 105 p. (unpublished).

Önen, A.P., and Unan, C., 1988. Kaman (Kırşehir) kuzeydoğusunda bulunan gabroların mineralojisi, petrografisi ve jeokimyası. Türkiye Jeol. Kur. Bült., 31, 23-28.

Pabst, A., 1955. Redescription of the single layer structure of the micas. American Mineralogists, 53, 201-215.

Palabora Mining Company Limited Mine Geological and Mineralogical Staff, 1976. The geology and the economic deposits of copper, iron and vermiculite in the Palabora Igneous Complex: a brief review. Economic Geology, 71, 177-192.

Pozzuoli, A., Vila, E., Franco, E.A., Ruiz-Amil, and Calle, C. de la, 1992. Weathering of biotite to vermiculite in quaternary lahars from Monti Ernici, Central Italy. Clay Minerals, 27, 175-184s.

Proust, D., Eymery, J.P., and Beaufort, D. 1986. Supergene vermiculitization of a magnesian chlorite: Fe and Mg removal process. Clays and Clay Minerals, 34(5), 572-580.

Rosenblum, S., 1958. Magntic susceptilities of minerals in the Frantz isodynamic magnetic separator. American Mineralogist, 43, 170-173.

Rowins, S.M., Lalonde, A.E., and Cameron, E.M., 1991. Magmatic oxidation in the syenitic Murdock Creek intrusion, Kirkland Lake, Ontario: evidence from the ferromagnesian silicates. Journal of Geology, 99, 395-414.

Roy, R., 1949. Decomposition and resynthesis of the micas. Jour. Amer. Ceram. Soc., 32, 202-210.

Roy, R., and Romo, L.A., 1957. Weathering studies: I New data on vermiculite. Journal of Geology, 65, 603-610.

Sekine, T., and Whllie, P.J., 1982a. Phase relationships in the system $KAlSiO_4$ - Mg_2SiO_4 - SiO_2 - H_2O as a model for hybridization between hydrous siliceous melts and peridotite. Contrib. Mineral. Petrol., 79, 368-374.

Sekine, T., and Whllie, P.J., 1982b. Synthetic systems for modeling hybridization between hydrous siliceous magmas and peridotites in subduction zones. Journal of Geology, 90, 734-741.

Sekine, T., and Whllie, P.J., 1982c. Phase relationships for mixtures of granite and peridotite, with applications to subduction zone hybridization. Contrib. Mineral. Petrol., 81, 190-202.

Sekine, T., and Whllie, P.J., 1983. Experimental simulation of mantle hybridization in subduction zones. Journal of Geology, 91, 511-528.

Serratosa, J.M., and Sanz, J., 1985. Dehydroxilation of micas and vermiculites: The effect of octahedral composition and interlayer saturing cations. Mineral. Petrogr. Acta, 29-A, 399-408.

Seymen, İ., 1981a. Kaman, (Kırşehir) dolayında Kırşehir Masifinin stratigrafisi ve metamorfizması: Türkiye Jeol. Kur. Bült., 24(2), 101-108.

Seymen, İ., 1981b. Kaman, (Kırşehir) dolayında Kırşehir Masifinin metamorfizması: Türkiye Jeol. Kur. 35. Bil. ve Teknik Kurultayı, İç Anadolu'nun Jeolojisi Sempozyumu, 12-15.

Seymen, İ., 1982. Geology of Kırşehir Massif around Kaman region. Habil. Thesis, İstanbul Techn. Univ., 164 p (unpublished).

Singer, A., and Stoffer, P., 1981. Hydrothermal Vermiculite from the Atlantis II Deep, Red Sea. Clays and Clay Minerals, 29(6), 454-458.

Smith, J.V., and Yoder, H.S., 1956. Experimental and theoretical studies of the mica polymorphs. Mineralogical Magazine, 31, 209-235.

Smykatz-Kloss, W., 1974. Differential Thermal Analysis: Application and Results in Mineralogy. Springer-Verlag, New York-Heidelberg-Berlin, 185 p.

Streckeisen, A.L., 1976. To each rock its proper name. Earth Science Reviews, 12, 1-33.

Sudo, A., and Tatsumi, Y., 1990. Phlogopite and K-amphibole in the upper mantle: implication for magma genesis in subduction zones. Geophys. Res. Lett., 17, 29-32.

Suquet, H., Malard, C., Quarton, M., Dubernat, J., and Pezeart, H., 1984. Etude du biopyribole forme par chauffage des vermiculites magnesiennes. Clay Minerals, 19, 217-227.

Tarhan, N., 1987. Orta Anadolu metamorfik ve granitik kayalarının kökeni ve evrimi. İstanbul Üniv. Müh. Fak. Yerbilimleri Dergisi, 6(1/2), 57-68.

Thompson, A.B., 1992. Water in the Earth's upper mantle. Nature, 358, 295-302.

Todor, D.N., 1976. Thermal Analysis of Minerals, Tunbridge Wells, Kent, Abacus Press, 256 p.

Toksoy, F., and Göncüoğlu, M.C., 1998. Phlogopitic metagabbro within Central Anatolian Ophiolites, Kurançalı (Kırşehir), Turkey. Third International Turkish Geology Symposium, Middle East Technical University, 31 August-4 September, 1998, Ankara-Turkey, Abstracts, p. 175.

Tribuzio, R., Riccardi, M.P., and Messia, B., 1997. Amphibolitization of Mg- and Fe-rich gabbroic dykes within mantle derived serpentinites from Northern Apennine ophiolites evidence for high temperature hydration of the oceanic lithosphere. Ofioliti, 22(1), 71-79.

Türeli, T.K., 1991. Geology, petrography and geochemistry of Ekecikdağ plutonic rocks (Aksaray Region-Central Anatolia): Ph.D. Thesis in Geological Engineering, Middle East Technical University, Ankara, 194 p. (unpublished).

Vali, H., and Hesse, R., 1992. Identification of vermiculite by transmission electron microscopy and x-ray diffraction. Clay Minerals, 27, 185-192.

Varley, E.R., 1948. Vermiculite deposits in Kenya. Imperial Inst. Bull., 46, 348-352.

Velde, B., 1978. High temperature metamorphism vermiculites. Contrib. Mineral. Petrol., 66, 319-323.

Velde, B., 1985. Clay Minerals (Physico-Chemical Explanation of their Occurences), Developments in Sedimentology, Elseiver, Amsterdam, Oxford, New York, Tokyo, 427 p.

Vicente, M.A., Razzaghe, M., and Robert, M., 1977. Formation of aluminum hydroxy vermiculite (intergrade) and smectite from mica under acidic conditions. Clay Minerals, 12, 101-112.

Vorovikov, P.P., 1973. Genetic types, conditions of formation and economic evaluation of vermiculite deposits in Perlite and Vermiculite (Geology, Exploration and Production Technology), Gosudarstvennoe Nauchno-Tekhnicheskoe Izdarel'stvo Literatury Po Geologii I Okhrano Nedr., Moscow (translated from Russian by the Indian Nat. Science Documentation Centre for the US Dept. of the Interior), 139-176.

Walker, G.F., 1949. The decomposition of biotite in soils. Mineralogical Magazine, 28, 693-703.

Walker, G.F., 1950a. Trioctahedral minerals in soil clays. Mineralogical Magazine, 28, 704-714.

Walker, G.F., 1950b. Vermiculite-organic complexes. Nature, 166, 695-697.

Walker, G.F., 1951. Vermiculite and some related mixed-layer minerals in X-ray Identification and Structures of Clay Minerals, Mineralogical Society of Great Britain Monograph, 199-223.

Walker, G.F., 1956. Mechanism of dehydration of Mg-vermiculite. Natl. Acad. Sci. Publ., 456, 101-115.

Walker, G.F., 1957. On the differentiation of vermiculites and smectites in clays. Clay Minerals Bull., 3(17), 154-163.

Walker, G.F., and Cole, W.F., 1957. The vermiculite minerals in The Differential Thermal Investigations of Clays, Mineralogical Society, London, 191-206.

Wones, D.R., and Dodge, F.C.W., 1977. The stability of phlogopite in the presence of quartz and diopside. In: Fraser, D.G. (ed.), Thermodynamics in Geology, Dordrecht-Holland, D. Reidel Publishing Co., 229-247.

Wones, D.R., and Eugster, H.P., 1965. Stability of biotite: Experiment, theory, and application. American Mineralogist, 50, 1228-1272.

Wones, D.R., and Gilbert, M.C., 1982. Amphiboles in the igneous environment. Reviews in Mineralogy 9B, Mineral. Soc. Amer., 355-390.

Wyllie, P.J., and Sekine, T., 1982. The formation of mantle phlogopite in subduction zone hybridization. Contrib. Mineral. Petrol., 79, 375-380.

Yalınız, M.K., 1996. Petrology of the Sarıkaraman Ophiolite (Aksaray-Turkey). Ph.D. Thesis in Geological Engineering, Middle East Technical University, Ankara, 270 p. (unpublished).

Yalınız, M.K., and Göncüoğlu, M.C., 1998. General geological characteristics and distribution of the Central Anatolian Ophiolites. H.U. Yerbilimleri Dergisi, 20, 19-30.

Yalınız, M.K., Floyd, P.A., and Göncüoğlu, M.C., 1996. Supra-subduction zone ophiolites of Central Anatolia: geochemical evidence from the Sarıkaraman Ophiolite, Aksaray, Turkey: Mineralogical Magazine, 60(402), 697-710.

Yalınız, K., Göncüoğlu, M.C., and Floyd, P.A., 1994. Geochemical characteristics and geodynamic interpretation of supra-subduction Sarıkaraman ophiolite, Central Anatolia, Turkey: Int. Volcanological Congress, Ankara, 12-16 September, 1994, Abstracts, 144.

Yalınız, K., Parlak, O., Özkan-Altıner, S., and Göncüoğlu, M.C., 1997, Formation and emplacement ages of supra-subduction-type ophiolites in Central Anatolia; Sarıkaraman Ophiolites, Central Turkey: Çukurova Univ. 20. Anniv. Of Geol.Educ., 30 April-3 May 1997, Adana, Abstracts, 61-62.

Yılmaz-Şahin, S., Boztuğ, D., 1997. Petrography and wholerock chemistry of the gabbroic, monzogranitic and syenitic rocks from the Çiçekdağ region, N of Kırşehir, Central Anatolia, Turkey. In: Boztuğ, D., Yılmaz-Şahin, S., Otlu, N., and Tatar, S. (eds.), Proceeding of TÜBİTAK-BAYG/NATO-D PROGRAM on Alkaline Magmatism (Theoretical Consideration and Field Excursion in Central Anatolia), 2-10 October, 1997, Dept. of Geology, Cumhuriyet University, Sivas-Turkey, 29-42.

Yılmaz-Şahin, S., Boztuğ, D., 1998. Petrogenesis of the Çiçekdağ Igneous Complex, NW Kırşehir, Central Anatolia, Turkey. 51th Geological Congress of Turkey, Ankara, Abstracts, 33-35.

Yoder, H.S., 1959. Experimental studies on micas: a review. Proceedings of the 6th National Clay Conference, Pergamon Press, New York, 42-60.

Zeck, H.P., and Ünlü, T., 1987. Parallel whole rock isochrons from a composite, monzonitic pluton, Alpine Belt, Central Anatolia, Turkey. N. Jb. Miner. Mh., 5, 193-204.

Zhelyaskova-Panayotova, M., 1989. The Balkan Peninsula - A New Vermiculite-bearing province. Comptes Rendus de l'Académie Bulgare des Sciences, Geologie - Mineralogie, 42(11), 75-78.

Zhelyaskova-Panayotova, M., Laskou, M., Economou, M., and Stefanov, D., 1992. Vermiculite occurrences from the Vavdos and Gerakini Areas of the W. Chalkidiki Peninsula, Greece. Chem. Erde, 52, 41-48.

Zelyaskova-Panayotova, M., Economou-Eliopoulos, M., Petrov, P.M., Laskou, M., and Alexandrova, A., 1993. Vermiculite deposits in the Balkan Peninsula. Bull. Geol. Soc. Greece, 28, 451-461.

APPENDIX A

MAGNETIC SUSCEPTIBILITIES OF MINERALS

BY FRANTZ ISODYNAMIC SEPARATOR

A chart showing magnetic susceptibilities for common minerals by Frantz isodynamic separator which is adjusted to forward slope of 15° and site tilt of 25° (After Rosenblum, 1958; Flinter, 1959).

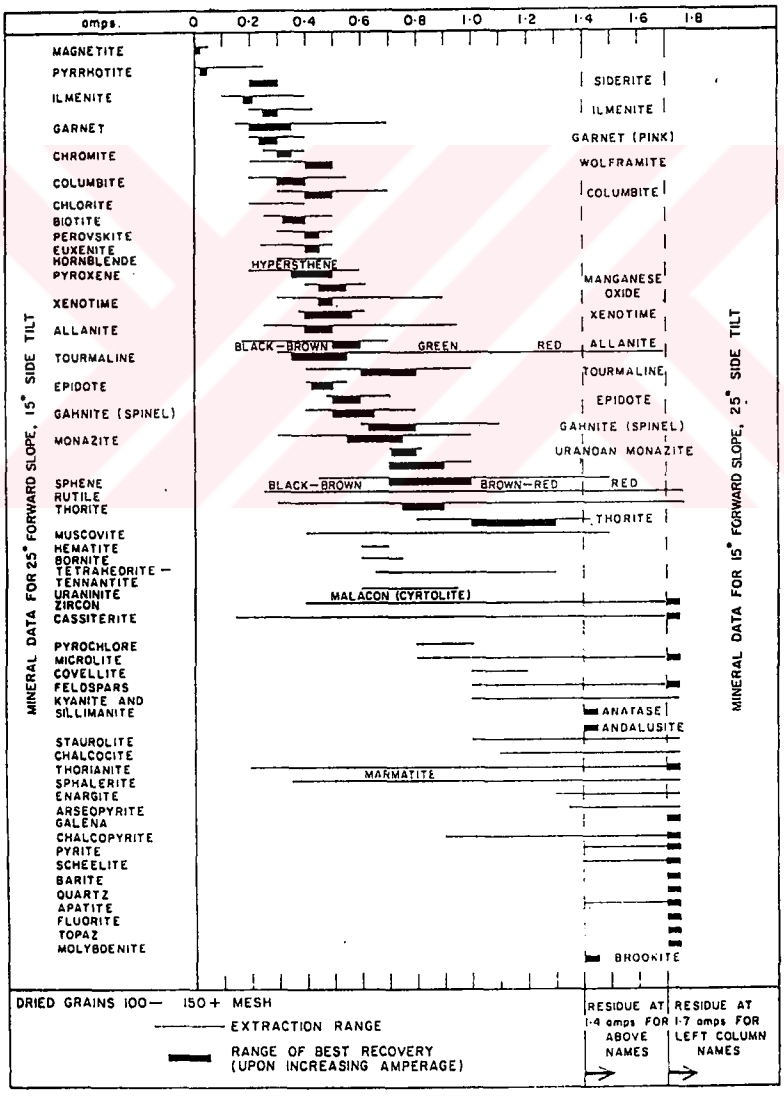

APPENDIX B

SOLUTION PREPARATION FOR CHEMICAL ANALYSES

1. Preparation of Solution to Measure Major Oxides by Inductively Coupled Plasma Spectrometry (ICP)

About 0.1 mg of the powder sample, fractionated to less than 100 μm, is mixed with 10 ml of H_2O_2 and waited for 10 mins to remove the organic matters. Then other materials are added to the specimen in the order of 10 ml of H_2SO_4, 10 ml of H_3PO_4, 10 ml of distilled water and 5 ml of HCl and the mixture is waited for 5 mins. Finally 5 ml of HF is added to the waited mixture. Teflon beaker containing the mixture is tightly covered and placed into razor. The mixture is dissolved in a microwave furnace with a program; waiting for 5 mins at 250 watt, waiting for 5 mins at 400 watt, waiting for 10 mins at 350 watt and ventilated for 5 mins. The material dissolved in furnace is poured into a volumetrical flask and completed to 250 ml with distilled water. This final solution is used to read the major oxides by ICP. The measurements obtained from the instrument are converted to percentages. Calculation for each read oxides is made by:

$$\% \text{ of oxide} = \frac{\text{measured value of oxide} \times 100}{\text{used sample weight}}$$

The used standard samples are of PE PURE (atomic spectroscopy standard) and their 1.000 vg/ml number is different for each oxides. For example; the standard number is N930-0150 belonging to PE PURE for silicon.

The ignition loss at 1060°C is also measured from 1 g of the sample dried at 100°C and waited for 4 hrs. It is not important to measure loss of

ignition whether before or after solution is prepared because it is only necessary during the calculation of the results.

2. Preparation of Solution to Calculate Fe^{2+} (FeO) Content by Spectrophotometry

10.0 mg of powdered sample, sieved to less than 100 μm, is put into teflon beaker. The materials are added to specimens in the order of 1 measure of powdered pure orthophenanthroline, 3 ml of H_2SO_4 and 0.5 ml of HF. The mixture is dissolved by heating on water bath for 30 mins. During dissolution of the mixture, 5 ml boric acid is poured into 100 ml volumetric flask. After 30 mins heating the mixture, 20 ml sodium citrate is immediately added to teflon beaker. Then the content of the beaker is poured into volumetric flask containing boric acid and the solution is completed to 100 ml with distilled water. During the solution preparation, solution for one blank sample and one standard must also be prepared. Taking blank as reference, measurements are made by using both 555 μm and 640 μm wavelenghts on spectrophotometer. The determination of FeO content of the sample is calculated by the following relationship;

a = (record at 555 μm wavelenght) - (record at 640 μm wavelenght)

$$b = \frac{(\%FeO)_{standard}}{a_{standard}}$$

$$(\%FeO)_{sample} = b \times a_{sample}$$

or

$$\frac{(\%FeO)_{standard} \quad a_{standard}}{X \quad a_{sample}}$$

$$X = \frac{a_{sample} \times (\%FeO)_{standard}}{a_{standard}}$$

where; $X = (\%FeO)_{sample}$

APPENDIX C

CALCULATION OF STRUCTURAL FORMULA FROM A MINERAL ANALYSIS BY DEER ET AL. (1980)

(1) The composition of the mineral expressed in the usual manner as weight percentages of the constituent oxides is listed.

(2) Molecular proportion of each constituent oxide is obtained by dividing weight percentage of the corncerned oxide by the molecular weight of the oxide concerned.

(3) Anion proportion is obtained by multiplying by the number of oxygen atoms in the oxide concerned. It thus gives a set of numbers proportional to the numbers of oxygen atoms associated with each of the elements concerned. Anion proportions of all the oxides are summed.

The F factor is obtained by dividing the formula based upon the number of oxygens (representing half the content of the unit cell) by total anion .

Number of oxygens based for formula calculations:

4 oxygen for olivine
6 oxygen for pyroxene
24 oxygen for amphibole (hydrous form)
23 oxygen for amphibole (anhydrous form)
24 oxygen for mica (hydrous form)
22 oxygen for mica (anhyrous form)

(4) Cation proportion is obtained by multiplying the molecular proportion by the number of cations in each oxides (e.g., for SiO_2 there is one silicon for 2

oxygens, so molecular proportion of SiO_2 multiplied by one. In the same way, there is 2 aluminum for 3 oxygens for Al_2O_3, so molecular proportion of Al_2O_3 is multiplied by 2).

(5) F factor is multiplied by cation proportion of each oxide to find the number of ions (unit cell content) in formula.

(6) It is assumed that the tetrahedral sites, which are not filled by Si are occupied by Al, and the remaining Al atoms are used in octahedral coordination.

APPENDIX D

NOMENCLATURE OF AMPHIBOLE BY LEAKE (1978)

The classification is based on the chemical contents of a standard amphibole calculated to 24(O,OH,F,Cl), but it is recognized that where there is no determination of H_2O^+ (e.g. electron microprobe analyses), or there is reason to suppose that the reported H_2O^+ is erroneous, or where it is probable that reported F or Cl may be substantial, then the basis of 23(O) should be used to calculate the cation contents of the standard formula. This formula unit contains eight tetrahedral sites and corresponds to the half unit cell for monoclinic amphiboles and to one quarter of the unit cell for orthorhombic amphiboles.

The standard amphibole formula is taken to contain 8 tetrahedral sites and the general form of the standard formula is:

$$A_{0\text{-}1}B_2C_5{}^{VI}T_8{}^{IV}O_{22}(OH,F,Cl)_2$$

In the calculation of standard amphibole formula, the following procedure is recommended.

If the water and hologen contents are well established, or if there is physical evidence that the amphibole is oxy-amphibole, the formula should be calculated to 24(O,OH,F,Cl).

If the water plus halogen content is uncertain the formula should be calculated on a water-free (and halogen-free) basis to 23(O) and 2(OH,F,Cl) assumed, unless this leads to an impossibility of satisfying any of the following criteria, in which case appropriate change in the assumed number of (OH+F+Cl) should be made.

(3) Sum T to 8.00 using Si, then Al, then Cr^{3+}, then Fe^{3+}, then Ti^{4+}.

(4) Sum C to 5.00 using excess Al, Cr, Ti, Fe^{3+} from (3), then Mg, then Fe^{2+}, and then Mn.

(5) Sum B to 2.00 using excess Fe^{2+}, Mn, Mg from (4), then Ca, then Na.

(6) Excess Na from (5) is assigned to A, then all K. Total A should be between 0.00 and 1.00, inclusive.

These assignments normally correspond to the occupancies of the tetrahedral sites (T), the M1 + M2 + M3 sites (C), the M4 sites (B) and the A sites (A).

When a standard amphibolite formula has been determined in this way it is classified first into one of four principal amphibole groups on the basis of the numbers of atoms of $(Ca+Na)_B$ and Na_B. Within each groups it can be named using the number of Si atoms and the ratio of $Mg/(Mg+Fe^{2+})$. The name so found is the name of the defined end-member to which the formula most closely approximates. The four principal amphibole groups are defined as:

Iron-magnesium-manganese amphibole group: $(Ca+Na)_B < 1.34$

(b) Calcic amphibole group: $(Ca+Na)_B \geq 1.34$ and $Na_B < 0.67$, usually $Ca_B > 1.34$.

In this group, tschermakitic hornblende is to be used for amphiboles chemically defined with respect to the standard formula as follows: $(Ca+Na)_B \geq 1.34$; $Na_B < 0.67$; $(Na+K)_A < 0.50$; $Mg/(Mg+Fe^{2+}) \geq 0.50$; Si between 6.25 and 6.49 inclusive: $Ti < 0.50$.

Sodio-calcic amphibole group: $(Ca+Na)_B \geq 1.34$ and $0.67 \leq Na_B < 1.34$, usually $0.67 < Ca_B < 1.34$

(d) Alkali amphibole group: $Na_B \geq 1.34$